GEOLOGICAL SURVEY OF DENMARK AND GREENLAND BULLETIN 26 • 2012

Review of Survey activities 2011

Edited by
Ole Bennike, Adam A. Garde and W. Stuart Watt

GEOLOGICAL SURVEY OF DENMARK AND GREENLAND
MINISTRY OF CLIMATE, ENERGY AND BUILDING

Geological Survey of Denmark and Greenland Bulletin 26

Keywords
Geological Survey of Denmark and Greenland, survey organisations, current research, Denmark, Greenland.

Cover photographs from left to right
1. Retrieving a sediment core in Sermilik fjord, South-East Greenland. Photograph: Robert S. Fausto.
2. Field work in Vietnam. Photograph: Flemming Larsen.
3. This Danish beech forest on Fyn was farm land during the Iron Age. Photograph: Ole Bennike.
4. Small-scale miners in Nigeria. Worldwide, *c.* 100 million people depend on small-scale mining. Photograph: John Tychsen.

Frontispiece: facing page
In the summer of 2011, GEUS carried out extensive reconnaissance work in South-East Greenland. The aim is to assess the mineral potential of the region, which is one of the least known regions of Greenland. The geologist is panning stream sediments in order to separate heavy minerals, possibly including gold. Photograph: Jakob Lautrup.

Printers: Rosendahls-Schultz Grafisk A/S, Albertslund, Denmark
Manuscripts received: 6 January 2012 – 8 May 2012
Final versions approved: 13 February 2012 – 23 May 2012
Printed: 10 July 2012

ISSN 1604-8156
ISBN 978-87-7871-339-1

Citation of the name of this series
It is recommended that the name of this series is cited in full, viz. *Geological Survey of Denmark and Greenland Bulletin*.
If abbreviation of the name of this volume is necessary, the following form is suggested: *Geol. Surv. Den. Green. Bull*. 26, 88 pp.

Available from
Geological Survey of Denmark and Greenland (GEUS)
Øster Voldgade 10, DK-1350 Copenhagen K, Denmark
Phone: +45 38 14 20 00, fax: +45 38 14 20 50, e-mail: *geus@geus.dk*. See also *www.geus.dk/publications/bull*

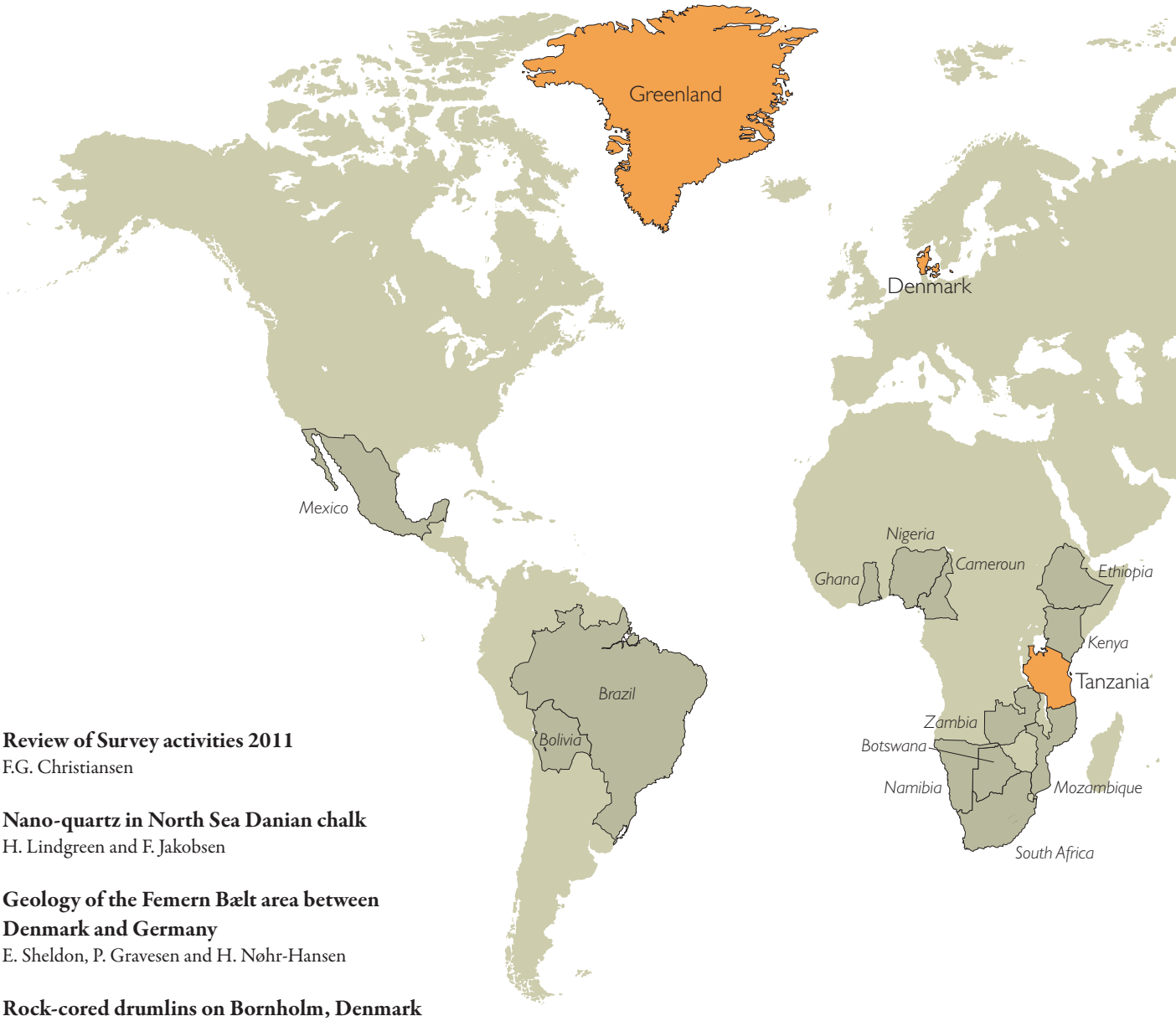

GEUS working areas 2011.
Orange areas are covered in this volume.

Review of Survey activities 2011

Flemming G. Christiansen
Deputy Director

2011 was a good year for the Geological Survey of Denmark and Greenland (GEUS) with fruitful discussions of strategies, handling of challenges posed to our society that has strong needs for growth and investments, and consequently for developing new projects for the future within the many fields where GEUS is involved.

GEUS has been through a long – but very constructive – process of putting together a new strategy that reflects the changes in society and new demands from many different stakeholders. This new strategy, 'Geology for society – knowledge for growth and welfare', covers the period up to 2020 and is based on an analysis of key driving forces such as transition from fossil fuel to sustainable energy, adaptation to changing climate conditions, need for water resources locally and globally, and international competition for critical minerals. The strategy includes a number of specific strategic topics. As these topics have been discussed between scientists and management over a long period and in some cases are related to new and on-going Survey projects, these topics are reflected in many of the papers in this year's issue of Review of Survey activities.

The reader will find contributions covering several of our new strategic topics such as: 'Past and future climate', 'Geology across land and sea', 'Geology in the public arena', 'Water resources under pressure', 'Oil and gas supply and transition to green energy' and 'Geothermal energy and heat storage', as well as papers on other subjects from GEUS' very broad project portfolio. Some of them describe specific, short projects, and others focus on results from some of our long-term monitoring projects on for example groundwater, gas storage, ice and earthquakes.

GEUS' activities and research in Denmark cover many different subjects such as fossil fuel and renewable energy, water, climate history and monitoring and adaptation to climate changes, nature protection, input to large infrastructure projects and data management.

Chalk is the main oil reservoir in the Danish part of the North Sea and understanding its mineralogy and diagenesis has crucial implications for production parameters. One paper proposes a new model for the formation of flint from studies of nano-quartz.

As part of planning the fixed link across Femern Bælt between Denmark and Germany, GEUS has been involved in geological and geotechnical investigations. Results of a multidisciplinary biostratigraphic study of pre-Quaternary deposits (especially Paleocene and Eocene) are summarised here.

Although the surface morphology of Denmark is well mapped and described in detail, there is still room for new observations and reinterpretation of some glacially formed features like rock-cored drumlins from Bornholm that are described for the first time.

Understanding methane distribution in young marine sediments is important for long-term use and protection of areas such as the Baltic Sea. GEUS has been partner in the Baltic Gas project with a key role to map the occurrence of free gas, to quantify the flux of gas and to study the processes and parameters governing methane generation and consumption. Natura 2000 is a network of nature protection areas under the Habitats Directive of the European Union. Some results from mapping of a Natura 2000 area with bubbling reefs in the inner Danish waters are presented in this volume. Another paper describes how Øresund became a strait between 8000 and 9000 years ago due to sea-level rise after an earlier history of being dry land with some bogs and lakes, and later a fjord.

The coastal cliff Stevns Klint is a classical locality for field trips, especially for studying the world's best exposed Cretaceous–Tertiary boundary, but also for the beautiful scenery. For this reason an understanding of the risks of cliff collapse is crucial, and an analysis of the different collapse types including volumetric considerations based on photogrammetric studies is given in one of the papers.

With a strong Danish ambition to reduce the dependence on fossil fuel by using renewable energy sources, shallow geothermal energy can be economically competitive. One paper introduces this concept with comments on exploitation, modelling and groundwater protection. The latter is very important in Denmark where almost all drinking water comes from groundwater. The Danish policy on this topic and the role of the authorities and water supply companies are discussed. GEUS is also involved in long-term monitor-

 Geological Survey of Denmark and Greenland Bulletin 26, 7–8. Open access: www.geus.dk/publications/bull

ing of groundwater above the gas storage facility at Stenlille on Sjælland. There has been no evidence of leakage through the geological barriers, and only one short incident with traces of gas from an injection well. Earthquake activity is low in an intra-plate region like Denmark, but prediction of seismicity is important, and the question whether geological and geodetic observations should be included in the assessment is discussed.

In 2011 there was a high level of field activities in Greenland with a major mapping and geochemical programme in South-East Greenland, a large field and shallow-core drilling programme of poorly known Cretaceous sediments in North-East Greenland and the EAGER cruise offshore North-East Greenland, which was part of the Danish Continental Shelf Project. Results from these large projects will be presented later; in this issue results from other completed and on-going projects are presented.

This volume also contains a discussion of the possibility to use anorthosite from Greenland as a future raw material for aluminium instead of bauxite. Based on regional knowledge and geochemical data, it is suggested that the Fiskenæsset complex is especially interesting. 3D mapping and modelling is high on the agenda in the new GEUS strategy in both Denmark and Greenland. Different methods are used in the crystalline areas of Greenland, for sedimentary basins or for Quaternary deposits in Denmark. A case study from the Skaergaard intrusion in southern East Greenland is presented.

In Greenland, the Bureau of Minerals and Petroleum in Nuuk is preparing licensing rounds offshore North-East Greenland for 2012 and 2013, and part of the regional preparation for this work is described. There is a high level of exploration activities throughout the West Greenland shelf in these years, and one paper brings a case study of bitumen from crystalline rocks in South Greenland.

Climate models predict a marked warming in the Arctic that may lead to the release of large amounts of methane bound in permafrost areas or in gas hydrates. The background of and some preliminary results from a scientific cruise to Disko Bugt in 2011 are related. The important monitoring programme of the Greenland Ice Sheet (PROMICE) continues to develop, and a paper summarises the results of ablation observations from 2008 to 2011. GEUS takes part in operating many seismic stations in Denmark (5) and Greenland (18), and it is very time-consuming to analyse all data manually. Test of an automatic method is described in another paper, and although the method is efficient, manual processing is still required to detect all earthquakes and for quality control purposes.

GEUS works in many different countries with many different types of projects. The last two papers in this issue are about Vietnam and Tanzania. GEUS has been active in Vietnam together with our sister organisation Vietnam Petroleum Institute and universities in Hanoi for almost twenty years. In Tanzania a Geocenter Denmark project has studied the possibilities of restoring soil fertility by using locally quarried rock phosphate and lime.

Nano-quartz in North Sea Danian chalk

Holger Lindgreen and Finn Jakobsen

The main oil reservoir in the Central Graben in the North Sea is chalk of the Maastrichtian Tor Formation, which has high porosity and relatively high permeability. The chalk of the Danian Ekofisk Formation is an additional reservoir, but with highly variable porosity and permeability. Whereas the Tor Formation is almost pure calcite primarily consisting of coccolith debris, the Ekofisk Formation also comprises significant proportions of phyllosilicates (clay minerals) and quartz in addition to coccolith debris. For decades the quartz was assumed to be a normal crystalline α-quartz such as is present in quartz sand, and the clay fraction was assumed to consist predominantly of phyllosilicates. However, Maliva & Dickson (1992) reported the presence of presumably authigenic submicron-size quartz crystals arranged in clusters, and suggested that these clusters were transformed opal-CT lepispheres. Investigations by nano-structural methods (X-ray diffraction and atomic force microscopy (AFM)) revealed that the prevailing quartz component in the North Sea chalk comprises α-quartz appearing as nano-size quartz spheres (Jakobsen *et al.* 2000; Lindgreen *et al.* 2010). Nano-quartz spheres were first observed in indurated chalk in the Ekofisk Formation in the Ekofisk Field and later in the South Arne Field. Subsequent analyses of the Ekofisk Formation in different chalk fields showed that the content of nano-quartz varies throughout the chalk succession and to some degree reflects the cyclic development of the chalk. The proportion of dispersed nano-quartz in the chalk is highly variable, from 10% to more than 80% in the Lower Danian (Lindgreen *et al.* 2010). This paper describes the nano-quartz, its formation and structure and presents a model for the formation of flint from nano-quartz in the North Sea Ekofisk chalk.

Material and methods

We have investigated core samples from the Ekofisk Formation in the South Arne Field wells SA-1 and Rigs-1, in the Halfdan Field wells Sif-1 and Nana-1 and in the Gorm Field well N-22 (Fig. 1). Most samples contained large amounts of calcite, so calcite-free residues were prepared by dissolving the calcite in an acetate-acetic acid buffer at pH 4.5–5. In this buffer, non-calcite minerals and especially fine-grained nano-quartz and clay minerals are not corroded or dissolved.

Scanning electron microscopy (SEM) is routinely used for investigations of chalk minerals and in special cases micron-sized particles can be identified (Hjuler & Fabricius 2009). However, rock samples dominated by nano-sized quartz are at the limit of resolution in the SEM and generally give poor SEM images due to poor current transmission in the fine-grained matrix. We used X-ray diffraction and AFM to characterise the ultra-fine particles in the chalk, such as nano-quartz and clay minerals.

X-ray diffraction scanning using 10 s/0.1 °2Θ was applied routinely to determine the mineralogical composition of both core piece samples and of non-calcite residues. High statistic scanning using 100 s/0.02 °2Θ was used to characterise the nano-quartz.

AFM (Binnig *et al.* 1986) generates topographic images by scanning a sharp tip across a surface and can produce images at atomic resolution of both conductors and non-conductors. For AFM we used a Rasterscope 3000 instrument under room conditions with a force of 0.175 nN and a scanning speed of 500 nm/s. In the present investigation of the topography of raw surfaces, AFM was run in non-contact

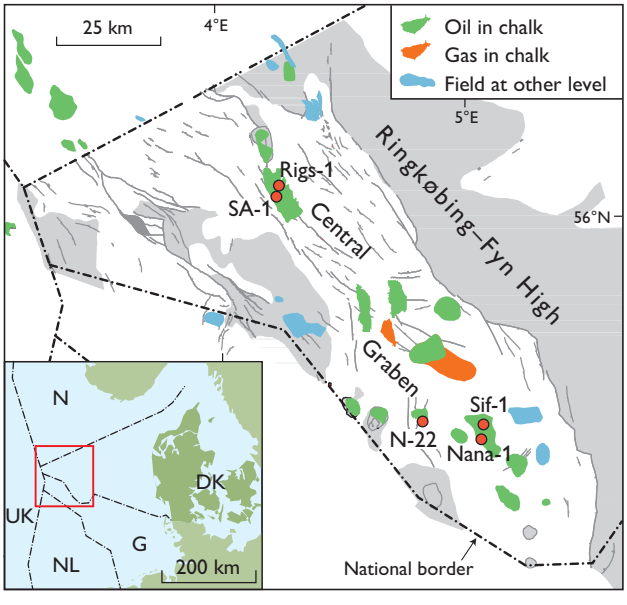

Fig. 1. Map of the Danish Central Graben showing the locations of the investigated wells.

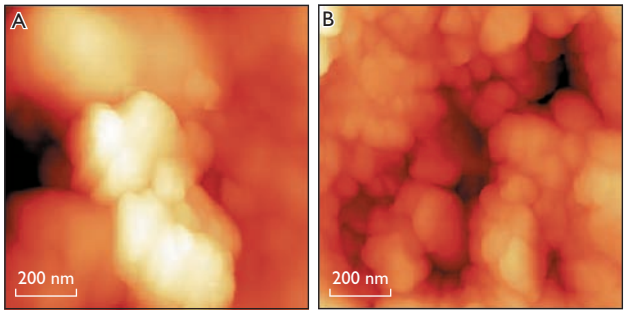

Fig. 2. Atomic force microscopy images of spherical grains of quartz. Non-contact mode, room conditions, force 0.175 nN, scanning speed 500 nm/s. A: Calcite-free residue deposited on graphite from well SA-1, 3344.15 m. B: Intact flint from Nana-1, 2135.7 m.

mode. Intact rock samples of small pieces of chalk or flint were glued onto gold-coated sample holders. In chalk samples, non-calcite minerals were identified and imaged from the insoluble residue. For such samples, the residue was dispersed ultrasonically in distilled water and the samples prepared by leaving a drop of the suspension to dry under room conditions on a block of highly oriented pyrolytic graphite.

Structure of the nano-quartz particles

AFM of non-calcite residues deposited on graphite showed that the nano-quartz consists predominantly of rather uniform, *c.* 600 Å large spherical particles (Fig. 2A). AFM images of intact flint surfaces showed that the flint consists of similar spherical particles with a diameter of *c.* 500 Å or more (Fig. 2B) and some irregularly shaped particles. X-ray diffraction showed that the non-calcite residues and the flint and quartz layers are composed of α-quartz having practically identical patterns and resembling the pattern of standard quartz (Fig. 3). It is remarkable that the quartz in all the examined samples of dispersed quartz and flint have almost identical unit cell *a* and *c* parameters and sizes of coherent scattering domains (Lindgreen *et al.* 2011).

At high angles peak broadening was pronounced for the nano-quartz particles and careful recording revealed a broad and distorted pattern of the (212), (203) and (301) reflections compared to the reflection from standard quartz (Fig. 4). These distortions are due to larger *a* and *c* parameters compared to those of normal quartz (Lindgreen *et al.* 2011). The nano-quartz spheres had colloidal properties and flocculated in suspensions with sufficient ionic strength, such as sea water (Fig. 5).

Formation of quartz particles

The nano-quartz spheres are anticipated to be of a type that might crystallise in a marine environment which is slightly enriched in silicon (Williams & Crerar 1985). The source of silicon was probably opal-A from radiolarians, which were the main silica-bearing organism in the chalk sea (Maliva & Dickson 1992). It is important that the non-crystalline Si in radiolarians will dissolve at the low concentration of Si, which is sufficient to precipitate fine quartz, and that the quartz will be the first silica phase to crystallise.

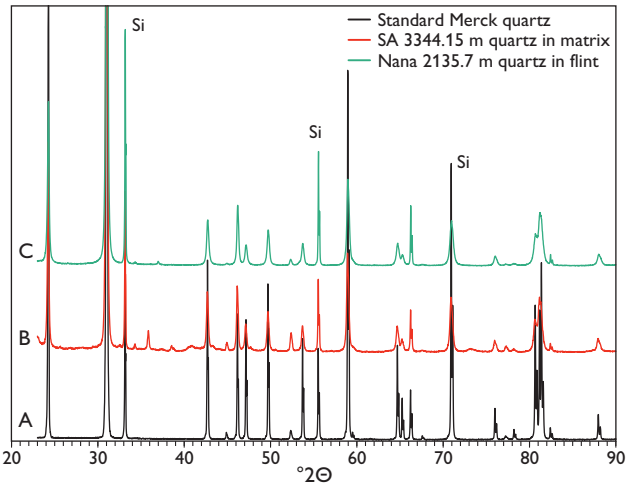

Fig. 3. **A:** X-ray diffraction pattern of standard Merck quartz. **B:** of calcite-free residue from chalk, South Arne Field, well SA-1, 3344.15 m, **C:** and of flint layer in Halfdan Field, well Nana-1, 2135.7 m. Co-K_α radiation, 5% Si added as internal standard.

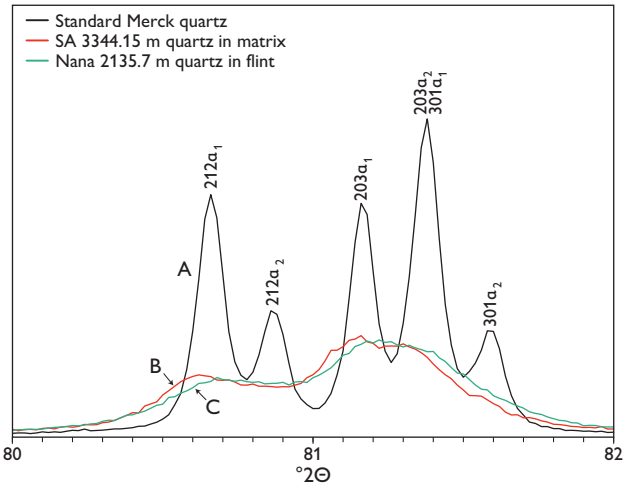

Fig. 4. X-ray diffraction patterns. A: Region of (212), (203) and (301) reflections of standard Merck quartz. B: The same region for calcite-free residue from chalk, South Arne Field, well SA-1, 3344.15 m. C: The same region for flint layer in Halfdan Field, well Nana-1, 2135.7 m. Co-K_α radiation.

Fig. 5. Flocculation of nano-quartz particles. Residue from well SA-1, 3353.0 m. Left: quartz dispersed in distilled water. Right: quartz dispersed in 0.2 M $CaCl_2$.

Data from Williams *et al.* (1985) indicate that the *c.* 500 Å diameter quartz spheres observed in the chalk and in the flint of the North Sea Danian chalk can form at SiO_2 concentrations of *c.* 12 ppm. The North Sea chalk is a deep water deposit and present-day deep sea water has a concentration of 1–10 ppm SiO_2 (Millot 1970; Calvert 1974). We think that only a minor increase in Si concentration would result in crystallisation of nano-quartz spheres. The colloidal quartz spheres could then have flocculated and been deposited on the sea floor mixed with coccolith ooze. Flocculation is important for sedimentation of silica and the rate of sedimentation for the formation of layers rich in quartz.

Chemical environment in the water column

As described above, we assume that silica was not deposited as biogenic opal-A. Therefore the variation in proportion of nano-quartz cannot be caused by changes in the supply of silicon to the sea as such changes would be reflected in changes in size and mineralogy of the silica. An alternative is variation in the sedimentation of coccoliths. Such variation may be due to a decrease in pH which may cause coccoliths to be partly or totally dissolved in the water column.

Such a decrease in pH requires significant amounts of an acidifier. This acidifying agent was most probably atmospheric CO_2, which by mixing with sea water has been found to decrease the calcification of marine plankton (Riebesell *et al.* 2000; Feely *et al.* 2004). CO_2 released in large quantities during volcanic eruptions (Holmes 1965; Zimmer & Erzinger 2003; Frondini *et al.* 2004; Schuiling 2004; Self *et al.* 2006) could be a cause of the dissolution of the coccoliths in parts of the Danian chalk deposits in the North Sea.

Sensitivity analysis has indicated that only massive and short-lived volcanism could cause the $CaCO_3$ undersaturation of seawater (Berner & Beerling 2007). Age determinations of lavas from the British Tertiary igneous province have yielded ages of 63–65 Ma (Saunders *et al.* 1997), corresponding to a Danian age. We therefore propose that the pronounced quartz enrichment in the Danian chalk of the North Sea was associated with frequent volcanic eruptions in this period at and after the Cretaceous–Tertiary boundary. Our model implicates that the degree of dissolution of the coccoliths in the sedimentary environment determines the proportion between calcite and nano-quartz in the chalk.

Theories for flint formation

The new theory for the formation of flint and dispersed nano-quartz in the North Sea by crystallisation of nano-quartz in the marine environment is totally different from the generally accepted theory for flint formation in chalk based on studies of chalk from onshore outcrops (Bromley & Ekdale 1986; Clayton 1986; Zijlstra 1987; Madsen & Stemmerik 2010). According to the current theory for flint formation, opaline tests and sponge spicules in the sediment are dissolved during burial and the Si is recrystallised as opal-CT and quartz in hollows and by replacement of calcite. However, the generally accepted theory does not agree with our results obtained for the silica in the investigated North Sea chalk. We support our point of view by observing that the type of α-quartz dispersed in chalk is identical with the type constituting the flint nodules and flint horizons and with the type constituting the α-quartz horizons in the chalk. We find it highly unlikely that the same size and shape of particles will crystallise in the chalk and in the hollows during dissolution or reprecipitation, whereas the particles are of the type which can possibly crystallise in the marine environment that is slightly enriched in silicon (Williams & Crerar 1985). A sedimentary origin of the silica-rich chalk layers is supported by the presence of a flint bed in well N-22. The flint layer includes a calcite-filled burrow within

a matrix comprising nano-quartz spheres. The occurrence of a burrow in rather pure α-quartz sediment shows that the α-quartz was soft when biological activity took place.

A sedimentary origin of the flint fits well with our results for the North Sea Tertiary chalk, which is a deposit in relatively deep water. However, it cannot be generally applied to other areas and deposits in different settings without further investigations.

Conclusions

We have proposed a new model for the formation of flint in North Sea chalk: (1) The nano-quartz in the flint, like the nano-quartz in the chalk matrix, has crystallised in the marine chalk-sea environment. The colloidal quartz particles have then flocculated and have been deposited on the sea floor mixed with coccolith ooze. (2) Regional variations in the concentration of nano-quartz particles in the sediment reflect different degrees of acidification of the chalk sea. (3) This resulted in areas with a high concentration of nano-quartz spheres that could form flint layers. In areas with lower concentration of nano-quartz spheres, indurated chalk with abundant nano-quartz particles are now preserved. (4) The acidification may have been caused by enhanced atmospheric CO_2 linked to massive volcanic eruptions.

References

Berner R.A. & Beerling D.J. 2007: Volcanic degassing necessary to produce a $CaCO_3$ undersaturated ocean at the Triassic–Jurassic boundary. Palaeogeography, Palaeoclimatology, Palaeoecology **244**, 368–373.

Binnig, G., Quate, C.F. & Gerber, Ch. 1986: Atomic force microscope. Physics Revue Letters **56**, 930–933.

Bromley R.G. & Ekdale, A.A. 1986: Flint and fabric in the European chalk. In: Sieveking, G.D.G. & Hart, M.B. (eds): The scientific study of flint and chert, 71–82. Cambridge: Cambridge University Press.

Calvert S.E. 1974: Deposition and diagenesis of silica in marine sediments. International Association of Sedimentologists, Special Publication **1,** 273–300.

Clayton C.J. 1986: The chemical environment of flint formation in Upper Cretaceous chalk. In: Sieveking, G.D.G. & Hart, M.B. (eds): The scientific study of flint and chert, 43–54. Cambridge: Cambridge University Press.

Feely, R.A., Sabine C.L., Lee, K., Berelson, W., Kleypas, J., Fabry, V.J. & Millero, F. J. 2004: Impact of anthropogenic CO_2 on the $CaCO_3$ system in the oceans. Science **305**, 362–366.

Frondini, F., Chiodini, G., Caliro, S., Cardellini, C., Granieri, D. & Ventura, G. 2004: Diffuse CO_2 degassing at Vesuvio, Italy. Bulletin of Volcanology **66,** 642–651.

Hjuler, M.L. & Fabricius, I.L. 2009: Engineering properties of chalk related to diagenetic variations of Upper Cretaceous onshore and offshore chalk in the North Sea area. Journal of Petroleum Science and Engineering **68**, 151-170.

Holmes, A. 1965: Principles of physical geology, 1288 pp. London: Nelson.

Jakobsen, F., Lindgreen, H. & Springer, N. 2000: Precipitation and flocculation of spherical nano silica in North Sea chalk. Clay Minerals **35**, 175–184.

Lindgreen, H., Jakobsen, F. & Springer, N. 2010: Nano-size quartz accumulation in reservoir chalk, Ekofisk Formation, South Arne Field, North Sea. Clay Minerals **45**, 171–182.

Lindgreen, H., Drits, V.A., Salyn, A.L., Jakobsen, F. & Springer, N. 2011: Formation of flint horizons in North Sea chalk through marine sedimentation of nano-quartz. Clay Minerals **46**, 525-537.

Madsen, H.B. & Stemmerik, L. 2010: Diagenesis of flint and porcellanite in the Maastrichtian chalk at Stevns Klint, Denmark. Journal of Sedimentary Research **80**, 578–588.

Maliva, R.G. & Dickson, J.A.D. 1992: Microfacies and diagenetic controls of porosity in Cretaceous/Tertiary chalks, Eldfisk Field, Norwegian North Sea. AAPG Bulletin **76**, 1825–1838.

Millot, G. 1970: Geology of clays, 429 pp. New York: Springer.

Riebesell, U., Zondervan, I., Rost, B., Tortell, P.D., Zeebe, R.E. & Morel, F.M.M. 2000: Reduced calcification of marine plankton in response to increase atmospheric CO_2. Nature **407**, 364–367.

Saunders, A.D., Fitton, J.G., Kerr, A.C., Norry, M.J. & Kent, R.W. 1997: The North Atlantic Igneous Province. In: Mahoney, J.J. & Coffin, M.F. (eds): Large igneous provinces. Geophysical Monograph Series **100**, 45–97.

Schuiling, R.D. 2004: Thermal effects of massive CO_2 emissions associated with subduction volcanism. Comptes Rendus Geoscience **336,** 1053–1059.

Self, S., Widdowson, M., Thordarson, T. & Jay, A.E. 2006: Volatile fluxes during flood basalt eruptions and potential effects on the global environment: a Deccan perspective. Earth and Planetary Science Letters **248,** 518–532.

Williams, L.A. & Crerar, D.A. 1985: Silica diagenesis, II. General mechanisms. Journal of Sedimentary Petrology **55**, 312–321.

Williams, L.A., Parks, G.A. & Crerar, D.A. 1985: Silica diagenesis, I. Solubility controls. Journal of Sedimentary Petrology **55**, 301–311.

Zijlstra, H.J.P. 1987: Early diagenetic silica precipitation, in relation to redox boundaries and bacterial metabolism, in Late Cretaceous chalk of the Maastrichtian type locality. Geologie en Mijnbouw **66**, 343–355.

Zimmer, M. & Erzinger, J. 2003: Continuous H_2O, CO_2, ^{222}Rn and temperature measurements on Merapi Volcano, Indonesia. Journal of Volcanology and Geothermal Research **125,** 25–38.

Authors' address

Geological Survey of Denmark and Greenland, Øster Voldgade 10, DK-1350 Copenhagen K, Denmark. E-mail: *hl@geus.dk*

Geology of the Femern Bælt area between Denmark and Germany

Emma Sheldon, Peter Gravesen and Henrik Nøhr-Hansen

Geological and geotechnical investigations in the Femern Bælt area were undertaken from 1995 to 2010 (Rambøll Arup JV 2011) in preparation for the fixed link between Lolland in Denmark and Fehmarn in Germany. As a result, new data have been acquired on the stratigraphy and distribution of the deposits and the major structures and tectonic influence on the layers close to the surface. Previous investigations of Cretaceous–Palaeogene deposits on southern Lolland (Fig. 1) were limited due to lack of outcrops and borehole data. Two deep boreholes and geophysical surveys (1952–1953) revealed: (1) the presence of a salt diapir at Rødbyhavn, (2) upper Maastrichtian chalk 29–143 m below Quaternary deposits and (3) an erosional window in the Palaeogene cover. Boreholes to the east of Rødbyhavn (1992–1994) revealed the sediment distribution on southern Lolland and showed that Cretaceous and Palaeogene deposits are cut by several NW–SE-orientated faults. This paper presents a summary of lithostratigraphic and biostratigraphic investigations and a brief description of the geological development in the area.

Methods

A multidisciplinary biostratigraphic study was undertaken of 170 samples from 46 wells drilled in 2009–2010 in the Femern Bælt region. The wells were drilled to depths of 50–100 m and were fully cored in the pre-Quaternary deposits.

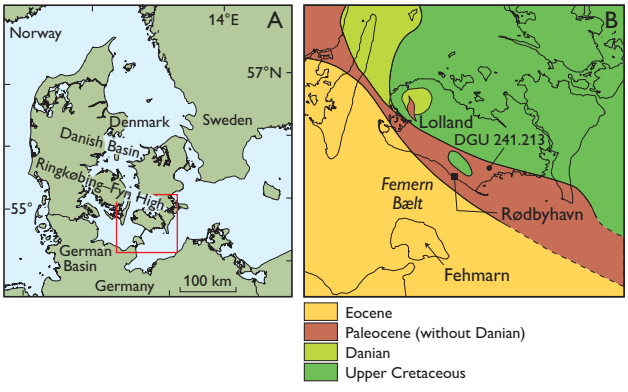

Fig. 1. **A:** Map of Denmark and northern Germany showing the proposed location of the fixed link across the Femern Bælt. **B:** Geological map of the Femern Bælt region (after Håkansson & Pedersen 1992).

One to ten samples from each well were selected for biostratigraphic analysis by Rambøll Arup JV. Nannofossil analysis was carried out on all samples. Supplementary analyses were carried out using microfossils and dinoflagellate cysts (dinocysts) when necessary. Nannofossils are particularly useful for dating chalk and clay, microfossils for chalk, sand and clay and dinocysts for clay. The use of three fossil groups allowed for well-constrained and reliable dating and formation identification (Sheldon & Nøhr-Hansen 2010). In addition, 13 samples from DGU core 241.213, a water well from 2011 on Lolland, were analysed.

Biostratigraphy and lithostratigraphy

A chronostratigraphic, biostratigraphic and lithostratigraphic correlation is presented in Fig. 2. The lithologies and selected marker fossils reported in this article are as follows (see also Fig. 3):

Tor Formation equivalent (Campanian–Maastrichtian) – The Tor Formation of the North Sea was originally described by Deegan & Scull (1977) as homogeneous white or grey chalk, bioturbated pelagic chalk, laminated chalk and redeposited chalk. The Femern Bælt area chalk is slightly indurated, with <5% flint nodules.

Biostratigraphic marker fossils: *Tranolithus orionatus, Reinhardtites levis, Nephrolithus frequens, Arkhangelskiella maastrichtiana, Eiffellithus turriseiffelii, Prediscosphaera spinosa, Cribrosphaerella daniae* (nannofossils), *Bolivinoides laevigatus, Praebulimina levis, Reusella szajnochae szajnochae, Bolivina incrassata, Stensioeina pommerana* (foraminifera), *Cannosphaeropsis utinensis, Montanarocysta aemiliana* and *Xenascus wetzelii* (dinocysts).

Danian limestone (lower–middle Danian) – comprises fossiliferous limestone, rich in echinoderm, bryozoan and bivalve fragments and is recognised as a thin layer on Lolland (DGU core 241.213).

Biostratigraphic marker fossils: *Prinsius tenuiculus, Prinsius dimorphosus, Chiasmolithus danicus, Cruciplacolithus tenuis, Neochiastozygus modestus* (nannofossils), *Eoglobige-*

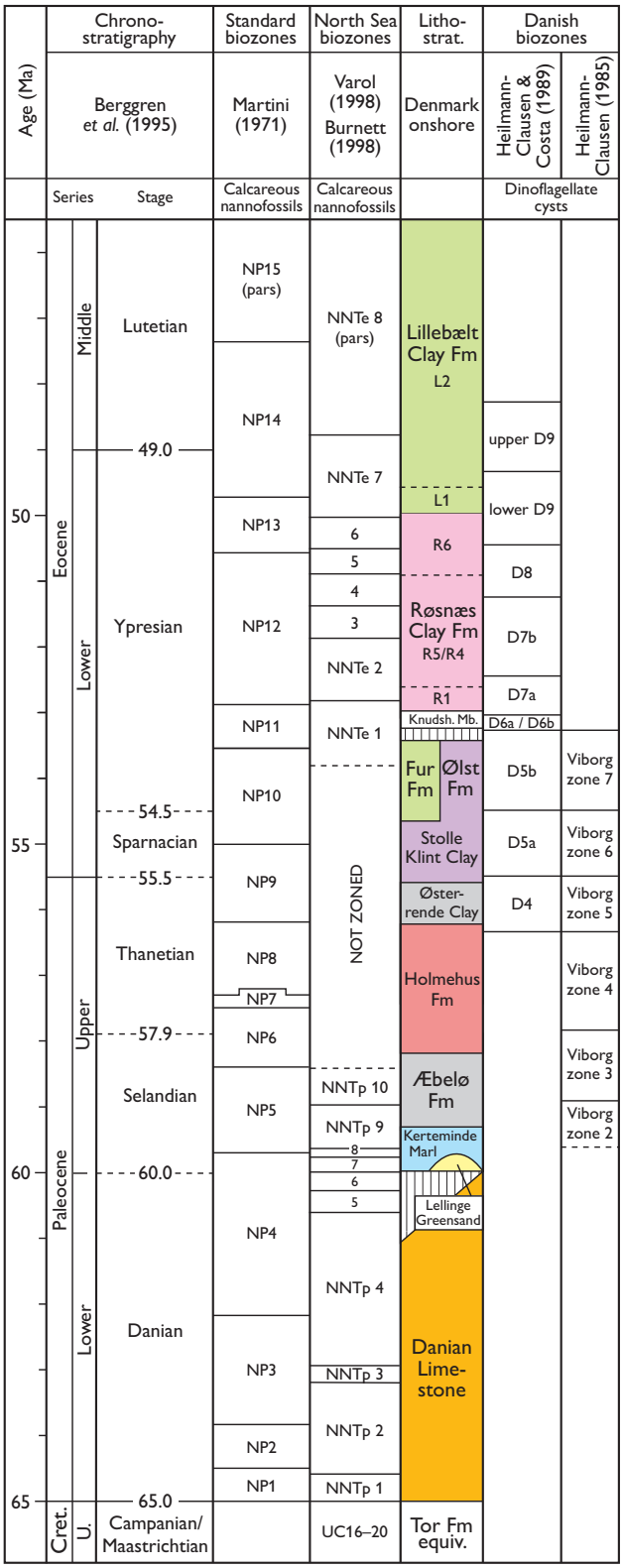

Fig. 2. Chrono-, bio- and lithostratigraphy of the Campanian–Eocene in Denmark. Note, not all formations have been found in the investigated area.

rina edita, Globoconusa daubjergensis and *Cibicidoides succedens* (foraminifera).

Lellinge Greensand (lower Selandian) – In DGU core 241.213, Lellinge Greensand (originally described by Gry 1935) comprises olive-grey, glauconitic, sandy, hard limestone intercalated with fine-grained clay with brown phosphate nodules and pyrite. Lellinge Greensand is also encountered in a number of Femern Bælt boreholes.

Biostratigraphic marker fossils: common *Neochiastozygus perfectus* and *Prinsius martinii* (nannofossils), *Globanomalina ehrenbergi, Bulimina trigonalis* (common) and *Gavelinella danica* (foraminifera) with reworked Danian and Upper Cretaceous nanno- and microfossils (Danian limestone and Tor Formation equivalent) and macrofossil debris.

Ælbelø Formation (middle Selandian) – The Ælbelø Formation (Heilmann-Clausen *et al.* 1985) comprises slightly calcareous to non-calcareous, silty – very silty, grey clay.

Biostratigraphic marker fossils: *Chiasmolithus edentulus, Chiasmolithus eograndis* (nannofossils), *Isabelidinium? viborgense* and *Palaeoperidinium pyrophorum* (dinocysts).

Holmehus Formation (Selandian–Thanetian) – The Holmehus Formation (Heilmann-Clausen *et al.* 1985) consists of non-calcareous, greenish, brownish and reddish, very fine-grained clay with minor sand and phosphatic or sideritic concretions.

Biostratigraphic marker fossils: *Transversopontis pulcheroides, Zygodiscus adamas, Neococcolithes protenus* (nannofossils), *Cyclammina amplectens,* (foraminifera), *Alisocysta* sp. 1 Heilmann-Clausen 1985 and *Cerodinium medcalfii* (dinocysts).

Ølst Formation (lower Ypresian) – The Ølst Formation (Heilmann-Clausen *et al.* 1985) is a grey to almost black, sandy, silty and mainly non-calcareous clay, interbedded with layers and laminae of black or grey volcanic ash.

Biostratigraphic marker fossils: *Sphenolithus editus, Tribrachiatus orthostylus, Lophodolithus nascens* (nannofossils), *Fenestrella antiqua, Coscinodiscus morsianus moelleri, Triceratium* spp. (diatoms), *Apectodinium hyperacanthum* and *Deflandrea oebisfeldensis* (dinocysts).

Røsnæs Clay Formation (middle Ypresian) – The Røsnæs Clay Formation (Dinesen *et al.* 1977; Heilmann-Clausen *et al.* 1985) comprises red, brown and yellow-brown, very fine-grained, plastic marine clay with glauconitic beds at the base and greenish volcanic ash layers throughout.

Biostratigraphic marker fossils: *Discoaster kuepperi, Imperiaster obscurus, Toweius occulatus, Rhabdosphaera pinguis, Discoaster lodoensis* (nannofossils), *Turrilina brevispira, Clavulina anglica*, *Pseudohastigerina wilcoxensis, Gaudryina hiltermanni, Subbotina patagonica* (foraminifera), *Dracodinium? condylos, Ochetodinium romanum, Wetzeliella astra, Dracodinium solidum, Eatonicysta ursulae* and *Dracodinium varielongitudum* (dinocysts).

Lillebælt Clay Formation (upper Ypresian – lower Lutetian) – The Lillebælt Clay Formation is a green-grey, non-calcareous, very fine-grained plastic clay containing concretions, with red-brown clay beds in the lower part (Dinesen *et al.* 1977; Heilmann-Clausen *et al.* 1985).

Biostratigraphic marker fossils: *Vaginulinopsis decoratus* (foraminifera), *Membranilarnacia compressa, Charlesdowniea columna* and *Eatonicysta furensis* (dinocysts).

Geological development

Lolland is located to the south of the Ringkøbing–Fyn High, in the German Basin. During the Late Cretaceaous, fully marine conditions characterised the Danish area including the northern highs and chalk of the Campanian – upper Maastrichtian Tor Formation equivalent was deposited. Danian limestone and Lellinge Greensand have recently been found *in situ* on southern Lolland and are documented here for the first time. The Danian limestone is *c.* 2 m thick. Danian nannofosssils and microfossils are also found in small limestone clasts within the Selandian deposits, indicating that Danian sediments were eroded and partially redeposited at the end of the Danian and probably also in the earliest Selandian.

The lower Selandian glauconitic and conglomeratic deposits of the Lellinge Greensand rest on Danian sediments on Sjælland, especially in the Copenhagen area (Stouge *et al.* 2000). Clasts, microfossils and nannofossils from the lower Selandian also indicate deposits from the Lellinge Greensand in the Femern Bælt area. The Lellinge Greensand is at least 12–13 m thick; the top is eroded and covered by Quaternary deposits. In DGU core 241.213 the Lellinge Greensand is found 138 m below ground surface. The encountered glauconitic deposits from the Lelllinge Greensand rest on Danian limestone in a small subsided fault block, demonstrating that the lowermost Selandian was probably deposited in the area and subsequently eroded.

The early–middle Paleocene sea was more restricted than in the Cretaceous and several highs bordered the marine area (Clausen & Huuse 2002). The Danian was dominated by erosion, rising sea level characterised the early Selandian and erosion dominated again during the late early Selandian. These two erosional episodes may have resulted in sediment removal, but it is also possible that the area was subaerial during part of the Danian–Selandian. Continued erosion or nondeposition characterised the upper Selandian and therefore deposits from the Kerteminde Marl Formation (up to 100 m thick on Sjælland) are not found in the area, probably due to uplift during this time.

Clastic marine sedimentation resumed during the upper Selandian sea-level rise, and the North Sea, Denmark

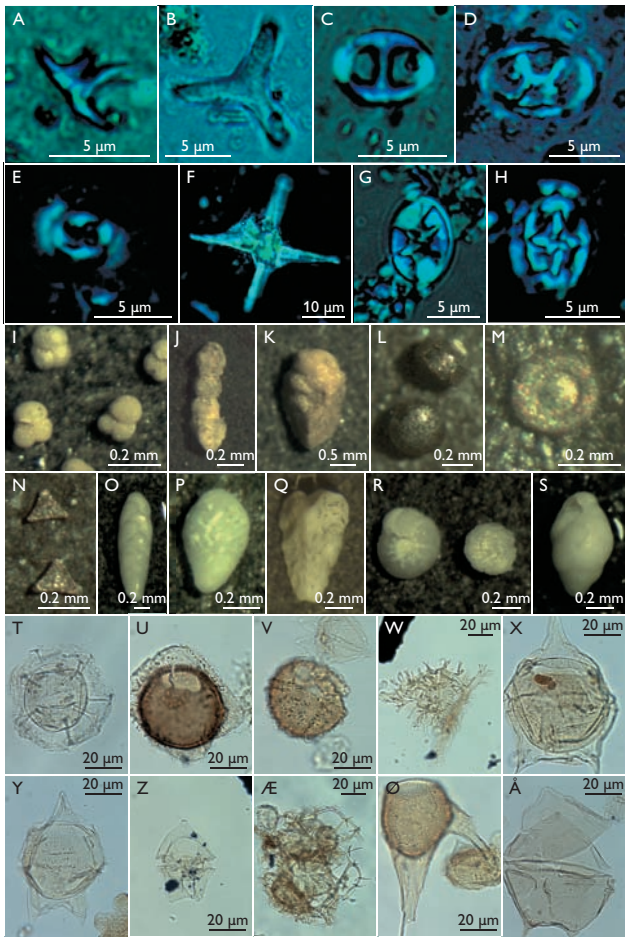

Fig. 3. Selected important nannofossils (A–H), microfossils (I–S) and dinocysts (T–Å). **A:** *Discoaster kuepperi*, **B:** *Tribrachiatus orthostylus*, **C:** *Lophodolithus nascens*, **D:** *Neococcolithes protenus*, **E:** *Toweius occulatus*, **F:** *Imperiaster obscurus*, **G:** *Eiffellithus turriseiffelii*, **H:** *Prediscosphaera spinosa*, **I:** *Subbotina patagonica*, **J:** *Clavulina anglica*, **K:** *Gaudryina hiltermanni*, **L:** *Fenestrella antiqua*, **M:** *Coscinodiscus morsianus moelleri*, **N:** *Triceratium* spp., **O:** *Bolivina incrassata*, **P:** *Bolivinoides laevigatus*, **Q:** *Reusella szajnochae szajnochae*, **R:** *Stensioeina pommerana*, **S:** *Praebulimina levis*, **T:** *Eatonicysta furensis*, **U:** *Dracodinium? condylos*, **V:** *Ochetodinium romanum*, **W:** *Apectodinium hyperacanthum*, **X:** *Deflandrea oebisfeldensis*, **Y:** *Cerodinium medcalfii*, **Z:** *Isabelidinium? viborgense*, **Æ:** *Cannosphaeropsis utinensis*, **Ø:** *Xenascus wetzelii*, **Å:** *Palaeoperidinium pyrophorum*.

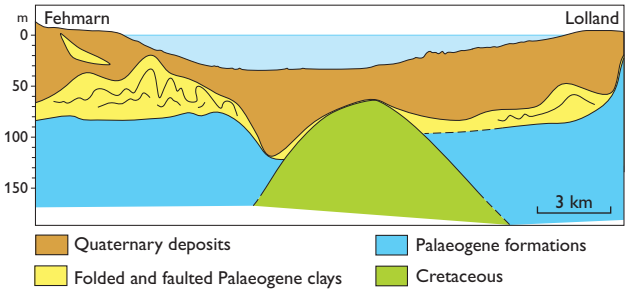

Fig. 4. Simplified geological cross-section across the Femern Bælt. The folding shown in the Palaeogene clay is for illustrative purposes only; the real nature of the disturbance (folding and faulting) is much more intense and complicated than shown (modified after Rambøll Arup JV 2011).

and the German Basin formed a partly enclosed shelf area. The remainder of the Palaeogene (Æbelø, Holmehus, Ølst, Røsnæs Clay and Lillebælt Clay) formations mainly consist of fine-grained, plastic clay but there were many lithological shifts during this time. Deposition occurred in a relatively deep marine basin, although proximal to the shore. The changes in depositional conditions were related to changing circulation patterns in the North Sea and shifts in clay mineral provenance and periods of regression and non-deposition also occurred (Heilmann-Clausen *et al*. 1985). Intense volcanic activity caused by the opening of the North Atlantic resulted in ash deposition during the late Paleocene and Eocene.

Quaternary glacial activity eroded, faulted and folded the Palaeogene sediments resulting in their present distribution (Fig. 4). The new biostratigraphic studies indicate that the Røsnæs Clay Formation is strongly folded with repeated stratigraphy, indicating movements along faults. The youngest formation in the area, the Lillebælt Clay Formation, occurs only as floes in the glacial sediments. On land, the Palaeogene clay seems to be undisturbed towards the north whereas disturbances increase towards the south.

Conclusions

The recent biostratigraphic study has provided important information about the pre-Quaternary deposits under the *c.* 18 km wide Femern Bælt, imperative to planning the construction of the Femern Bælt fixed link. The Cretaceous–Palaeogene Tor Formation equivalent, Danian limestone, Lellinge Greensand, Æbelø, Holmehus, Ølst, Røsnæs and Lillebælt Formations have been identified in multiple boreholes using multidisciplinary biostratigraphy. This information, coupled with physical rock properties (Rambøll Arup JV 2011) allows a geological cross-section of the Femern Bælt to be established and demonstrates the complex nature of the depositional and structural history of the area. In addition, *in situ* Danian limestone has been discovered for the first time, along with Lellinge Greensand on Lolland in DGU core 241.213. The new data from >500 m fully cored boreholes provide an excellent basis for future detailed biostratigraphic, sedimentological and basin analysis of the Palaeogene deposits in the area.

References

Berggren, W.A., Kent, D.V., Swischer III, C.C. & Aubry, M.-P. 1995: A revised Cenozoic geochronology and chronostratigraphy. In: Berggren, W.A. *et al.* (eds): Geochronology, time scale and global stratigraphic correlation. Society for Sedimentary Geology (SEPM) Special Publication **54**, 129–212.

Burnett, J.A. 1998: Upper Cretaceous. In: Bown, P.R. (ed.): Calcareous nannofossil biostratigraphy. British Micropalaeontological Society Series, 132–199.

Clausen, O.R. & Huuse, M. 2002: Mid-Paleocene palaeogeograhpy of the Danish area. Bulletin of the Geologocal Society of Denmark **49**, 171–186.

Deegan, C.E. & Scull, B.J. 1977: A standard lithostratigraphical nomenclature for the central and northern North Sea. The Institute of Geological Sciences Report **77/25**, 36 pp.

Dinesen, A., Michelsen, O. & Lieberkind, K. 1977: A survey of the Paleocene and Eocene deposits of Jylland and Fyn. Danmarks Geologiske Undersøgelse Serie **B1**, 15 pp.

Gry, H. 1935: Petrology of the Paleocene sedimentary rocks of Denmark. Danmarks Geologiske Undersøgelse II. Række **61,** 180 pp.

Heilmann-Clausen, C. 1985: Dinoflagellate stratigraphy of the uppermost Danian to Ypresian in the Viborg 1 borehole, central Jylland, Denmark. Danmarks Geologiske Undersøgelse Serie **A7,** 69 pp.

Heilmann-Clausen, C., Nielsen, O.B. & Gersner, F. 1985: Lithostratigraphy and depositional environments in the Upper Paleocene and Eocene of Denmark. Bulletin of the Geological Society of Denmark **33**, 287–323.

Heilmann-Clausen, C. & Costa, L.I. 1989: Dinoflagellate Zonation of the Uppermost Paleocene? to lower Miocene in the Würsterheide Research Well, northwest Germany. Geologisches Jahrbuch **A111**, 431–521.

Håkansson, E., & Pedersen, S.S. 1992: Kort over den danske undergrund. København: Varv (map sheet).

Martini, E. 1971: Standard Tertiary and Quaternary calcareous nannoplankton zonation. In: Farinacci, A. (ed.): Proceedings of the Second Planktonic Conference Roma. Edizioni Tecnoscienza, Rome **2**, 739–785.

Rambøll Arup JV 2011: Summary of geological conditions. Geotechnical Data Report **01.3-002**, 53 pp. Virum: Femern A/S.

Sheldon, E. & Nøhr-Hansen, H. 2010: Fehmarn Belt fixed link pre-Quaternary biostratigraphy – a final status report for Rambøll Arup Joint Venture. Danmarks og Grønlands Geologiske Undersøgelse Rapport **2010/134,** 53 pp.

Stouge, S., Hjortkjær, B.F., Rasmussen, J.A., Roncaglia, L. & Sheldon, E. 2000: Micro- and nannofossil biostratigraphy across the Danian/Selandian (Paleocene) stage boundary at Gemmas Allé, Copenhagen, Denmark. GFF **122,** 161–162. Stockholm: Geological Society of Sweden.

Varol, O. 1998: Palaeogene. In: Bown, P.R. (ed.): Calcareous Nannofossil Biostratigraphy. British Micropalaeontological Society Series, 200–224.

Authors' address

Geological Survey of Denmark and Greenland, Øster Voldgade 10, DK-1350 Copenhagen K, Denmark. E-mail: *es@geus.dk*

Rock-cored drumlins on Bornholm, Denmark

Peter Roll Jakobsen

The surface morphology of Denmark is predominantly of glacial origin, created in depositional, deformational and erosional environments. In addition, postglacial marine, freshwater and aeolian processes have formed a variety of landforms. Overviews of the Danish landscape were published as geomorphological maps (Milthers 1948; Schou 1949; Smed 1981), and a new one is currently in preparation. On Bornholm, the morphology differs from the rest of the country because bedrock is present at or near the surface. This paper describes drumlins formed on bedrock on Bornholm, which have not previously been recognised.

New geomorphological map of Denmark 1:200 000

The purpose is to create a map based on the Geographical Information Systems (GIS). To draw the boundaries of the different landform types as precisely as possible, the morphology was re-interpreted on the basis of topographical maps, LiDAR (light detection and ranging) data, geological maps as well as available literature. The scale of the new map is 1:200 000, but it is compiled at 1:100 000 and will be published in both a printed and a digital version, the former in four map sheets (Jacobsen in press): (1) northern Jylland, (2) central Jylland, (3) southern Jylland and Fyn and (4) Sjælland, surrounding islands and Bornholm. So far, a preliminary version of southern Jylland has been published (Gravesen *et al.* 2004), and the map sheet covering Sjælland, the surrounding islands and Bornholm is completed.

Most of the surface features have already been described (Milthers 1948; Schou 1949; Smed 1981). However, the morphological elements shown on these maps vary to some degree. The new geomorphological map of Denmark also differs significantly from older maps, and some surface elements are re-interpreted. New elements include mega-scale glacial lineations and Rogen moraines, and on Lolland a valley formerly classified as a tunnel valley is re-interpreted as a fracture valley.

Bornholm

Large parts of Bornholm consist of pre-Quaternary crystalline bedrock with a discontinuous, thin cover of Quaternary sediments and is classified as glacially scoured bedrock on the geomorphological map (Fig. 1). During the Quaternary glaciations, the bedrock was affected by overriding glaciers. It mainly shows erosional features such as fracture valleys and mega-scale glacial lineations, but also smaller features, not shown on the map, such as roches moutonnées and glacial striae (Grönwall & Milthers 1916; Gravesen 1996).

One of the most pronounced terrain features on Bornholm is fracture valleys, which are subglacially eroded faults and fracture zones within the basement rocks. These valleys outline the fault systems from multiple deformation phases in the Sorgenfrei–Tornquist Zone (Grönwall & Milthers 1916; Graversen 2009). The main orientations of the fracture valleys are N–S, NNE–SSW and NE–SW. A few are oriented NW–SE.

On Bornholm, the orientations of glacial striae show two general directions: NE–SW and ESE–WNW (Fig. 2; Grönwall & Milthers 1916). Mega-scale glacial lineations within the glacially scoured bedrock terrain are parallel with the measured glacial striae, and most of them are oriented NE–SW.

In general, the two populations of glacial striae on Bornholm occur in two different groups of pre-Quaternary rocks. In the southern part of Bornholm, the pre-Quaternary geology is dominated by sandstone, shale and unconsolidated or poorly consolidated sediments, which are softer than the granites and gneisses in the rest of the island. The southern part of Bornholm is dominated by a till plain. Mega-lineations in this till plain show a slightly curved ESE–WNW trend and are parallel to the dominant orientation of glacial striae in the area (Figs 1, 2).

Marginal moraines are not as distinct as in other parts of Denmark. They occur as scattered sandy and gravelly hills, and outline three ice marginal stages in the central and northern parts of Bornholm (Fig. 2). A N–S-trending ridge in the south-eastern part of Bornholm, associated with a kame, is also interpreted as a marginal moraine (Fig. 1). It is a low ridge that separates a till plain with mega-lineations to the west from a smooth till plain to the east. A few small outwash plains are found in south-western Bornholm. Raised beaches and beach ridges from the Baltic Ice Lake are found along the coast at different levels, especially towards the east and north (Fig. 1).

 Geological Survey of Denmark and Greenland Bulletin 26, 17–20. Open access: www.geus.dk/publications/bull

Rock-cored drumlins

In the northernmost part of Bornholm, within the glacially scoured bedrock terrain, there are ten elongated hills with typical drumlin shapes (Figs 1, 3). Drumlins are subglacial bedforms that were generated by the activity of overriding ice. Drumlins are oval-shaped hills that formed beneath an ice sheet and aligned in the direction of ice flow, and they are common and widespread in formerly glaciated regions. The formation of drumlins has been widely discussed, and they are one of the most studied glacial landforms on Earth (Clark *et al.* 2009; Johnson *et al.* 2010). On Bornholm, LiDAR data have been invaluable in recognising these features (Fig. 3). Like other drumlins, those on Bornholm are oval, and the surface has smooth contours with gradual fall to all

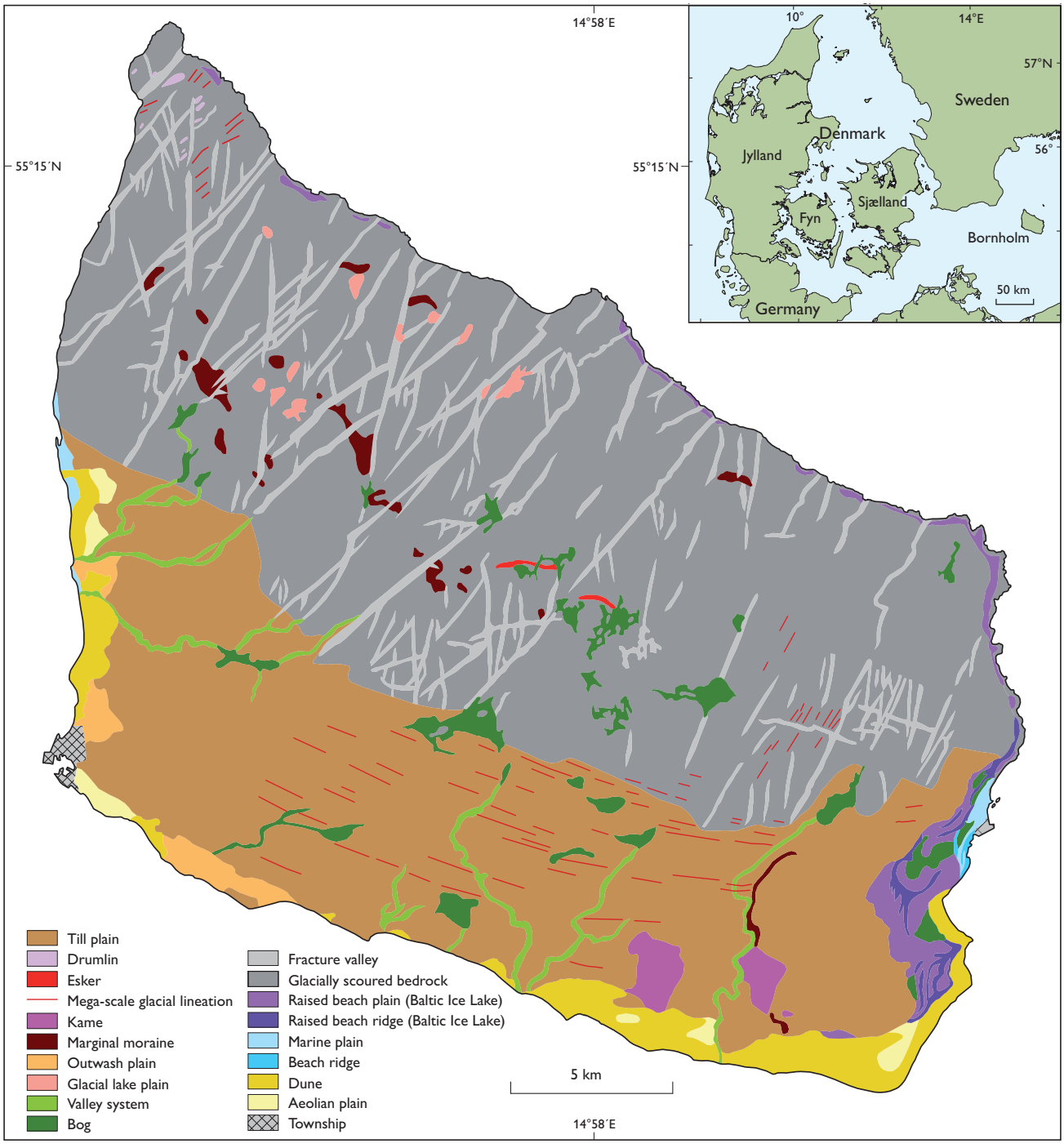

Fig. 1. Geomorphological map of Bornholm.

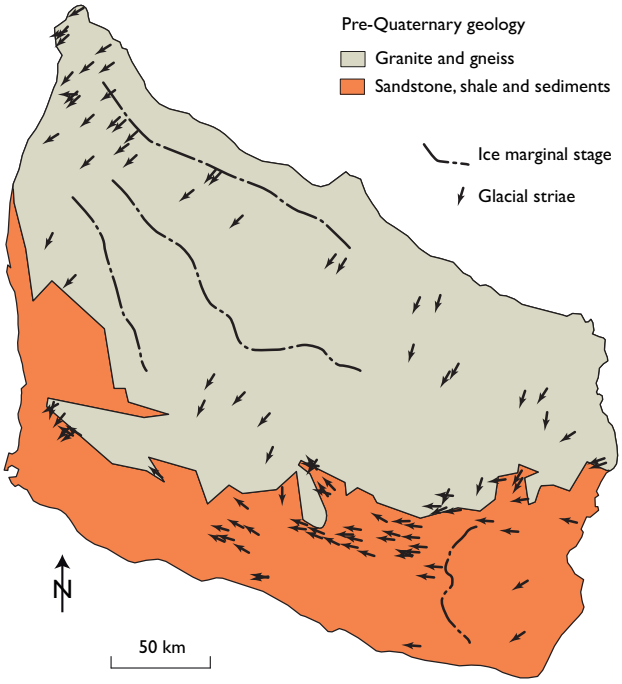

Fig. 2. Map of Bornholm showing orientation of glacial striae on bedrock, the distribution of crystalline and sedimentary bedrock types and ice marginal stages (after Grönwall & Milthers 1916; Hansen & Poulsen 1977).

sides. The length of the drumlins varies from 140 m to a little more than 600 m and their heights from 5 m to 31 m (Table 1). Their length to width ratio varies from 1.6 to 2.9 with an average of 2.3. The orientation of the hills is NE–SW, with an average of 50°.

The drumlins have a core of granite and are more or less covered by till (Fig. 3) that has predominantly been deposited towards the south-west on the lee side of the drumlins. The ice movement direction, indicated by glacial striae, is from the north-east (Grönwall & Milthers 1916), and the till cover is thickest on the south-western lee side of the drumlins.

Table 1. Dimensions of the drumlins on Bornholm

Number/ Name	Length (m)	Width (m)	Height (m)	L:W ratio	Orientation (°)
1 Langebjerg	612	211	31	2.9	60
2 Kælderbakke	140	67	7	2.1	65
3 Høje Meder	177	102	25	1.7	46
4 Kajbjerg	332	160	10	2.1	48
5 Byggehøj	532	205	8	2.6	46
6 Hestenshøj	330	145	10	2.3	56
7 Blåholtshus	395	137	10	2.9	51
8 Brogård	225	98	5	2.3	47
9 Blåholtsgård	391	148	10	2.6	43
10 Hammershus	389	239	25	1.6	39

Discussion

In the northern part of Bornholm, the drumlins and glacial striae indicate an ice-movement direction from the north-east to the south-west and are developed on crystalline bedrock. A few glacial striations have an E–W orientation (Fig. 2). In the southern part of Bornholm, only ice-movement directions from E to W are seen within the softer bedrock. These E–W erosional features were formed during a subsequent ice-stream event, which erased earlier NE–SW features in the southern part, but did not have the capacity to erode the harder crystalline bedrock. It appears that the subglacial conditions during the ice advances from the north-east were suitable for erosion of the granites on the northern part of Bornholm.

As indicated by the fracture valleys, the fault pattern is in N–S, NNE–SSW and NE–SW directions in this part of Bornholm, which is probably also true for the joint pattern. This joint and fault pattern could also favour formation of the elongated hills in this NE–SW direction, and would result in a preferred direction of erosional features by the ice advances from the north-east.

The orientations of the erosional features range from 39° to 65° and could reflect several ice advances, although they cannot clearly be separated into two or more directions. Investigations of drumlins in Sweden (Hättestrand *et al.* 2004) show that rock-cored drumlins are formed by successive phases of erosion. If this also holds for the drumlins of Bornholm, then they may have been formed during several ice advances or even ice ages, and only by glaciers advancing from the north-east.

Conclusions

On the northern part of Bornholm, ten bedrock-cored drumlins are recognised and are included in the new digital, geomorphological map of Denmark at a 1:200 000 scale. The LiDAR data were of great value in recognising them, although they are also recognisable from the contours of the topographic maps. The drumlins have a core of granite and are more or less covered with till that was predominantly deposited towards the south-west on the lee side of the drumlins. The lengths vary from 140 m to 612 m, and the height from 5 m to 31 m.

The orientation of the drumlins is NE–SW, with an average strike of 50° formed by subglacial processes during one or several ice advances from the north-east. The orientation of the fracture valleys could very well intensify the preferred erosional orientation parallel to the drumlins, and thus be an important factor in the drumlin formation.

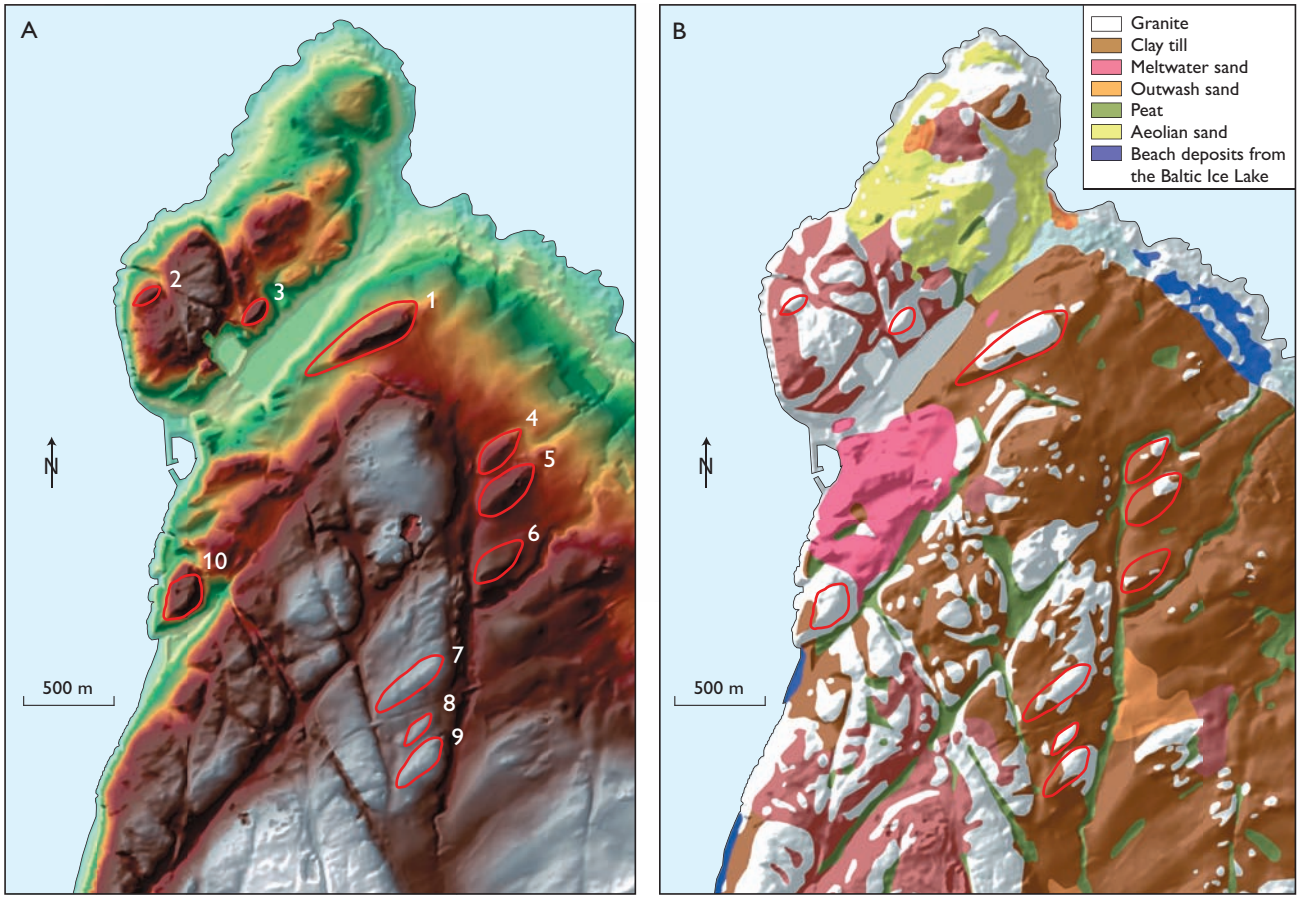

Fig. 3. **A**: LiDAR map of the northernmost part of Bornholm. The elevation varies from sea level to 118 m, and the highest parts are shown in white. The drumlins are indicated with red lines. The numbers refer to Table 1. **B**: Geological map of the same area.

References

Clark, C.D., Hughes, A.L.C., Greenwood, S.L., Spagnolo, M. & Ng, F.S.L. 2009: Size and shape characteristics of drumlins, derived from a large sample, and associated scaling laws. Quaternary Science Reviews **28**, 677–692.

Gravesen, P. 1996: Geologisk set – Bornholm. En beskrivelse af områder af national geologisk interesse, 208 pp. København: Miljøministeriet, Skov- og Naturstyrelsen og Danmarks og Grønlands Geologiske Undersøgelse.

Gravesen P., Jakobsen, P.R., Binderup, M. & Rasmussen, E.S. 2004: Geologisk set – Det sydlige Jylland. En beskrivelse af områder af national geologisk interesse, 188 pp. København: Miljøministeriet, Skov- og Naturstyrelsen og Danmarks og Grønlands Geologiske Undersøgelse.

Graversen, O. 2009: Structural analysis of superimposed fault systems of the Bornholm horst block, Tornquist Zone, Denmark. Bulletin of the Geological Society of Denmark **57**, 25–49.

Grönwall, K.A. & Milthers, V. 1916: Beskrivelse til geologisk Kort over Danmark i Maalestok 1:100 000, Kortbladet Bornholm. Danmarks Geologiske Undersøgelse I. Række **13**, 281 pp. + atlas.

Hansen, M. & Poulsen, V. (eds) 1977: Geologi på Bornholm, 96 pp. Varv ekskursionsfører **1**. København: Tidsskriftet Varv.

Hättestrand, C., Götz, S., Näslund, J.O., Fabel, D. & Stroeven, A.P. 2004: Drumlin formation time: evidence from northern and central Sweden. Geografiska Annaler **86A**, 155–167.

Jakobsen, P.R. in press: Geomorphological map of Denmark, 1:200 000, 4 map sheets. Copenhagen: Geological Survey of Denmark and Greenland.

Johnson, M.D., Schomacker, A., Benediktsson, Í.Ö., Geiger, A.J., Ferguson, A. & Ingólfsson, Ó. 2010: Active drumlin field revealed at the margin of Múlajökull, Iceland: a surge-type glacier. Geology **38**, 943–946.

Milthers, V. 1948: Det danske Istidslandskabs Terrænformer og deres Opstaaen. Danmarks Geologiske Undersøgelse III. Række **28**, 233 pp.

Schou, A. 1949: Atlas of Denmark, **I**, Landscapes, 160 pp. + atlas. Copenhagen: Det Kongelige Danske Geografiske Selskab.

Smed, P. 1981: Landskabskort over Danmark, sheet 4, Sjælland, Lolland, Falster, Bornholm. Brenderup: Geografforlaget.

Author's address

Geological Survey of Denmark and Greenland, Øster Voldgade 10, DK-1350 Copenhagen K, Denmark. E-mail: *prj@geus.dk*

Methane distribution in Holocene marine sediments in the Bornholm Basin, southern Scandinavia

Jørn Bo Jensen and Rudolf Endler

The Baltic Sea is an ideal natural laboratory to study the methane cycle in the framework of diagenetic processes. In this paper we present preliminary geological mapping results from project *Baltic Gas*, a research project with the overall aim to contribute to the development of a scientific basis for long term sustainable use and protection of the Baltic Sea ecosystem. The Baltic Sea is a marginal sea with a strong permanent haline stratification, which leads to oxygen-poor bottom waters, and which is sometimes interrupted by oxygen-rich saltwater flowing in from the North Sea. The history of the Baltic Sea has resulted in deposition of organic-rich Holocene marine sediments that overlie glacial, late-glacial and early Holocene organic-poor sediments.

The aims of *Baltic Gas*, a project within the BONUS-169 Joint Baltic Sea Research Programme running from 2009 to 2011, were (1) to map the occurrence of free shallow gas in Holocene sediments, (2) to quantify methane fluxes through the sediments and into the water column and the atmosphere, and (3) to investigate the processes and parameters governing methane generation and consumption. The contribution by the Geological Survey of Denmark and Greenland, reported here, was to map the thickness and structure of organic-rich marine deposits and the distribution of gas-bearing sediments in co-operation with partners. The authors have also compiled acoustic data which were used to select sites for a comprehensive coring programme. The sediment cores were used for physical characterisation of the gas-bearing sediments and for biogeochemical analyses. These included measurements of the concentrations of methane, sulphide, sulphate, iron and other elements and compounds. Here we present data from the Bornholm Basin, one of several key study areas (Fig. 1).

Methods

On shallow seismic profiles, the acoustic return signal is reduced in areas rich in gas-bearing sediments. The most pronounced reduction is seen when the frequency used during the seismic survey is near the resonance of the gas bubbles. Their size controls the resonance frequency, and multi-frequency data from the project show maximum bubble resonance close to 4.2 kHz, which indicates gas bubbles with a radius of 0.5–2 mm. Many of the acoustic/gas relationships were established by Anderson & Hampton (1980a, b).

Acoustic data acquired during the project comprised swath bathymetry data, multibeam backscatter data, multi-

Fig. 1. Map of the Baltic Sea region showing the location of the project *Baltic Gas* in the Bornholm Basin (red rectangle) and the location of other place names mentioned in the text. **1**: Eckernförder Bucht, **2**: Mecklenburger Bucht, **3**: Arkona Basin.

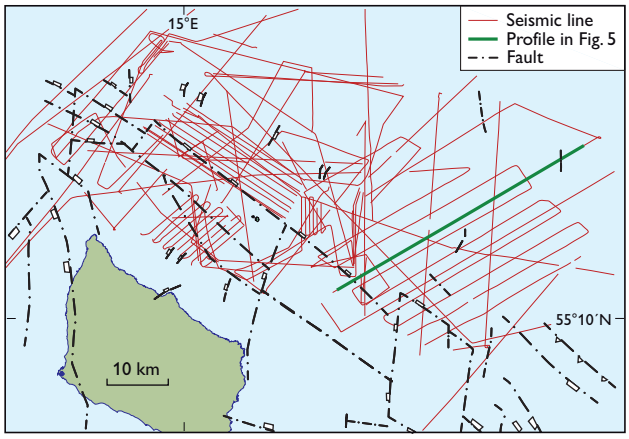

Fig. 2. Map of the Bornholm Basin showing the distribution of shallow seismic lines and deep faults. The location of the seismic profile of Fig. 5 is shown in green.

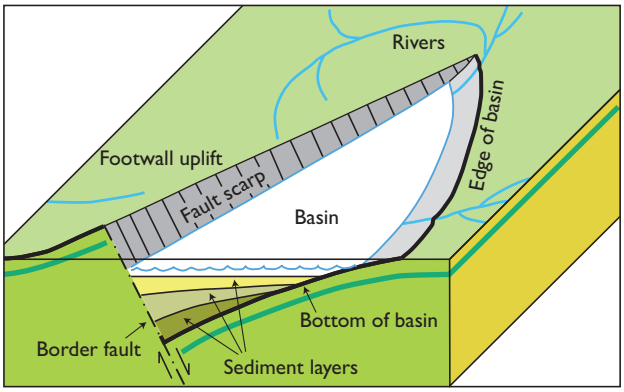

Fig. 3. Model of syn-sedimentary infill in a half-graben.

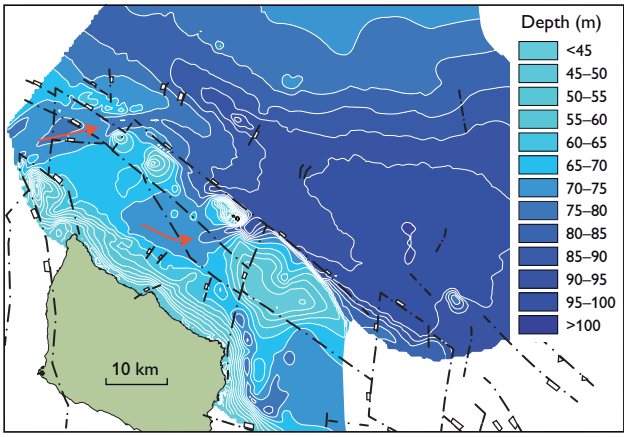

Fig.4. Map of the Bornholm Basin showing the bathymetry and deep faults (black stippled lines). The red arrows show inflow channels.

frequency single beam data (5–100 kHz), echo sounder data as well as high frequency seismic data. Sediment acoustic work using a 5–100 kHz signal was mainly carried out in areas known to be rich in gas at shallow depths in Mecklenburger Bucht, the Arkona Basin and the Bornholm Basin in the western Baltic. Data from Parasound and an Innomar sediment echo sounder were acquired simultaneously for all acoustic lines. Extensive seismic data were acquired from the gas-rich part of the Bornholm Basin (Figs 1, 2). The sediment acoustic records were used to select places for collection of water-column data and bottom sediments during the cruises. The simultaneous recording with different devices allowed comparison of the different responses to the occurrence of gas at shallow depths.

The new seismic field data collected during project *Baltic Gas* was loaded onto a seismic work station and combined with seismic archive data from the same area. The seismic dataset was interpreted and combined with physical characteristics of the sediments plus additional seabed data to compile a map of the gas distribution in the Baltic Sea. Multisensor core logging of 6–12 m long gravity cores were used for estimating the basic physical properties of sediments with and without gas bubbles. Split cores were used for core description, sub-sampling and sedimentological analyses.

Gas distribution mapping in the Bornholm Basin

As stated in the introduction, the main aim of the project was to produce a map of the seabed gas distribution in the

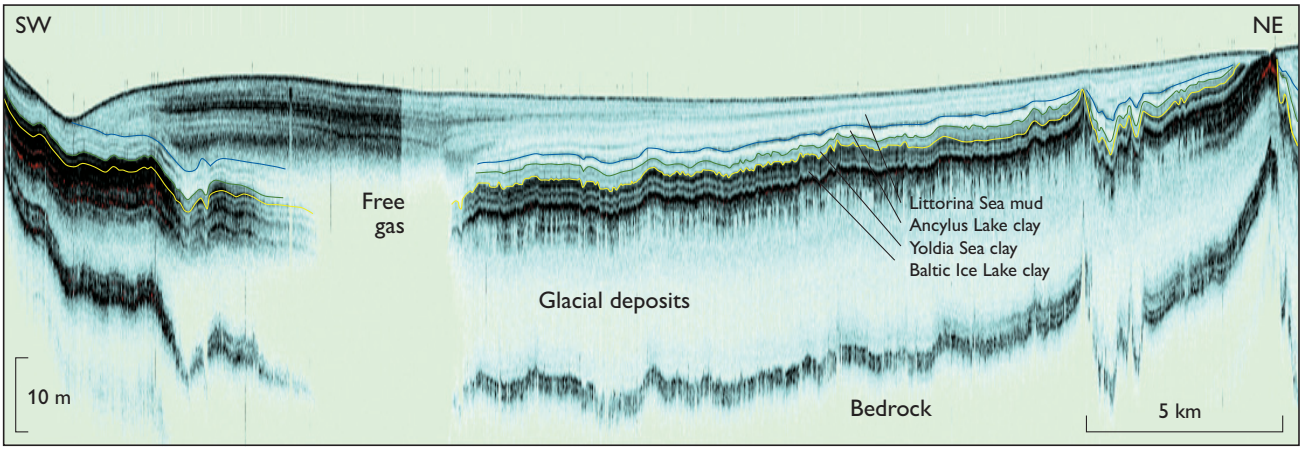

Fig 5. Seismic profile 2005-06222 obtained by an Innomar sediment echo sounder (10 kHz). The profile crosses the Bornholm Basin (for location see Fig. 2). Deposits from the Baltic Ice Lake, the Yoldia Sea and the Ancylus Lake drape the glacial basin surface whereas mud from the Littorina Sea shows asymmetrical infill. Acoustic blanking due to free gas occurs where the thickness of the organic-rich Littorina mud exceeds 6–8 m.

Baltic Sea. Such a map shows only the general pattern, so in order to understand the mechanism of gas production below the seabed it was necessary to make detailed studies in a few key areas. The Bornholm Basin was selected as one of these key areas, because it is well known for gas-rich sediments and because seismic data from previous surveys together with the new data made it possible to get a full coverage of the basin with limited supplementary work during the cruises (Fig. 2).

The Bornholm Basin is located north-east of the island of Bornholm in an area that has been influenced by block faulting. It is possible that faulting continued into the Holocene. The Bornholm Basin is bounded by major faults and has been interpreted as a half-graben (Fig. 3; Vejbæk 1985; Wannäs & Flodén 1994; Sviridov *et al.* 1995) in which thick packages of late glacial and Holocene sediments have been deposited. In spite of the post-half-graben sedimentation history, the present bathymetry clearly reflects the deeper structures (Fig. 4). Two inflow channels are found in the south-eastern part of the basin.

It is a characteristic feature of the basin that late glacial and early Holocene clay deposits drape the glacial surface, whereas the marine Holocene mud sediments form a wedge-like sediment body (Fig. 5). This difference reflects different sedimentation mechanisms, from vertical settling of sediment particles to settling influenced by inflowing currents during the marine Littorina Sea stage.

A map showing the thickness of the Holocene marine mud based on the depth of the seabed and the bottom of the Holocene marine mud is shown in Fig. 6. A clear connection between the thickness of the mud and the down-faulted blocks is seen; the mud reaches a thickness of more than 12 m in the vicinity of the fault scarp of the half-graben, but only a few metres in the deepest, central part of the Bornholm Basin.

Acoustic blanking is seen in many seismic profiles. This is caused by scattering due to gas bubbles in the sediment. A gas distribution map has been compiled showing the depth from the seabed to the top of the acoustic gas front (Fig. 7). Experience tells us that a critical thickness of organic-rich Holocene marine mud must be reached before free gas bubbles form. In the Bornholm Basin where water depths in the order of 90 m are found, acoustic blanking starts where the Holocene organic-rich mud reaches a thickness of 6–8 m. The depth from the seabed to the top of the acoustic gas front is an important parameter in modelling methane fluxes. Our study shows that in the Bornholm Basin the gas front is located less than 0.5 m below the seabed, in areas with the highest sedimentation rates of organic-rich mud.

Acoustic properties and physical characteristics of gas-charged sediments

The data acquired from multi-sensor core logging and sedimentological analyses were used for geo-acoustic models and interpretation of the seismo-acoustic records. The physical properties and the geo-acoustical data were used to investigate the influence of gas bubbles on the acoustic properties and the strength of the muddy sediments.

The acoustic properties such as sound velocity and attenuation are strongly influenced by gas bubbles in the sediments, as illustrated in the sediment echo sounder and seismic records (Fig. 5). The behaviour of acoustic signals is very complex and controlled by environmental parameters including pressure and temperature, the sound frequency and the physical properties of the different sedimentary components (solid grains, water and gas bubbles). The physical properties determined on sediment cores or samples from sediment

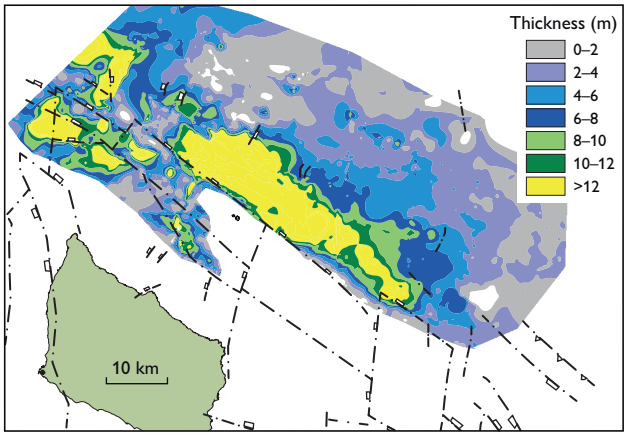

Fig. 6. Map of the Bormholm Basin showing the thickness of Holocene marine mud. Deeper structures are represented by the faults (black stippled lines).

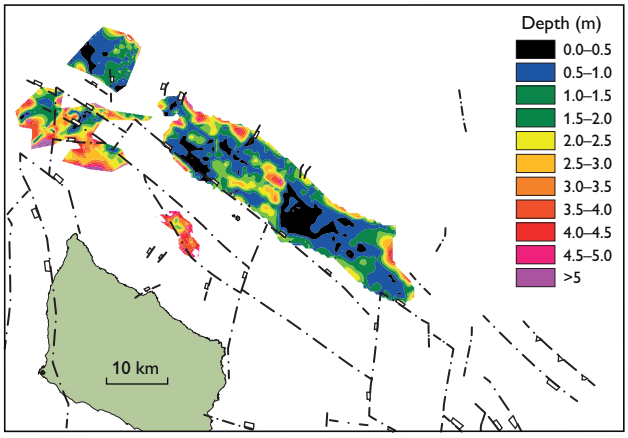

Fig. 7. Mapped areas with acoustic blanks caused by scattering due to gas bubbles in the sediment. The depth from the seabed to the top of the acoustic gas front is shown.

samples (wet bulk density, porosity, gravimetric bulk water content, loss on ignition and vane shear strength) showed no significant differences between gas-charged and gas-free mud. The reason may be that gas bubbles only constitute a small part of the sediment and hence do not change the bulk properties significantly. Similar results were reported by Wilkens & Richardson (1998) for Eckernförder Bucht where the gas volume ranged from 0 to 2%, with bubble diameters of 0.6–1 mm.

Concluding remarks

Mapping of the methane distribution in the Baltic Sea surface sediments and sediment analyses have led to a number of conclusions:

1. Acoustic blanking in seismic profiles is caused by scattering due to gas bubbles in the sediment. The bubble size controls the resonance frequency, and the results indicate a maximum bubble resonance close to 4.2 kHz, corresponding to bubble diameters in the order of 1–4 mm.
2. Accumulations of near-surface gas in the Baltic Sea in general are restricted to near-shore archipelagos and geologically controlled sediment traps with high sedimentation rates.
3. A direct link between the occurrence of near-surface gas and a minimum thickness of Holocene marine organic-rich sediments is seen. A characteristic feature for the Bornholm Basin is that acoustic blanks are seen where the organic-rich mud reaches a thickness of more than 6–8 m.
4. The acoustic properties of gas-free and gas-charged sediments are very different, as demonstrated by sound-velocity changes and attenuation in the seismic records. The behaviour of acoustic signals is extremely complex and influenced by environmental parameters such as pressure and temperature.
5. Comparisons of gas-charged and gas-free mud show no significant difference in bulk properties of various basic physical parameters determined in the sediment. This may reflect that gas bubbles only constitute 0–5% of the Holocene muddy sediments.

Acknowledgement

Project *Baltic Gas* was funded by The Baltic Organisations Network (BONUS).

References

Anderson, A.L. & Hampton, L.D. 1980a: Acoustics of gas-bearing sediments I. Background. Journal of the Acoustical Society of America **67**, 1865–1889.

Anderson, A.L. & Hampton, L.D. 1980b: Acoustics of gas-bearing sediments II. Measurements and models. Journal of the Acoustical Society of America **67**, 1890–1903.

Sviridov, N.I., Frandsen, J.V., Larsen, T.H., Friis-Christensen, V., Madsen, K.E. & Lykke-Andersen, H. 1995: The geology of Bornholm Basin. Aarhus Geoscience **5**, 15–35.

Vejbæk, O.V. 1985: Seismic stratigraphy and tectonics of sedimentary basins around Bornholm southern Baltic. Danmarks Geologiske Undersøgelse, Serie A **8**, 30 pp.

Wannäs, K.O. & Flodén, T. 1994: Tectonic framework of the Hanö Bay area, southern Baltic Sea. Technical Report: Svensk Kärnbränslehantering AB, 1994, 50 pp., *http://www.skb.se/upload/publications/pdf/TR94-09webb.pdf*

Wilkens, R.H. & Richardson, M.D. 1998: The influence of gas bubbles on sediment acoustic properties: in situ, laboratory, and theoretical results from Eckernförde Bay, Baltic sea. Continental Shelf Research **18**, 1859–1892.

Authors' addresses

J.B.J., *Geological Survey of Denmark and Greenland, Øster Voldgade 10, DK-1350 Copenhagen K, Denmark*. E-mail: *jbj@geus.dk*

R.E., *The Leibniz Institute for Baltic Sea Research, Seestrasse 15, Warnemünde, D-18119 Rostock, Germany.*

Natura 2000 habitat mapping in Kattegat, Denmark: an example from Læsø Trindel

Zyad K. Al-Hamdani and Laura G. Addington

Natura 2000 is a network of nature protection areas established by the European Union under the Habitats Directive (European Union 1992). The aim is to assure long-term survival of the most valuable and endangered species and habitats in Europe. The network comprises special areas of conservation and protection designated by the member states under, respectively, the Habitats Directive and the Birds Directive. The establishment of the network of protected areas also fulfils a community obligation under the Convention of Biological Diversity of the United Nations.

The member states of the European Union are obliged to ensure full compliance with Natura 2000 legislation and must work out a management plan for each Natura 2000 area. In the marine environment, detailed information on the Natura 2000 areas is necessary to make informed management plans in fulfilment of national and international obligations and regulate human activities. The data may come from geophysical mapping or from biological sampling or from both.

This paper presents some of the results of a habitat mapping project performed in 2011 covering almost all Natura 2000 areas and pre-designated, aggregate extraction areas in the inner Danish waters. Due to time and resource limitations, the Natura 2000 areas in Danish waters were mapped by geophysical methods to produce seabed sediment maps, followed by biological sampling at selected stations. This is a fast and reliable method for producing a broad-scale habitat map of large areas in a limited time.

The areas were mapped and classified according to the Habitats Directive (European Union 1992; European Commission 2007). The mapping was also conducted to conform to the Marine Strategy Framework Directive, which requires the member states to provide an initial assessment of their marine waters by July 2012 (European Union 2008).

The Geological Survey of Denmark and Greenland (GEUS) carried out the geological and geophysical work, and Orbicon A/S undertook the biological investigations in 18 Natura 2000 areas in Kattegat and the southern Baltic Sea (Fig. 1). Læsø Trindel is a Natura 2000 area with a significant biodiversity and a wide range of habitat types of which three are of special interest: (1) boulder reefs, (2) sandbanks and (3) 'bubbling reefs' which are structures formed by leaking gas.

Geological setting

Læsø Trindel is located north-east of Læsø, the largest island in Kattegat. The Læsø Trindel area is located in the NW–SE-trending Fennoscandian Border Zone and has been affected by neotectonic deformation (Hansen 1995). In this area there is a succession of Weichselian clay and silt with scattered stones and boulders, locally overlain by till. After isostatic rebound and erosion of the sediments in the Holocene, a widespread residual layer of boulders or patches of boulders has been left. Hermansen & Jensen (2000) produced a regional (1:500 000 scale) seabed sediment map of the Danish waters, which shows the presence of till deposits in the area on and around Læsø Trindel. However, at that time there were insufficient data for a detailed sediment map of the area.

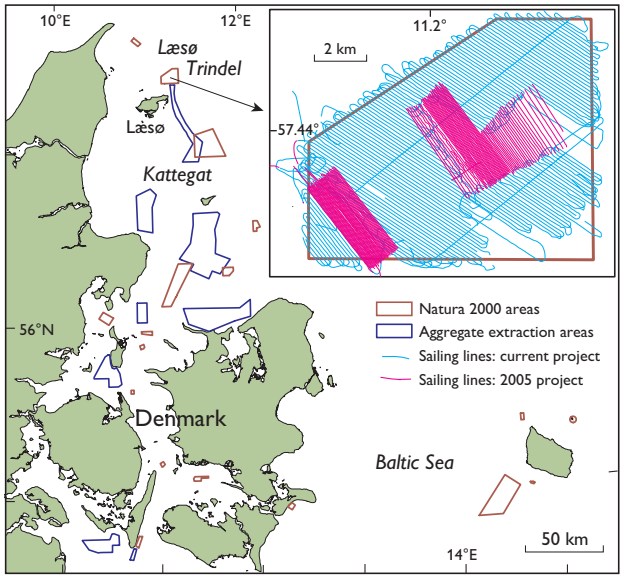

Fig. 1. Map of inner waters in Denmark showing the locations of the Natura 2000 and the aggregate extraction areas mapped in 2011. Inset: 2005 and 2011 sailing lines in the Læsø Trindel area.

 Geological Survey of Denmark and Greenland Bulletin 26, 25–28. Open access: www.geus.dk/publications/bull

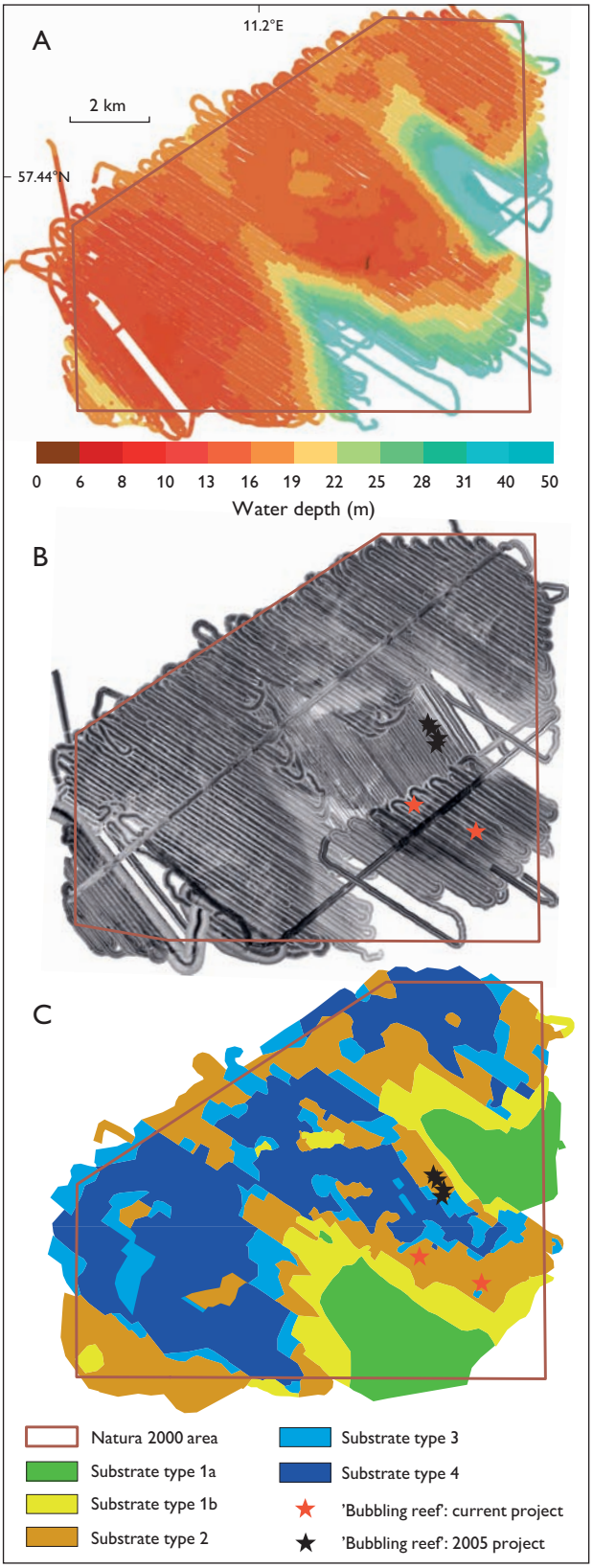

Fig. 2. The Læsø Trindel Natura 2000 area. **A**: Bathymetry. **B**: Side-scan sonar mosaic. The grey scale reflects hard (dark) to soft (light) sediments. **C**: Interpreted distribution of substrate types and Natura 2000 habitats.

A more recent study undertaken by GEUS in 2005 yielded echo sounder, side-scan sonar and ground truth data from the central part of Læsø Trindel (Fig. 1; Leth & Al-Hamdani 2008) showing that it consists of a 2 × 2 km shallow platform with water depths of 4 to 13 m. In the eastern and south-eastern parts of the survey area, the water depth increases to 45 m (Fig. 2A). The platform consists mainly of till with boulders and cobbles that vary in size and distribution throughout the area. Its central part shows the highest density of cobbles and boulders, and this is the main boulder reef of the region. The surrounding part is characterised by gravelly sand and sand patches with scattered boulders.

Methods

Field work in 2011 was carried out in two phases: In phase one, bathymetry data were collected with a single-beam echo sounder, and overlapping seabed backscatter images were obtained using side-scan sonar with 100 and 400 kHz frequencies. Information on the sub-bottom layers was obtained with a chirp profiler (1–10 kHz; providing high resolution but low penetration) and a sparker (1 kHz; providing deeper penetration but lower resolution). The area was surveyed with 100 m line spacing to ensure full seabed coverage. Cross lines with 4 km spacing were surveyed for cross-verification (Fig. 1).

In phase two, which succeeded preliminary interpretation of the acoustic data, areas of special interest were video filmed with a camera mounted on a remotely operated vehicle, and surface sediment samples were collected with a Van Veen grab sampler. Finally, sediment cores were collected with a 6 m long vibrocorer. The acoustic data, the video films and the grab and core samples were used together with older data for the final interpretation and habitat mapping .

Results and discussion

The data from 2005 and 2011 cover almost the entire Læsø Trindel Natura 2000 area (Fig. 1) and were used to map the bathymetry along the sailing lines, to compile a side-scan mosaic and to map the distribution of various substrates and nature types. The depth data from 2011 compare well with the depth data from 2005 which were acquired with a highly accurate multibeam echo sounder (Fig. 2A).

The side-scan backscatter mosaic image shows variation in substrate reflectivity due to the different signatures of the different sediments (Fig. 2B). The interpretation of the image was carried out by dividing the image into 50 × 50 m blocks and manually classifying the sediments in each block.

Interpretation of the side-scan images together with ground truth samples allowed us to produce a map that shows the distribution of substrate types and the occurrence of Natura 2000 habitat types, using the classification categories suggested by the Danish Nature Agency (Table 1; Fig. 2C). The chirp profiles were also used for the interpretation. The different types of sediments give different seismic signals that enhance the final seabed sediment interpretation significantly.

Boulder reefs (substrate type 4) cover *c.* 38% of the Natura 2000 area. Between these, substrate type 2 with sand and scattered boulders dominates. The deeper south-eastern parts of the surveyed area are dominated by soft sediment. Sandbanks are not well defined in the Læsø Trindel area, but

Table 1. Substrate classification

Substrate type	Description
1a	Soft bottom sediment with silt and mud
1b	Sand, including sandbanks
2	Sand, gravel and small stones <10 cm. May also comprise scattered stones >10 cm that cover <10% of the area
3	Sand, gravel and small stones <10 cm. May also comprise scattered stones >10 cm that cover 10–25% of the area
4	Stones >10 cm with >25% coverage; also with sand, gravel and scattered, small stones

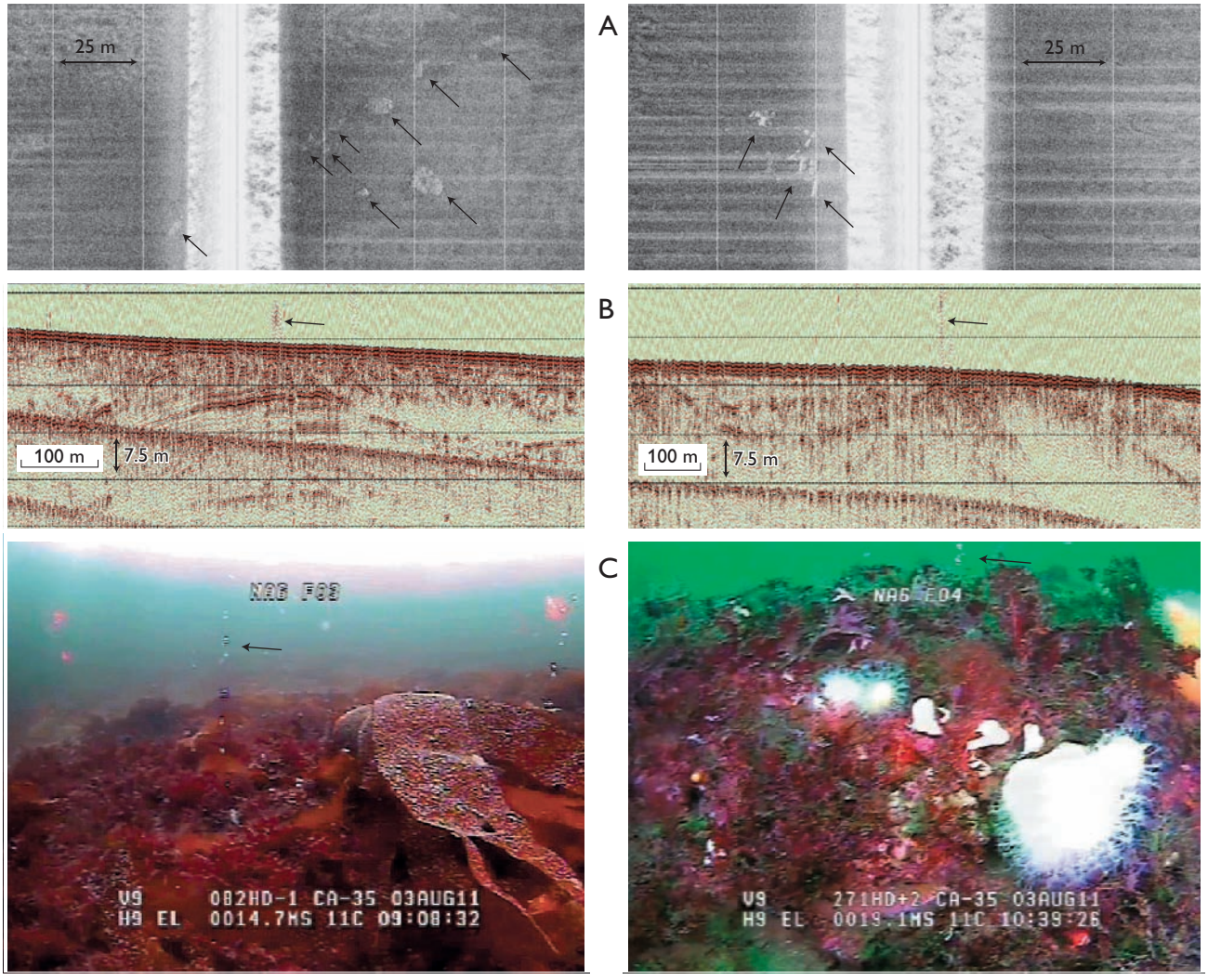

Fig. 3. Examples of 'bubbling reefs'. **A**: On side-scan images 'bubbling reefs' appear as small areas with lowered reflectivity (arrows). **B**: Shallow seismic sparker profiles with sites where the water column is disturbed by gas seeping out from the sediments (arrows). **C**: Snapshots from a video film taken with a camera mounted on a remotely operated vehicle. Gas bubbles are seen in the water column above the 'bubbling reefs' (arrows). The reefs have a rich epiflora and epifauna.

some sand accumulations (substrate type 1b) are found in the eastern and southern parts.

'Bubbling reefs' form at sites where methane gas seeping up from Eemian and early Weichselian marine deposits has led to carbonate cementation of sand in the methane oxidation zone (Jensen *et al.* 1992; Laier *et al.* 1992). In some areas, cemented sand slabs have been exposed by subsequent erosion producing a hard substrate, which can be colonised by plants and animals that form a rich epiflora and epifauna. The geology, geochemistry and biology of the 'bubbling reefs' have been intensively studied, and their structure, origin and formation have been described by Jørgensen (1989), Jensen *et al.* (1992) and Laier & Jensen (2007).

'Bubbling reefs' are fairly common in the Læsø Trindel region where they were discovered by chance by fishermen and sport divers. Some 'bubbling reefs' were recorded on side-scan images during previous surveys (Leth & Al-Hamdani 2008), and additional occurrences of these structures were recorded in the side-scan data from 2011 (Fig. 2C). They are distinctive on the side-scan images (Fig. 3A), but can also be detected on shallow seismic profiles (Fig. 3B) where gas-prone structures can be mapped, and sometimes gas bubbles can be seen in the water column. The 'bubbling reefs' occur mainly in areas with sandy seabed (substrate type 1b). The reefs support benthic communities rich in species (Fig. 3C) and have many cavities where animals can find shelter.

Concluding remarks

1. Habitat mapping using geophysical methods in combination with ground truth observations and sampling is a cost-effective means of mapping large seabed areas in a relatively short time.
2. Some Natura 2000 habitats such as the 'bubbling reefs' were originally discovered by chance by fishermen and sport divers. Side-scan surveying is an effective way to map this habitat type over larger areas.
3. The results obtained during this project provide information on the physical features and the habitat types of Læsø Trindel. These two elements are important to assess the current environmental status of marine waters as required by the Marine Strategy Framework Directive (table 1 in annex III).
4. Management of human activities in the marine environment requires a management plan that ensures habitat protection and at the same time enhances sustainable economic growth of the region. This project provides information on Natura 2000 areas for decision makers in Denmark.

Acknowledgements

The Danish Nature Agency is thanked for financing the project and for permission to publish the results. We also thank Orbicon A/S for ground truth samples and films, and the captain and the crew of R/V *Laura* for help during the cruises.

References

European Commission 2007: Interpretation manual of European Union habitat, 142 pp. Brussels: European Commission, *http://ec.europa.eu/environment/nature/legislation/habitatsdirective/docs/2007_07_im.pdf*

European Union 1992: Council directive 92/43/EEC of 21 May 1992 on the conservation of natural habitats and of wild fauna and flora (Habitat Directive). Official Journal of the European Union **L 206**, 7–92, *http://eur-lex.europa.eu/LexUriServ/LexUriServ.do?uri=OJ:L:1992:206:0007:0050:EN:pdf*

European Union 2008: Directive 2008/56/EC of the European Parliament and of the Council establishing a framework of community action in the field of marine environment policy (Marine Strategy Framework Directive). Official Journal of the European Union **L 164**, 19–40, *http://eur-lex.europa.eu/LexUriServ/LexUriServ.do?uri=OJ:L:2008:164:0019:0040:EN:pdf*

Hansen, J.M. 1995: En ø's opståen, kystdannelse og vegetationsudvikling: Naturlige og menneskeskabte landskaber på Læsø. Geologisk Tidsskrift **2**, 1–74.

Hermansen, B. & Jensen, J.B. 2000: Digitalt kort over havbundssedimenter omkring Danmark 1:500.000. Danmarks og Grønlands Geologiske Undersøgelse Rapport **2000/68** (CD-ROM).

Jensen, P., Aagaard, I., Burke Jr., R.A., Dando, P.R., Jørgensen, N.O., Kuijpers, A., Laier, T., O´Hara, S.C.M. & Schmaljohann, R. 1992: 'Bubbling reefs' in Kattegat: Submarine landscapes of carbonate-cemented rocks support a diverse ecosystem at methane seeps. Marine Ecology Progress Series **83**, 103–112.

Jørgensen, N.O. 1989: Holocene methane-derived, dolomite cemented sandstone pillars from the Kattegat, Denmark. Marine Geology **88**, 71–81.

Laier, T. & Jensen, J.B. 2007: Shallow gas depth-contour of Skagerrak – western Baltic Sea region. Geo-Marine Letters **27**, 127–141.

Laier, T., Jørgensen, N.O., Buchardt, B., Cederberg, T. & Kuijpers, A. 1992: Accumulation and seepages biogenic gas in northern Denmark. Continental Shelf Research **12**, 1173–1186.

Leth, J.O. & Al-Hamdani, Z. 2008: Mapping of the Natura 2000 Annex 1 habitats 1170 and 1180 in N Kattegat, combining acoustic and ground truth methods. In: Dinesen, G.E. (ed.): Mapping and modelling of marine habitats in the Baltic Sea region. BALANCE Interim Report **27**, 75–89.

Authors' address

Geological Survey of Denmark and Greenland, Øster Voldgade 10, DK-1350 Copenhagen K, Denmark. E-mail: *azk@geus.dk*

Early Holocene sea-level changes in Øresund, southern Scandinavia

Ole Bennike, Martin Skov Andreasen, Jørn Bo Jensen, Matthias Moros and Nanna Noe-Nygaard

The Baltic Sea and Kattegat are connected via three straits: Storebælt, Lillebælt and Øresund (Fig. 1). Øresund is the shallowest with a threshold around 7 m deep and increasing water depths to the north (Fig. 2). In the early Holocene, global sea-level rise led to reflooding of Øresund. It started in northern Øresund which was transformed into a fjord. However, so far the timing of the transgression has not been well determined, but sediment cores collected north of the threshold, at water depths of 12 to 20 m, and a new series of radiocarbon ages help to constrain this. As the relative sea level continued to rise, the threshold in Øresund was also flooded, and Øresund became a strait. In mid-Holocene time, the relative sea level rose until it was 4–5 m higher than at present, and low-lying areas around Øresund became small fjords. During the late Holocene, the relative sea level fell again. Part of the data set discussed here was presented by Andreasen (2005).

Active glacier ice disappeared from the region around 17 cal. ka BP (calibrated kilo-years before present; Houmark-Nielsen & Kjær 2003). During deglaciation, the ice margin receded southwards and huge amounts of meltwater flowed northwards and formed deep holes and channels.

Shortly after the deglaciation of the region, marine waters inundated Øresund and remains of Arctic species such as polar cod (*Boreogadus saida*) and ringed seal (*Phoca hispida*) have been found and dated to around 16 and 17.6 cal. ka BP (Lagerlund & Houmark-Nielsen 1993). During this time, the relative sea level must have been high, reflecting the loading of the Fennoscandian Ice Sheet during the Last Glacial Maximum.

Somewhat later Øresund played an important role in draining the Baltic Ice Lake, and a major delta formed north of Øresund. Radiocarbon dating of marine mollusc shells from the delta has given ages between 16.3 and 11.8 cal. ka BP. Following isostatic rebound the relative sea level fell, and major parts of Øresund became dry land with forests, lakes and peat bogs. Submarine lake and peat deposits from the Younger Dryas and the early Holocene have been reported (Jessen 1923). Several now submarine former settlements have been reported from Øresund (Fischer 1993), which can be referred to the Mesolithic based on artefacts and radiocarbon dating.

Methods

Sediment coring was carried out with a 10 cm diameter vibrocorer from R/V *Alexander von Humboldt* and R/V

Fig. 1. Map of Denmark and the surrounding area showing the location of Øresund and other place names mentioned in the text.

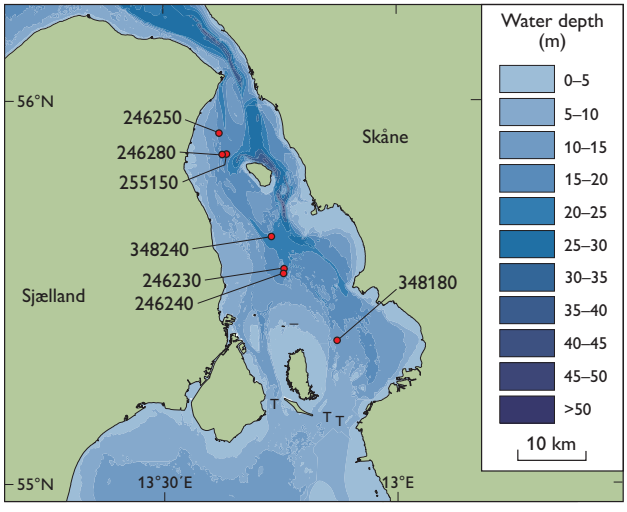

Fig. 2. Map of the Øresund region showing the bathymetry and the location of vibrocores. **T**: Threshold.

Table 1. Selected radiocarbon ages from Øresund

Core/ locality	N. lat. no.	W. long.	Lab. no.	Material	Depth bct* (cm)	Depth b.s.l. (m)	Age (^{14}C years BP)	Calibrated age (years BP)†
246230	55°46.801′	12°44.461′	AAR-8284	*Mytilus edulis*	105–115	21.2	8310 ± 70	8765–8981
246230	55°46.801′	12°44.461′	AAR-8285	*Mytilus edulis*	542	25.5	9155 ± 70	9840–10 101
246230	55°46.801′	12°44.461′	AAR-8286	*Phragmites australis*	560–570	25.7	9445 ± 70	10 569–10 781
246240	55°46.440′	12°44.392′	AAR-8287	*Macoma balthica*	120–130	18.0	9200 ± 70	9907–10 129
246240	55°46.440′	12°44.392′	AAR-8288	*Macoma balthica*	380–390	20.6	9380 ± 80	10 147–10 333
246250	55°57.811′	12°36.327′	AAR-8626	*Littorina littorea*	58–60	16.4	8455 ± 35	9003–9109
246250	55°57.811′	12°36.327′	AAR-8627	*Littorina littorea*	64–70	16.5	8565 ± 40	9113–9301
246250	55°57.811′	12°36.327′	AAR-8603	*Macoma balthica*	270–280	18.7	9475 ± 35	10 253–10 372
246250	55°57.811′	12°36.327′	AAR-8601	Woody plant roots	300–310	18.9	8820 ± 40	9740–10 115
246280	55°56.104′	12°36.696′	AAR-8628	*Cerastoderma edulis*	203–207	18.4	9270 ± 45	10 039–10 189
246280	55°56.104′	12°36.696′	AAR-8630	Wood	215–223	18.6	8940 ± 40	9941–10 193
246280	55°56.104′	12°36.696′	AAR-8604	*Phragmites australis*	220–230	18.6	8975 ± 50	9951–10 228
246280	55°56.104′	12°36.696′	AAR-8631	*Corylus avellana*	352–356	19.9	8740 ± 35	9606–9772‡
255150	55°56.144′	12°37.247′	AAR-8632	*Scirpus* spp.	190–200	20.3	8765 ± 40	9686–9887
348180	55°40.883′	12°51.410′	Poz-42496	*Cladium mariscus*	365–370	15.7	8660 ± 50	9546–9662
348240	55°49.398′	12°42.976′	Poz-42497	*Phragmites australis*	400	26.0	9240 ± 50	10 298–10 498
Pilhaken			AAR-1225	*Corylus avellana*		7.8	8120 ± 90	8980–9259$
Pilhaken			T-10667	*Quercus* sp.		7.8	7945 ± 75	8649–8977$
Svalerumpen			K-6036	Tree root		5.9	7680 ± 115	8386–8586$
Svalerumpen			T-10665	*Pinus sylvestris*		6.5	8225 ± 95	9031–9300$

* Below core top. † Calibration is according to the INTCAL09 data (terrestrial samples) and the Marine09 data (marine samples). ‡ Too young compared with the other dates from the core. $ Fisher (1993).

Professor Penck. Coring positions were selected from high-resolution shallow seismic profiles. The seismic equipment comprised a boomer, an X-star and a sediment echosounder. Differential GPS was used for navigation. The cores were split and described in the laboratory, and selected cores were subsampled for palaeoecological analyses. The samples were wet sieved on 0.4, 0.2 and 0.1 mm sieves, and the residue left on the sieves was analysed with a dissecting microscope. Macrofossils were identified using a reference collection. Remains of terrestrial plants and marine molluscs were used for accelerator mass spectrometry (AMS) radiocarbon age determination (Table 1).

Results

Most of the cores consisted of Holocene marine clayey and silty mud, sometimes with marine sand in the upper part. One core (348180) contained rootlet-peat overlain by sediment with numerous fruits of *Cladium mariscus* and shells of land gastropods. Core 348240 contained sediment with *in situ* rootlets tentatively identified as *Phragmites australis*.

Figure 3 shows an example of a macrofossil diagram. A total of 74 taxa were noted, but only 17 of them are shown in the simplified diagram. The sequence coarsens upwards; this is interpreted as an increased energy level as the sea level rose and the basin was transformed to a fjord. Common remains of tree birch (*Betula* sect. *Albae*) and pine (*Pinus sylvetris*, not shown) as well as rare remains of aspen (*Populus tremula*) indicate that the shore was not far away.

The lower part of the sequence is dominated by lacustrine taxa, such as the leach *Erpobdella* sp. and the bryozoan *Cristatella mucedo*. Shells and head shields of freshwater fleas (Cladocera) are also abundant. Macrolimnophytes are represented by, for example, *Najas minor* and *Zannichellia palustris*. Both can tolerate some brackish water influence, and the sediments contain rare remains of Hydroidea and the ostracode *Cythoromorpha fuscata*, implying a weak influence of brackish water. The presence of *Najas minor* seeds indicates that summer temperatures were slightly higher than at present (Bennike *et al*. 2001). This may be confirmed by the common presence of *Cladium mariscus* fruits in core 348180, but this plant is calciphilous and its abundance in early Holocene deposits may reflect that leaching of the soils was not as far advanced as today.

In the middle part of the sequence a marked peak in *Scirpus* spp. (mainly *Scirpus tabernaemontani*) fruits is seen, and at about the same level *Phragmites australis* seeds also show a maximum. This may imply erosion of reed beds as the sea level rose.

At around 220 cm depth *Hydrobia ulvae* and at around 180 cm depth *Ruppia* sp., *Potamogeton pectinatus* and *Littorina littorea* appear, indicating increased salinity, followed by *Nucula nucleus*, *Corbula gibba* and other marine species that indicate a salinity similar to present values.

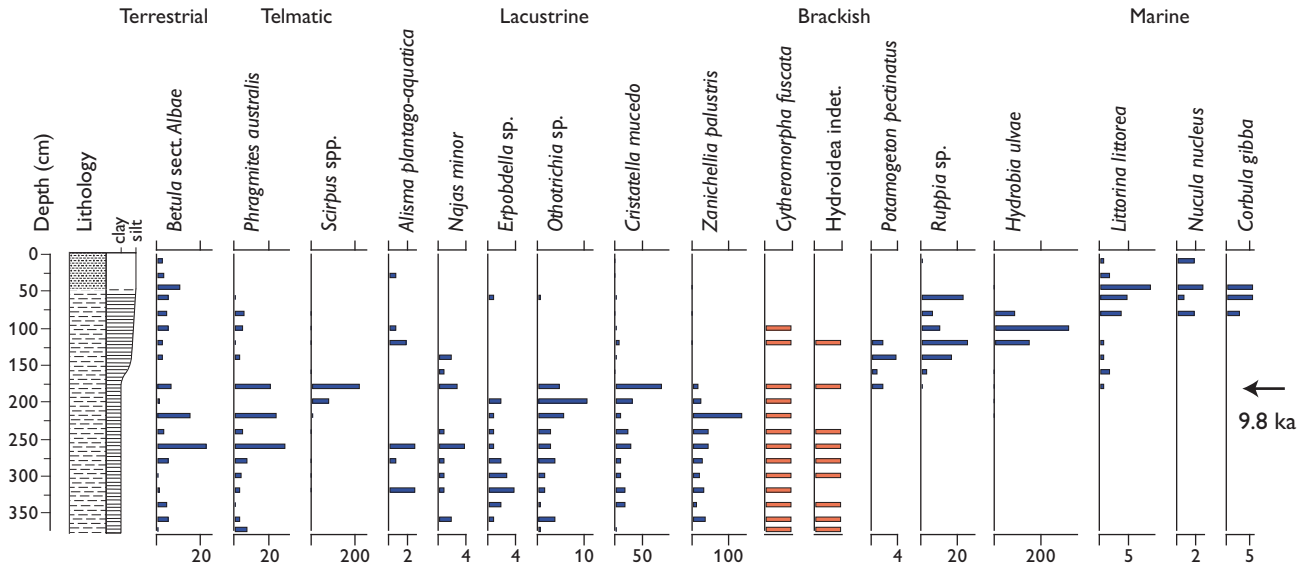

Fig. 3. Strongly simplified macrofossil concentration diagram of core 255150 from Øresund. The core consists of a lower unit of horizontally layered clay and silt and an upper unit of homogenous silty mud. A single sample has been dated to 9686–9887 cal. years BP (Table 1). The red bars show remains that were not counted.

Sea-level changes

Figure 4 shows a plot of the ages of radiocarbon dated samples against depth. We have included a few samples from archaeological sites (Table 1; Fisher 1993). The full black line shows relative sea-level changes during the mid-Holocene according to Christensen (2001), when a number of small transgressions and regressions occurred. A similar picture may have characterised the late Holocene, but due to lack of data we have drawn a straight, stippled line for this time period.

We have also drawn a straight line for the early Holocene. We consider this unlikely, but the data do not allow us to draw a more elaborate line. The marine and terrestrial samples should fall respectively below and above the line. However, it is not possible to draw the line so that this is fulfilled. This means that some of the ages are not correct. Several explanations for this can be offered. One factor to consider is differential isostatic rebound. The samples come from a fairly large region, but most of the isostatic rebound occurred prior to the Holocene, and the marine limit only falls from *c.* 5.5 to *c.* 4 m from north to south (Christensen 2001). Hence we suggest that the depth of the dated samples should be moved by only 1–2 m, which does not change the picture.

We consider two other factors more important. One is the marine reservoir effect, for which a value of 400 years was used, which is common for the region. However, large variations are seen from place to place, and in closed fjords it can be several hundred years greater than the regional value. Variations of several hundred years may also take place over time (Olsen *et al.* 2009). The other factor is that some mollusc species, such as *Macoma balthica* used in this study, can take up old carbon from the sediment, and dating of such species may therefore also produce ages that are several hundred years older than contemporaneous terrestrial samples (Mangerud *et al.* 2006).

Dating of terrestrial samples can also be problematic, and here we have excluded an age determination of a hazel (*Corylus avellana*) nut fragment that appears to be too young. An explanation for this could be contamination by modern carbon in the laboratory. We consider the other ages

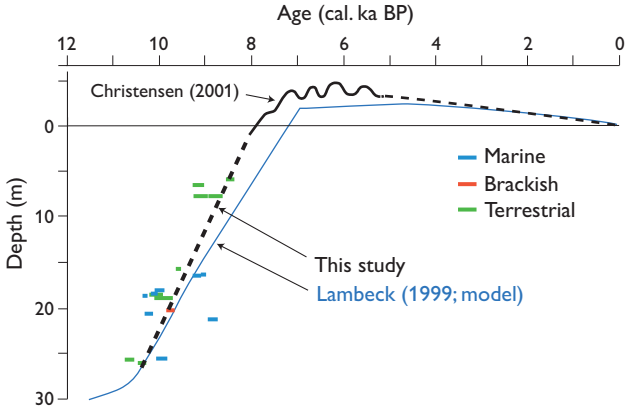

Fig. 4. Tentative curve showing relative sea-level changes in Øresund during the Holocene, based on radiocarbon dated samples. The curve is compared with a curve based on numerical, geophysical modelling by Lambeck (1999). **ka**: kilo-annum (one thousand years).

of terrestrial material to be reliable and have drawn the curve so that the terrestrial samples fall above it. According to the curve, the relative sea level rose *c.* 25 m to the present level from 10 to 8 ka BP. We have compared the curve with a curve constructed by Lambeck (1999), using numerical modelling, which shows a good fit (Fig. 4).

Discussion and conclusions

During the earliest Holocene, large parts of Øresund were dry land, but local lakes and bogs existed in depressions. The shore level of the southern Baltic Sea and Kattegat reached a lowstand (Björck 1995). As the water level in Kattegat began to rise, a fjord with brackish water and limited water exchange formed in northern Øresund.

Later, the ongoing eustatic sea-level rise led to increased salinity, and the fjord became larger. At the same time, the water level in the Baltic Basin also increased (Jensen *et al.* 1999). The threshold in Øresund was flooded between 9 and 8 ka, and Øresund developed into a strait.

The oldest dated marine shell from Øresund gave an age of 10.3–10.4 cal. ka BP, but we suggest that this is somewhat too old, and marine water probably did not reach a level of around 25 m b.s.l. until *c.* 10 ka. However, at the entrance to Øresund where the water depth is 35–40 m, marine waters may have begun to enter several millennia earlier according to Lambeck's model (Fig. 4). In Storebælt, the oldest dated marine shell gave an age of *c.* 8100 cal. years BP (Bennike *et al.* 2004), in the Lillebælt the oldest shell date is *c.* 7700 cal. years BP (Bennike & Jensen 2010) and in Mecklenburger Bucht, the oldest reported shell date is *c.* 7600 cal. years BP (Bennike & Jensen 1998). These differences partly reflect different threshold levels. However, freshwater drainage from the Baltic Basin through Storebælt may also have inhibited marine bivalves from entering this strait for centuries or millennia.

Acknowledgements

The captain and crew of the former R/V *Alexander von Humboldt* and R/V *Professor Penck* of the Institut für Ostseeforschung in Warnemünde are thanked for their help during marine cruises.

References

Andreasen, M.S. 2005: Træk af Øresunds udviklingshistorie gennem tidlig Holocæn, 151 pp. Unpublished cand. scient. thesis, Københavns Universitet, Danmark.

Bennike, O. & Jensen, J.B. 1998: Late- and postglacial shore level changes in the southwestern Baltic Sea. Bulletin of the Geological Society of Denmark **45**, 27–38.

Bennike, O. & Jensen, J.B. 2010: Postglacial, relative shore-level changes in Lillebælt, Denmark. Geological Survey of Denmark and Greenland Bulletin **23**, 37–40.

Bennike, O., Jensen, J.B. & Lemke, W. 2001: Late Quaternary records of *Najas* spp. (Najadaceae) from Denmark and surroundings. Review of Palaeobotany and Palynology **114**, 259–267.

Bennike, O., Jensen, J.B., Lemke, W., Kuijpers, A. & Lomholt, S. 2004: Late- and postglacial history of the Great Belt, Denmark. Boreas **33**, 18–33.

Björck, S. 1995: A review of the history of the Baltic Sea, 13.0–8.0 ka BP. Quaternary International **27**, 19–40.

Christensen, C. 2001: Kystbosættelse og havniveauændringer i stenalderen. In: Jensen, O.L., Sørensen, S.A. & Hansen, K.M. (eds): Danmarks jægerstenalder – status og perspektiver, 183–193. Hørsholm: Hørsholm Egns Museum.

Fischer, A. 1993: Stenalderbopladser på bunden af Øresund. Del 1, det centrale Øresund, 103 pp. Copenhagen: Miljø- og Energiministeriet, Skov- og Naturstyrelsen.

Houmark-Nielsen, M. & Kjær, K.H. 2003: Southwest Scandinavia, 40–15 kyr BP: palaeogeography and environmental change. Journal of Quaternary Science **18**, 769–786.

Jensen, J.B., Bennike, O., Witkowski, A., Lemke, W. & Kuijpers, A. 1999: Early Holocene history of the southwestern Baltic Sea: the Ancylus Lake stage. Boreas **29**, 437–453.

Jessen, K. 1923: En undersøisk Mose i Rungsted Havn og de senglaciale Niveauforandringer i Øresund. Danmarks Geologiske Undersøgelse IV. Række **1**(18), 18 pp.

Lagerlund, E. & Houmark-Nielsen, M. 1993: Timing and pattern of the last deglaciation in the Kattegat region, southwest Scandinavia. Boreas **22**, 337–347.

Lambeck, K. 1999: Shoreline displacements in southern-central Sweden and the evolution of the Baltic Sea since the last maximum glaciation. Journal of the Geological Society (London) **156**, 465–486.

Mangerud, J., Bondevik, S., Gulliksen, S., Hufthammer, A.K. & Høisæter, T. 2006: Marine ^{14}C reservoir ages for the 19th century whales and molluscs from the North Atlantic. Quaternary Science Reviews **25**, 3228–3245.

Olsen, J., Rasmussen, P. & Heinemeier, J. 2009: Holocene temporal and spatial variation in the radiocarbon reservoir age. Boreas **38**, 458–470.

Authors' addresses

O.B. & J.B.J., *Geological Survey of Denmark and Greenland, Øster Voldgade 10, DK-1350 Copenhagen K, Denmark*. E-mail: *obe@geus.dk*

M.S.A. & N.N.N., *Department of Geography and Geology, University of Copenhagen, Øster Voldgade 10, DK-1350 Copenhagen K, Denmark.*

M.M., *The Leibniz Institute for Baltic Sea Research, Seestrasse 15, Warnemünde, D-18119 Rostock , Germany.*

Cliff collapse at Stevns Klint, south-east Denmark

Stig A. Schack Pedersen and Tove Damholt

The scenic coastal cliff of Stevns Klint is a classical study locality that stretches for 15 km along the east coast of Sjælland and it holds arguably the best exposed Cretaceous–Tertiary boundary in the world (Fig. 1; Damholt & Surlyk 2012). The famous boundary separates the soft Cretaceous chalk from the harder overlying Tertiary bryozoan limestone (Fig. 2), and the difference between the two rock types controls the character of the frequent cliff falls. The relatively soft chalk at the base is eroded by storm waves and is subject to general debris shedding. The overlying bryozoan limestone, with its hardgrounds and flint layers, is more resistant to erosion and is strong enough to form overhanging projections of the coastal cliff that result in large and small recurring collapses.

The position of the Cretaceous–Tertiary boundary varies in altitude along the cliff from about 5 m below sea level in the southern part of the cliff to *c.* 35 m above sea level in the northern part. Hence the southern part of the cliff mainly consists of hard bryozoan limestone whereas the central and northern parts consist of soft chalk overlain by bryozoan limestone. Throughout the entire length of the cliff the carbonate rock is overlain by a few metres of glacial till.

Stevns Klint has recently been proposed for inclusion on the World Heritage Site List (Damholt & Surlyk 2012) and as part of the nomination process a risk assessment of the frequency of cliff collapse was conducted. This paper describes the analysis of erosion and rockfall that formed the background of the risk assessment.

Cliff-collapse analysis of Stevns Klint

The evaluation of the cliff-collapse risk at Stevns Klint included an analysis of the size and character of the present overhang, the vulnerability of the cliff to erosion and rockfall dimensions. The analysis was based on a photogrammetric investigation using a series of oblique photographs taken in April 2011. The cliff section was mapped in segments and detailed photogrammetric measurements were made using the software SocketSet in the photogrammetric laboratory at the Geological Survey of Denmark and Greenland. The result was stored in a GIS database using the ArcGis format (Pedersen & Strunck 2011).

Results from a previous photogrammetric investigation using oblique photographs taken in 1992 (Surlyk *et al.* 2006) were compared with our results to describe the changes in the cliff profile over the past 20 years. The general conditions of cliff erosion are described and the rockfall dynamics for the various types of cliff collapse are characterised.

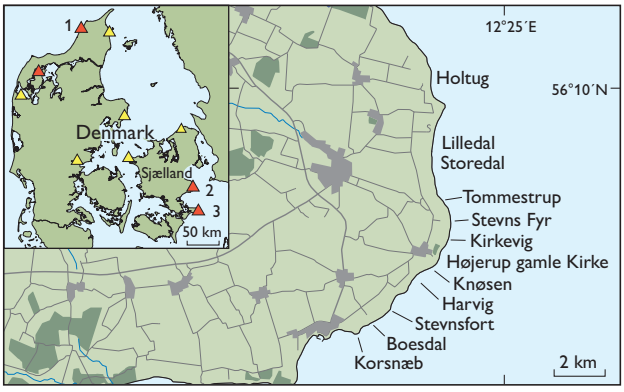

Fig. 1. Map of the Stevns Klint region showing place names mentioned in the text. The inset map shows the distribution of localities with major landslides in Denmark. Red trinangles: the most hazardous slides. Yellow triangles: clayey landslides. **1:** Lønstrup Klint, **2:** Stevns Klint, **3:** Møns Klint.

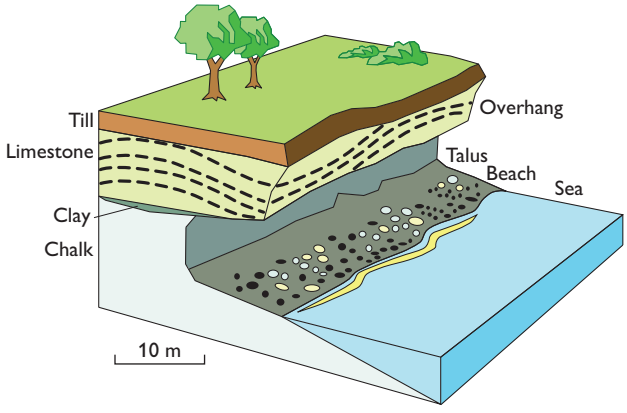

Fig. 2. Block diagram illustrating the morphology and rock types present in the Stevns Klint exposures. The succession consists of Maastrichtian chalkish clay, with the famous Cretaceous–Tertiary boundary at the base, Danian bryozoan limestone and Weichselian glacial till.

 Geological Survey of Denmark and Greenland Bulletin 26, 33–36. Open access: www.geus.dk/publications/bull

General erosion conditions at Stevns Klint

The rate of erosion is an essential factor for the assessment of cliff collapse. We estimated the average rate of coastal erosion at Stevns Klint to be 15 cm/year, based on comparisons of the position of the coastline in 1891 with that in 2010, provided by the National Survey and Cadastre. The highest rate (*c.* 35 cm/year) was found in the northern part of the cliff between Storedal and Lilledal (Fig. 1). In some places, progradation of the coastline occurs where beach ridges form or where old cliff slides act as wave breakers. Beach ridges are especially found at Korsnæb in the south (Fig. 1), where the accumulation rate amounts to 12 cm/year. A landslide north of Kirkevig and south of Storedal (Fig. 1) has resulted in a coastline progradation of 7–9 cm/year.

Limestone quarrying over the past few hundred years has also altered the cliff profile. Numerous small quarries were established directly on the cliff with quarry walls inclined towards the base of the limestone and resulted in considerable overhang. The quarries can contribute to cliff points projecting above the beach.

The erosion rate at Stevns Klint is modest when compared with the highest rate of coastal erosion in Denmark, which is 1.25 m/year at Lønstrup Klint that is formed in Quaternary sediments (Fig. 1; Pedersen 1986).

Types of cliff collapses at Stevns Klint

The largest type of cliff collapse at Stevns Klint can be called cliff slides (Fig. 3). This type of slide includes a major part of the cliff for several tens of metres along the coastline which slide simultaneously. In general a cliff slide takes place along a steeply dipping surface and it involves a volume of 5000 to 10 000 m³. Prior to a cliff-slide a whole section of the chalk has been eroded away at sea level, creating an undercut below the limestone and resulting in a considerable overhang. The size of the overhang has to be around 10–12 m and the thickness of the limestone and till in the overhang around 15–18 m before it becomes unstable.

The most famous event at Stevns Klint occurred in 1928, when a large cliff slide dramatically tore away the choir of

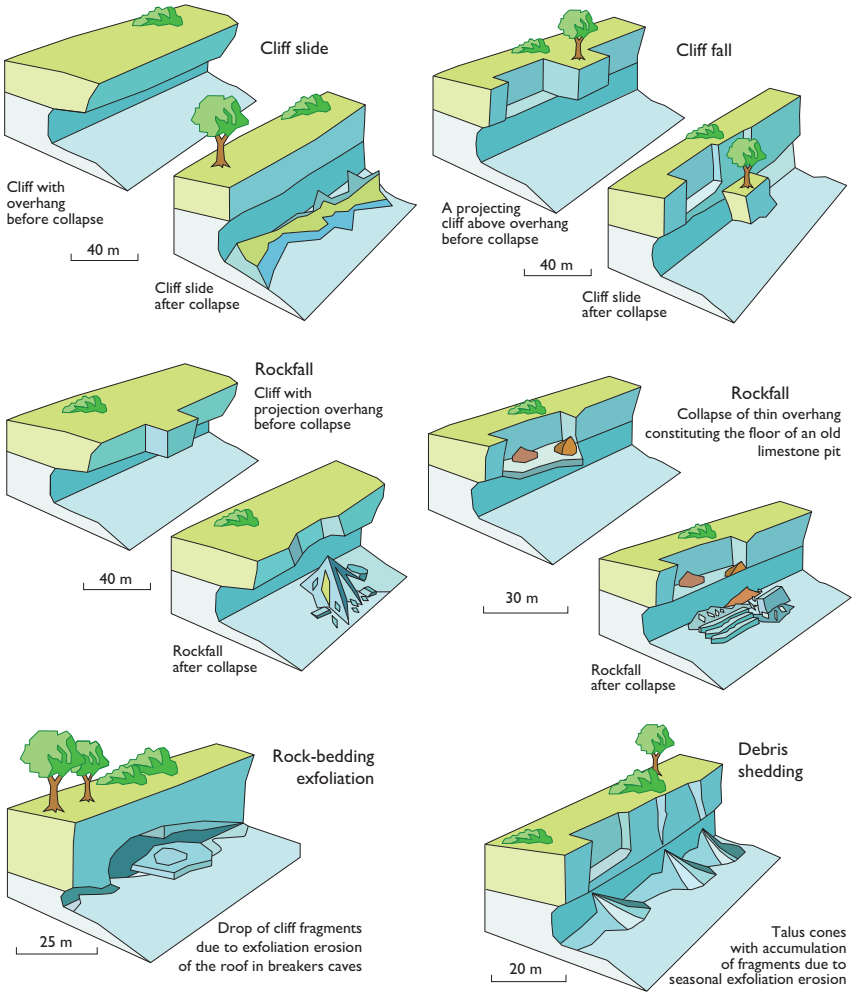

Fig. 3. Cliff-collapse types at Stevns Klint. The most hazardous type is the cliff slide involving volumes of 5000–10 000 m³. The volume of a cliff fall amounts only to 500–1500 m³, but still a cliff fall is an impressive sight with the bedding completely preserved in a displaced cliff fragment. The rockfall is the general type of cliff collapse and is illustrated by two examples, of which the plate-like overhang corresponds to a recent cliff collapse at Knøsen. The rock-bedding exfoliation generates platy 1–10 m³ limestone blocks, which drop from the underside of the overhang. The main erosion of the cliff is caused by debris shedding, which produces the talus at the foot of the cliff.

Fig. 4. Aerial photograph of the cliff section at Højerup gamle Kirke (medieval church).

Højerup gamle Kirke (a medieval church) that rested on a 15 m thick overhang. The slide continued several tens of metres out into the sea (Fig. 4). Shortly after the incident the cliff was protected by wave breakers to inhibit wave erosion and to secure the rest of the old church. Prior to the spectacular slide, the undercutting erosion had lasted for 160 years following an earlier slide in 1767 (Rasmussen 1967). Before the cliff collapse in 1928, the overhang amounted to *c.* 12 m measured perpendicularly to the orientation of the cliff and a similar overhang size is estimated for the collapse in 1767. An overhang of *c.* 12 m is thus regarded as a critical size for cliff slides where the overhang thickness is *c.* 15 m.

A significant cliff slide has occurred at Tommestrup (Figs 1, 5A) and another one in the inner part of Harvig. At both sites cliff-slide deposits will protect the cliff from erosion for the next decades.

In order of decreasing size, the next type of large collapse is the cliff fall (Fig. 3). Cliff falls only involve isolated projecting parts of the cliff with a considerable overhang and their volumes are 500–1500 m^3. The cliff fall is a simple drop of part of the cliff where the bedding of the fallen block is preserved after the fall. The average relation between thickness and depth of the overhanging limestone prior to cliff fall is 3 to 2 as illustrated in the cliff fall below the lighthouse of Stevns Fyr (Figs 1, 5B).

The third type of collapse is classified as rockfalls (Fig. 3), which in this analysis varies in size from 1 to 500 m^3. This type may occur together with block slides, in which bigger blocks are displaced together with finer-grained material such as clayey till and sand. The resulting aggradation of material on the shore after a rockfall is a chaotic breccia. In general, rockfalls leave a concave escarpment in the cliff and the aggradation of debris results in a cone expanding out into the sea.

Platy rockfall, caused by rock-bedding exfoliation, involves rock volumes of around 1 m^3 and is a significant type of collapse at Stevns Klint (Fig. 3). Rock-bedding exfoliation occurs in caves eroded by storm waves in the lower part of the cliff. Layers are peeled off from the roofs of the cave due to exfoliation, and dish-shaped fragments of rock drop to the cave floor. Caves are prominent north of Boesdal (Fig. 1) and

Fig. 5. Cliff sections showing various types of rockfalls at Stevns Klint. **A:** Cliff slide at Tommestrup. **B:** Cliff fall at the lighthouse of Stevns Fyr.

Fig. 6. The cliff collapse at Knøsen, which occurred in November 2011. The weight of fill deposited on top of the section added to the load of the overhang.

north of Stevnsfort where they are formed in limestone and extend up to 9 m into the cliff. Caves formed in chalk occur south of Storedal and at Holtug.

Finally, fragments of rock may fall from the cliff due to general shedding of debris (Fig. 3). In general, the material resulting from debris shedding is pebbles and cobbles, whereas clasts of boulder-size are loosened only occasionally from the cliff surface. The result is seen as an apron of talus along the foot of the cliff, typically with irregular conical shapes. Debris shedding results from contraction and expansion due to seasonal variation of frost and thaw in winter time and desiccation during the summer. The rate of erosion due to debris shedding is equal to the average rate of erosion, i.e. 15 cm/year.

Assessment of cliff collapse hazards at Stevns Klint

The size of the overhang is considered to be the most important factor in the assessment analysis of rockfall hazards at Stevns Klint. However, the likelihood of a collapse also depends on the thickness of the overhang. The shear strength of a rock increases with increasing normal pressure, which increases with the thickness of the rock. Therefore an overhang with a thickness of 20 m is more stable than one with a thickness of 10 m. The degree of exposure to the sea is also important, primarily because the exposed parts of the cliff are affected by wave erosion and secondly because the softness of chalk increases by salt water spray (Mortimore *et al*. 2004). Finally, the assessment of risk is proportional to the number of visitors. A more detailed description of the assessment is provided in a full report (Pedersen & Strunck 2011).

After our analysis, a rockfall of *c*. 300 m³ occurred at Knøsen (Fig. 1). The rockfall was discovered on 6 November 2011. It was caused by the collapse of a 5 m overhang with a thickness of 2 m that constituted the floor of an old limestone quarry (Figs 3, 6). The floor carried the weight of removed overburden, in the form of clayey till and chert-rich limestone rubble. The collapse shows that an overhang with a thickness of just 2 m can become unstable even if the overhang is only 5 m. In other instances an overhang with a thickness of 15 m can be stable even with an undercut of more than 10 m.

Discussion and conclusions

Our cliff-collapse hazard assessment of Stevns Klint is based on an investigation of cliff collapse processes along the cliff. Five types of cliff collapse are recognised: cliff slides, cliff fall, rockfall, platy rockfall caused by rock-bedding exfoliation and debris shedding. The cliff slides have large volumes and occur at low frequencies (1/100 years) whereas debris shedding of low volume occurs at high frequencies (seasonal). The resulting average rate of erosion is 15 cm/year. Rockfalls may be initiated by cycles of frost and thaw, saturation of cracks following rainy periods or desiccation after dry periods, but actual prediction of cliff collapses is not possible at present.

References

Damholt, T. & Surlyk, F. 2012: Nomination of Stevns Klint for inclusion in the World Heritage List, 159 pp. St. Heddinge: Østsjællands Museum.

Mortimore, R.N., Stone, K.J., Lawrence, J. & Duperret, A. 2004: Chalk physical properties and cliff stability. In: Mortimore, R.N. & Duperret (eds): Coastal chalk cliff instability. Geological Society (London), Engineering Geology Special Publications **20**, 75–88.

Pedersen, S.A.S. 1986: Rubjerg klint, Rubjerg klit, årsag og virkning. Varv **3**, 84–98.

Pedersen, S.A.S. & Strunck, M.N. 2011: Vurdering af fjeldskredsrisiko på Stevns Klint. Danmarks og Grønlands Geologiske Undersøgelse Rapport **2011/93**, 100 pp.

Rasmussen, H.W. 1967: Skrivekridtet og kalkstenene. In: Nørvang, A. & Meyer, T.J. (eds): Danmarks Natur 1, Landskabets opståen, 131–160. Copenhagen: Politikens Forlag.

Surlyk, F., Damholt, T. & Bjerager, M. 2006: Stevns Klint: Uppermost Maastrichtian chalk, Cretaceous–Tertiary boundary, and lower Danian bryozoan mound complex. Bulletin of the Geological Society of Denmark **54**, 1–48.

Authors' addresses

S.A.S.P., *Geological Survey of Denmark and Greenland, Øster Voldgade 10, DK-1350 Copenhagen K, Denmark*. E-mail: *sasp@geus.dk*

T.D., *Østsjællands Museum, Højerup Bygade 38, DK-4660 St. Heddinge, Denmark*.

Shallow geothermal energy in Denmark

Thomas Vangkilde-Pedersen, Claus Ditlefsen and Anker Lajer Højberg

The use of shallow geothermal energy instead of fossil fuels can lead to substantial reductions in CO_2 emissions. However, the use of shallow geothermal energy in Denmark is limited compared to, e.g. Sweden and Germany and we still lack know-how and experience with its use in Denmark. In co-operation with research and industry partners, the Geological Survey of Denmark and Greenland is conducting a three-year project *GeoEnergy, Tools for ground-source heating and cooling based on closed-loop boreholes* (*www.geoenergi.org*). The objective of the project is to acquire knowledge and develop tools and best practice for the design and installation of shallow geothermal energy systems.

Exploitation of shallow geothermal energy

In the shallow subsurface, solar energy absorbed and stored in the ground determines the temperature, whereas the temperature gradient is determined by the heat flux from the interior of the Earth. In Denmark the net insolation is *c.* 400 kWh/m²/year and in the upper few hundred metres, the heat flux from the interior is *c.* 0.20 to 0.35 kWh/m²/year (Balling *et al.* 1992). The geothermal gradient in Denmark is 25–30°C per kilometre (Mathiesen *et al.* 2009) with an upper zone of seasonal variations. The thickness of this zone has not been investigated in detail in Denmark, but a general thickness of 10–20 m may be expected (Fig. 1; Banks 2008). The shallow geothermal energy is exploited in combination with heat pumps bringing the temperature to the desired operating temperature of the heating (or cooling) system. A ground-source heat pump, however, requires energy in the form of heat or cold from the ground as well as electricity for the operation of the pump itself.

The energy extraction from the ground can be based on either open-loop systems or closed-loop systems. In open-loop systems, groundwater from a production well is used directly as an energy source for the heat pump and returned to the aquifer via an injection well. The efficiency is high due to a constant and relatively high temperature of the water (typically 8–10°C), but a suitable aquifer with sufficient yield is required and conflicts of interest with neighbouring installations or nearby drinking water catchment may arise. In closed-loop systems, water with antifreeze is circulated in the ground in high-density polyethylene pipes and acts as a heat exchanger. The heat capacity of soil and groundwater is relatively high, whereas the thermal conductivity is moderate and dependent on the local hydrogeology. Therefore the heat exchanger must be relatively large, i.e., the polyethylene pipes relatively long. They can either be installed horizontally at a depth of *c.* 1 m (horizontal closed-loop systems), or vertically in a borehole (borehole heat exchanger or vertical closed-loop system; Fig. 2).

Vertical systems are only influenced by seasonal temperature variations in the upper zone down to 10–20 m and have a higher efficiency than horizontal systems due to a higher and constant ground temperature. On the other hand, the temperature regime around a vertical system is only slowly re-generated and careful design with respect to the energy demand is necessary, and an accurate estimate of the energy consumption is needed to optimise the design of the system. Alternating operations with heating during winter and cooling during summer, supplemented with seasonal storage of

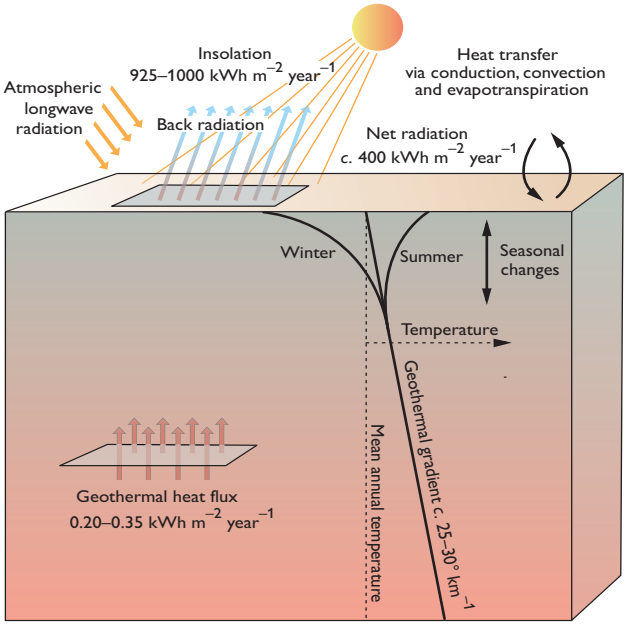

Fig. 1. Schematic block diagram showing the geothermal gradient and magnitude of geothermal heat flux and insolation with average values for Denmark as well as the seasonal zone of fluctuation in temperature (modified from Banks 2008).

heat from, e.g. solar panels, can optimise the efficiency of vertical systems.

Groundwater and environmental protection

Protection of the environment and groundwater is of paramount importance in shallow geothermal projects. The main issues are leakage of water with antifreeze, cross-connecting different aquifers, seepage of surface water along the borehole, drilling into artesian aquifers and unwanted thermal effects. All steps in the production and installation of a ground loop must be designed for optimum tightness and longevity of the loop. Installation procedures must minimise the risk of damaging the pipes, and a pressure test of the pipes must be carried out. The legislation also specifies which antifreeze agents can be used in the ground loop – only non-toxic and easily biodegradable fluids are allowed.

Closed-loop boreholes must be sealed with low permeable grout in order to prevent contact between the surface and aquifers or between individual aquifers and the quality of the sealing determines the protection of the groundwater, as for all other boreholes. Grouting is also necessary to improve the heat transfer from the ground to the pipes and in actual practice the entire borehole is sealed with grout.

Perforation of an artesian aquifer can cause large quantities of water to press through the drill pipe disrupting the grout. To avoid drilling closed-loop boreholes into artesian aquifers, local hydraulic heads must be checked prior to drilling (Ditlefsen 2012).

Possible problems with thermal pollution for horizontal systems are described by Banks (2008). Extraction of heat may cause freezing of the ground and frost heaving, which can potentially damage surface structures, buried installations and plant roots. Warming of the ground may cause vapour migration and progressive drying and perhaps even shrinkage of soils. Significant heating of the ground can also lead to consolidation and settling in clayey, unconsolidated soils and thermal interference between neighbouring ground-source energy schemes may occur. In the Danish legislation for closed-loop systems safety distances to other ground heat exchangers and to extraction wells for drinking water are specified, but not to buildings and other structures. For open- loop systems the limitations in the allowable thermal influence on the groundwater are rather strict.

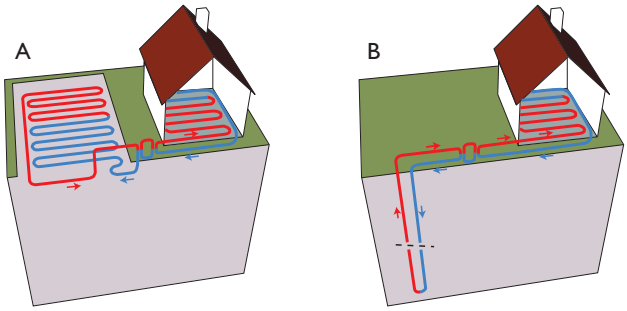

Fig. 2. Principles of horizontal (**A**) and vertical (**B**) closed-loop, ground-source heat-pump systems.

Evaluation of thermal properties of Danish sediments

In Denmark vertical systems are normally drilled to depths of 50–200 m. In order to evaluate the possible energy extraction from a specific new site and estimate the required depth and number of boreholes, information about the geology and hydrogeology is crucial. The greater part of Denmark is under-

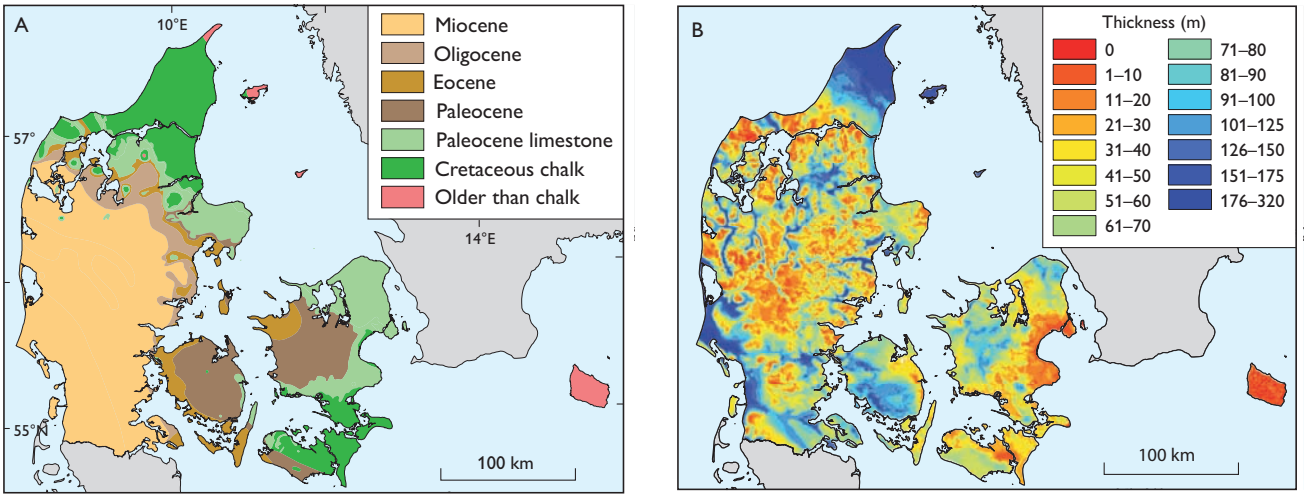

Fig. 3. Maps showing the pre-Quaternary geology (**A**) and the thickness of Quaternary sediments (**B**) in Denmark.

Table 1. Thermal conductivity of different sediment and rock types

Sediment/rock	Thermal conductivity W mK^{-1}	Recommended values W mK^{-1}	Estimated specific heat extraction rate (W m^{-1}) VDI (2001)	MCS (2011)
Clay and silt (dry)	0.4–1.0*	0.5*	–	–
Water-saturated clay and silt	1.1–3.1*	1.8*	35–50	21–34
Palaeogene clay, Denmark	1.34–1.56†	–	–	–
Sand (dry)	0.3–0.9*	0.4*	25	–
Water-saturated sand	2.0–3.0*	2.4*	65–80	26–45
Water-saturated gravel	1.6–2.5*	1.8*	–	–
Till/loam	1.1–2.9*	2.4*	–	–
Clayey till, Denmark	2.00–2.31‡	–	–	–
Chalk, England	1.79 ± 0.54§	–	–	–
Chalk, Denmark	1.45–1.86†	–	–	–
Quartzite	5.5–7.5§	6.0§	–	–
Granite	3–4§	3.4§	65–85	33–45

* VDI (2010). † Balling *et al.* (1981). ‡ Porsvig (1986). § Banks (2008).

lain by a sedimentary basin dominated by shallow marine to deep marine clastic and biogenic sediments (Fig. 3A), overlain by Quaternary deposits. In some areas the Quaternary cover is thin and limestone or Tertiary sand, silt and mud are found close to the surface. Thick successions of Quaternary sediments are common in the northern and south-western part of the country (Fig. 3B). In these areas the Quaternary sediments are dominated by marine and glaciomarine deposits. Thick successions of Quaternary deposits are also found in buried valleys (Jørgensen & Sandersen 2006). The geological variation within the Quaternary sediments is high and regional-scale geological models are not sufficiently detailed to estimate the possible energy extraction from a vertical system. Local information from boreholes and geophysical data are necessary to map the Quaternary strata and the elevation of the water table.

The potential flow of energy in and out of a vertical system is determined by the heat capacity and the thermal conductivity of the sediments or rocks surrounding the borehole. The process is dominated by heat conduction, but advective transport in the groundwater also plays a role. The thermal conductivity of geological materials depends on the porosity, water content and mineral composition. Rocks and sediments with a high content of quartz have high thermal conductivity, whereas porous, unsaturated sediments have low thermal conductivity due to the presence of air in the pore space. Thermal conductivity values for different rock and sediment types are compiled in Table 1 and show large variations for saturated clay and silt as well as for till deposits, which are common sediments in Denmark. Most of the values are from Germany and the UK and to get more information about common Danish lithologies new measurements are required.

Modelling of near-surface heat flow in a Danish context

Various model systems are available for calculating the efficiency of vertical systems in terms of energy extraction, ranging from simple and easy-to-use models to complex numerical models. The easy-to-use models consider the long-term aspects assuming homogeneous and constant subsurface thermal properties, whereas the complex models also take into account the effect of alternating system operation, heterogeneity in thermal properties as well as groundwater flow. Assuming standard design and 1800 hours of production per year, specific heat extraction rates for selected sediment and rock types have been estimated for German (VDI 2001) and British (MCS 2011) conditions based on vertical systems with double- and single-loop pipes, respectively (Table 1). The values indicate large variations between different sediment types and within specific geological facies as well as between the German and British studies, stressing the importance of establishing valid standard values applicable for Danish conditions and different systems. The possible energy extraction for 100 m vertical, closed-loop boreholes has been calculated for four simple geological successions (Fig. 4). The estimated energy extraction for the most unfavourable of the geological scenarios (7560 kWh) is only *c.* 60% of the energy extraction for the most favourable (12 537 kWh), thus giving an indication of the possible effect of different geological settings.

In addition to heterogeneity in geology and thermal properties, the efficiency of vertical systems is affected by possible groundwater flow. If the system is operating only in heating or cooling mode, groundwater flow will have a positive impact on the efficiency due to the continuous supply of energy. On the other hand, groundwater flow will have a negative

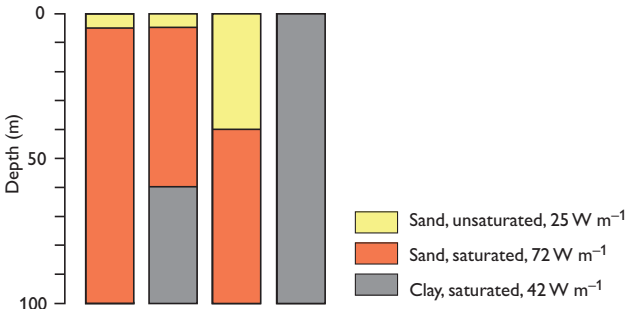

Fig. 4. Four simple geological successions with average, specific heat-extraction rates from Table 1 VDI (2001). The possible energy extraction has been calculated to 12 537; 10 373; 9576 and 7560 kWh (left to right), based on 1800 hours of production per year (borehole length × specific heat extraction rate × hours of production).

impact on systems using the subsurface for seasonal energy storage, because the flow will transport heat and cold away from the vertical system. To evaluate the importance of the hydrogeological heterogeneity observed in Denmark, modelling will be carried out based on a complex numerical model that allows the inclusion of subsurface heterogeneity as well as groundwater flow. The aim of the modelling is to identify the aspects that must be considered in the design phase of closed loop systems, and estimate the maximum energy that can be extracted under different hydrogeological conditions typical in Denmark.

Perspectives for shallow geothermal energy in Denmark

Shallow geothermal energy is a competitive, renewable energy resource as domestic heat pumps typically produce 3–4 times the amount of energy they consume in the form of electricity. Depending on how the electricity is generated and taking the generation and transmission loss into consideration, heating a building using ground-source energy produces only half of the CO_2 emission of fossil fuels used directly for heating (Banks 2008). Nevertheless, the application of shallow geothermal energy in Denmark is relatively limited. In 2008, the number of ground-source heat-pump installations was *c.* 25 000 (Willumsen 2008), with the vast majority being horizontal systems. So far, only a few hundred of the installed systems are based on closed-loop boreholes, and the number of groundwater-based open-loop systems is limited to a few tens. Hopefully the GeoEnergy project can pave the way for a wider use of shallow geothermal energy, but in order to fully exploit the resource, a systematic assessment of the potential is needed, including the potential for seasonal storage of waste heat. With the continuous focus on climate change and energy consumption, the number of installations is likely to increase rapidly in the coming years, especially after a political decision has been made to phase out domestic oil burners starting in 2012. The manifold exploitation of various shallow geological resources, including shallow geothermal energy, drinking water and minerals, will increase the demand for resource management and data availability.

Acknowledgement

The EUDP programme of the Danish Energy Agency is thanked for financial support to the GeoEnergy project.

References

Balling, N., Kristiansen, J.I., Breiner, N., Poulsen, K.D., Rasmussen, R. & Saxov, S. 1981: Geothermal measurements and subsurface temperature modelling in Denmark. GeoSkrifter **16**, 176 pp.

Balling, N., Nielsen, S.B., Christiansen, H.S., Christensen, L.D. & Poulsen, S. 1992: The subsurface thermal regime and temperature of geothermal reservoirs in Denmark. Synthesis report to the Commission of the European Communities, Contract EN3G-0029-DK, 91 pp. Århus: Department of Earth Sciences, University of Aarhus.

Banks, D. 2008: An introduction to thermogeology: ground source heating and cooling, 351 pp. Oxford: Blackwell.

Ditlefsen, C. 2012: D1 Geologi og jordvarmeboringer. Oversigt over geologiske forhold af betydning ved etablering af jordvarmeboringer. GeoEnergi – Energianlæg baseret på jordvarmeboringer – udvikling af markedsfremmende værktøjer og best practice. EUDP projekt, *J.nr.* 64011-0003.

Jørgensen, F. & Sandersen, P.B.E. 2006: Buried and open tunnel valleys in Denmark – erosion beneath multiple ice sheets. Quaternary Science Reviews **25**, 1339–1363.

Mathiesen, A., Kristensen, L., Bidstrup, T. & Nielsen, L.H. 2009: Vurdering af det geotermiske potentiale i Danmark. Danmarks og Grønlands Geologiske Undersøgelse Rapport **2009/59**, 30 pp.

MCS (Microgeneration Certification Scheme) 2011: Microgeneration installation standard: MIS 3005. Issue 3.0. London: Department of Energy and Climate Change.

Porsvig, M. 1986: Varmeovergangsforhold omkring jordslanger. Energiministeriets varmepumpeforskningsprogram **33**, 56 pp.

VDI (Verein Deutscher Ingenieure) 2001: Thermische Nutzung des Untergrundes: Erdgekoppelte Wärmepumpenanlagen. Richtlinie 4640, Blatt 2, 43 pp. Düsseldorf: Verein Deutscher Ingenieure.

VDI (Verein Deutscher Ingenieure) 2010: Thermische Nutzung des Untergrundes: Grundlagen, Genehmigungen, Umweltaspekte. Richtlinie 4640, Blatt 1, 33 pp. Düsseldorf: Verein Deutscher Ingenieure.

Willumsen, B. 2008: Jordvarmeanlæg. Teknologier og risiko for jord- og grundvandsforurening, 176 pp. Miljøprojekt nr. 1238. Copenhagen: Miljøstyrelsen.

Authors' address

Geological Survey of Denmark and Greenland, Lyseng Allé 1, DK-8270 Højbjerg, Denmark. E-mail: *tvp@geus.dk*

Efforts to include geological and geodetic observations in the assessment of earthquake activity in Denmark

Søren Gregersen and Peter H. Voss

Assessment of earthquake hazard is improved if geological and geodetic data are included in addition to seismological data. In earthquake regions like Japan and California, palaeoseismology combines data from geology and seismology, and networks of permanent GPS (global positioning system) stations situated on bedrock supplement the networks of seismographs. A combination of seismographs and GPS stations on ice is also used in current studies of glacial earthquakes in Greenland. In Denmark only broad-scale geodetic coverage is available (Khan *et al.* 2005) and only a few examples of geological input are found in the literature. However, more thorough geodetic evaluations of deformations are currently made in Nordic co-operation projects and we are looking forward to learn about the results. Also the number of permanent GPS stations in Denmark has recently been increased from 3 to 13. The geological input is limited but may hold some potential, and the aim of this article is to evaluate this. We also discuss new investigations of recent geological movements, both in projects on post-glacial uplift (and accompanying horizontal deformation) of Scandinavia, and more locally of geological indicators of uplift in selected areas. As seismologists, we are interested in a homogeneous evaluation of geological indicators in all of Denmark and its neighbouring areas.

In two recent seismological papers, we emphasised the very low earthquake activity in Denmark, even in the geologically significant Sorgenfrei–Tornquist Zone (Gregersen & Voss 2009, 2010). The recorded earthquake activity over

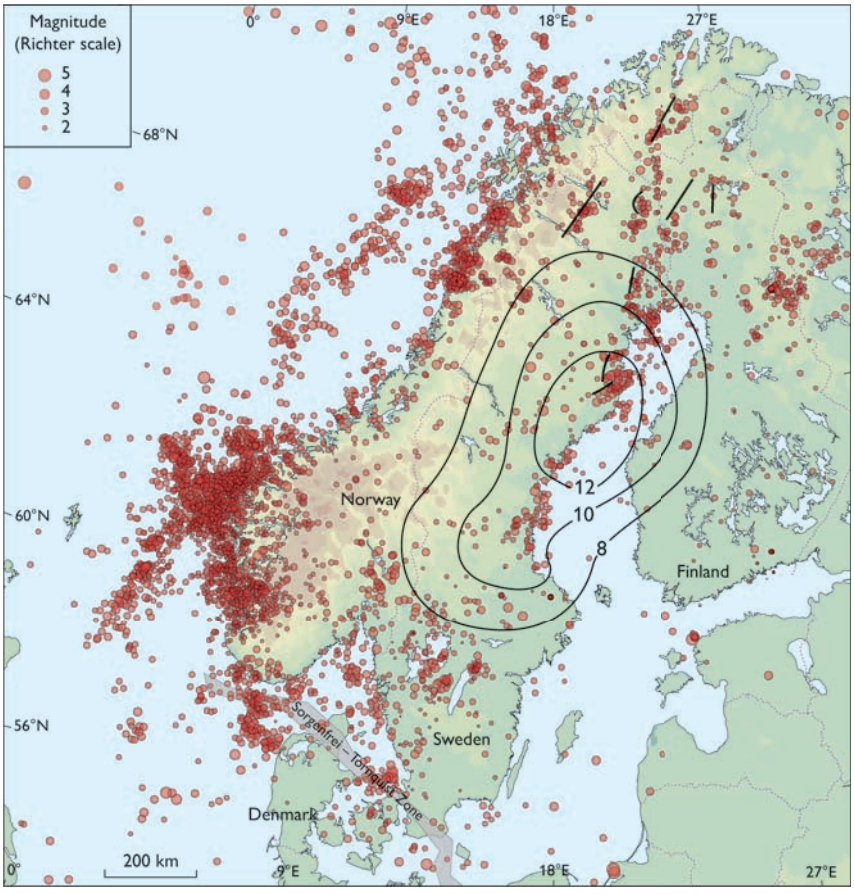

Fig. 1. Map of North-West Europe showing the locations of earthquakes recorded from January 1970 to December 2004. Earthquakes in Denmark are from a catalogue at the Geological Survey of Denmark and Greenland, and the other earthquake locations are from a Scandinavian catalogue at Helsinki University. Thick black lines show large postglacial faults *c.* 9000 years old, according to Lagerbäck (1991). The curves in central Scandinavia show an early common Scandinavian compilation in project BIFROST of uplift (mm/year). Updated earthquake files for Denmark are available at *.geus.dk* under seismology, and for the rest of Scandinavia at *www.seismo.helsinki.fi*. The map is modified from Gregersen & Voss (2009).

 Geological Survey of Denmark and Greenland Bulletin 26, 41–44. Open access: www.geus.dk/publications/bull

the last hundred years is even lower than that of northern Scandinavia (Fig.1). Historical reports from the past thousand years tell the same story. The stresses in Denmark are fairly homogeneous, mainly influenced by plate motion and only marginally by postglacial uplift, and the earthquake hazard is considered low (Giardini 1999). Here, we assess the longer geological perspective in an attempt to improve long term evaluation of hazard and to demonstrate the need for further geological investigations of stresses and strains in a time scale of several thousands of years. The area discussed is shown in Fig. 2, which also shows generalised, relative sea-level changes after the time of the Littorina Sea in the mid-Holocene (Christensen 2001).

Discussion of selected areas

Carlsberg fault, Copenhagen – This fault is one of the most significant faults in the Copenhagen area (Rosenkrantz 1937; Nielsen & Thybo 2004), and it has been very important for the Carlsberg brewery because large quantities of water could be extracted from the fault zone for brewing beer. Along the fault zone, cracks in house walls are observed, but it is an open question whether it is worse than in the adjacent area (Ovesen *et al.* 2002; O.W. Christensen, personal communication 1990s; B. Larsen, personal communication 2009; L. Nielsen, personal communication 2009). No earthquakes have been recorded near the fault. A more quantitative area mapping around the fault is needed.

Misfits in the Danish geodetic system have been ascribed to the Carlsberg fault. The base line of the distance measuring system on the island of Amager near Copenhagen has been described as deformed (Ovesen *et al.* 2002). However, a more probable explanation of this so-called deformation is movements of near-surface sediments at one of the end points of the base line before 1911 due to winter freezing and thawing (M. Aarestrup, personal communication 1991; K. Engsager, personal communication 2009). We consider it unlikely that deformation occurred in 1930 as suggsted by Rosenkrantz (1937) since no movements were registered between 1911 and 1933.

Another base line on Amager (in Danish called 'prøvebane', trial distance) has been reported as deformed (Ovesen *et al.* 2002). In this case the geodetic problem was identified from observations which showed that there were problems with the end point as mentioned above. One of the ends is sloping strangely, and it must have been disturbed by winter freezing and thawing (K. Engsager, personal communication 2009). We conclude that the Carlsberg fault is not active at present.

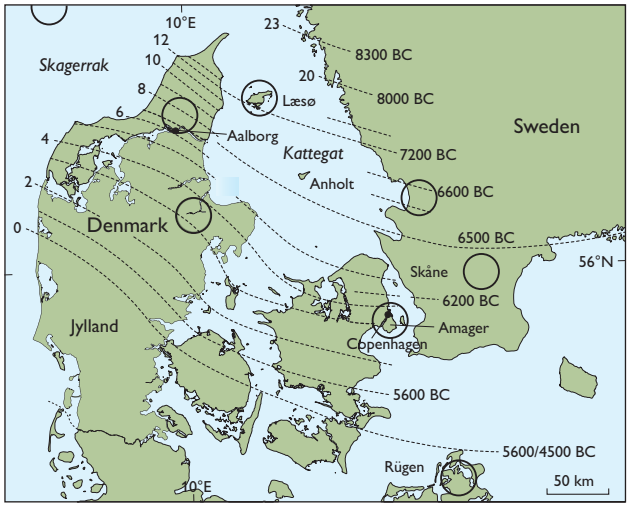

Fig. 2. Map of south-western Scandinavia, showing maximum elevations (m) and ages of shorelines from the Littorina Sea, according to Christensen (2001). The circles show areas discussed in the text.

Læsø – Indications of a large fault with a displacement of 4 m have been reported from geological investigations of sand deposits younger than 7000 years on the island of Læsø in Kattegat (Hansen 1977, 1980, 1994). No other sedimentary indications of earthquakes have been identified. Hansen suggested that Læsø does not fit into the post-glacial uplift pattern of the neighbouring coasts of Kattegat, but according to Christensen (2001) the elevations of the highest Littorina Sea shorelines on Læsø fit well into the regional pattern for Kattegat (Fig. 2).

A number of transgressions and regressions occurred over a period of several thousand years in the mid-Holocene in the Kattegat region (Christensen 2001). The last of these so-called Littorina transgressions ended around 4500 years ago. The structural differences in the Sorgenfrei–Tornquist Zone tell about an older geological regime, not the present intraplate inactivity.

Hansen (1980) presented a curve showing changes of tilt of a succession of shorelines based on shoreline elevation measurements without any evaluation of uncertainties. Each point in Fig. 3 represents an average of 10–15 individual measurements that span an elevation of *c.* 1 m. This 1 m can be taken as a rough estimate of four times the standard error. If an estimated standard error of 0.25 m is taken into account, the argument for variations in tilting becomes non-significant. We find that the observed differences and the standard errors are of the same magnitude (Fig. 3). The zig-zag line of Hansen (1980) goes through the average values of the slopes and the data may as well be explained by a straight line, i.e. within the belt of intervals determined by averages ± one standard error. Hence we conclude that the differences

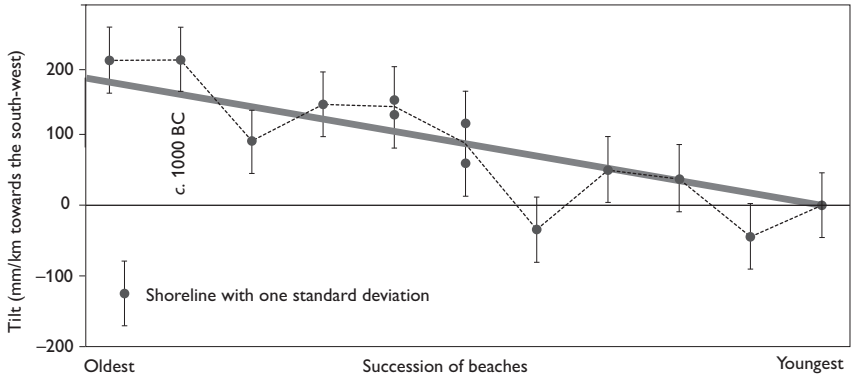

Fig. 3. Tilt of shorelines on Læsø (Hansen 1980, fig. 5) with our estimated standard errors added. Shorelines (dots) are plotted on the horizontal axis, with the youngest to the right. When the standard errors are included it appears that jumps in tilt values are not significant. The data can be interpreted as a steady change of tilt, approximated by the thick sloping line in the diagram, which is generally within one standard error and certainly within two standard errors.

in average tilt cannot be used as an argument for discontinuous and occasionally reverse tilting. The data may as well agree with steady uplift and tilting. The same magnitude of standard errors in the use of geological markers for tilt measurements, and for elevation measurements with respect to sea level, is used in a recent work on Anholt, also in the Kattegat. When changes in sea currents and stormy weather which can influence the development of shorelines are added, the observations on shoreline tilting (Fig. 3) cannot be used on their own as an argument for tectonic tilting.

On the basis of our assessment of old and new arguments we conclude that the bedrock subsurface below Læsø has been uplifted by the same amount as the rest of the Kattegat region, regularly or with minor irregularities. This means that there was no Læsø earthquake 4000–5000 years ago. The lower-lying parts of Læsø with many well-documented beach ridges have their own exciting history (Hansen *et al.* 2011), best explained by regular postglacial uplift together with coastal development influenced by sea currents, climate and weather. One hundred kilometres south-east of Læsø, in the Kattegat Sea, where earthquakes have been registered (Fig. 1), neotectonic small-scale faulting has been recognised (Jensen *et al.* 2002).

Northern Jylland – It has been suggested that a bend in the geodetic and geological uplift pattern north of Aalborg may reflect a fault (Lykke-Andersen & Borre 2000). However, according to follow-up measurements the bend could also be due to gradual creep with no indications of earthquakes (Gregersen & Schmidt 2001).

Central Jylland – Conspicuous so-called fracture valleys in central Jylland were recently discussed by Jakobsen & Pedersen (2009). The valleys may be related to a deep fault zone, but no evidence exists for present-day earthquakes in this region.

West coast of Sweden – Several localities on the west coast of Sweden have been discussed by Mörner (2003, 2009). Signs of geological movements at these localities include variations in postglacial uplift of shorelines, faulting and rock deformation in a few cases, and in many incidences rock slides. Also signs of liquefaction were found at several stratigraphic levels. We encourage a geological and geophysical assessment of these localities.

Skåne – In Skåne in southern Sweden repeated GPS measurements have indicated differential movements of the two sides of the Sorgenfrei–Tornquist Zone. However, these measurements are not considered statistically significant by Swedish geodesists.

Skagerrak – In Skagerrak and southern Norway more earthquake activity takes place than in Denmark (Fig. 1). An assessment similar to the present one has been carried out by Olesen *et al.* 2004.

Rügen – The bending phenomenon mentioned above is not confined to northern Jylland. Similar geodetic observations were reported from the island of Rügen in northern Germany (Fig. 2; R. Dietrich, personal communication 2008). However, seismological investigations show that northernmost Germany is an earthquake-free region like southernmost Denmark.

Discussion and conclusions

We have evaluated and discussed a number of reports on geological or geodetic indications of earthquake activity in Denmark. We found no signs of geologically recent faulting or recent crustal deformation. This corroborates that Denmark and its neighbouring areas are characterised by a small earthquake potential. The largest earthquakes recorded had a magnitude of just below 6 on the Richter scale. This is supported by the decrease of uplift stress after the last deglaciation. We conclude that earthquake hazard evaluations in Denmark in the foreseeable future are best based on seismological data

alone (Gregersen & Voss 2009). The earthquake zones are those found by historical and instrumental seismological investigations in the seas around Denmark (Fig. 1). Unfortunately this does not mean that destructive earthquakes cannot happen. The situation in Denmark is parallel to that of other intraplate regions. A totally unexpected destructive earthquake happens once every decade somewhere on Earth within a quiet lithospheric plate. Geodynamic stresses exist, which are occasionally released in structurally weak zones. Based on our present state of knowledge of seismology, geodesy and geology, we cannot foresee in which fault zone or region an earthquake may happen in Denmark, but no region is directly earthquake prone. Not even the very significant Sorgenfrei–Tornquist Zone is an earthquake zone (Gregersen *et al*. 2011).

Acknowledgments

We appreciate many good discussions with our colleagues Jens Morten Hansen, Peter Johannesen, Lars Henrik Nielsen, Tine B. Larsen, Tanni J. Abramovitz, Abbas Khan, Karsten Engsager, Holger Lykke-Andersen, Torben Bidstrup, Birger Larsen, Jørgen Leth, Lars Nielsen, Henrik Olsen, Hans Thybo and Lars B. Clemmensen.

References

Christensen, C. 2001: Kystbosættelse og havniveauændringer i stenalderen. In: Jensen, O.L., Sørensen, S.A. & Hansen, K.M. (eds): Danmarks jægerstenalder – status og perspektiver, 183–193. Hørsholm: Hørsholm Egns Museum.

Giardini, D. (ed.) 1999: The global seismic hazard assessment program (GSHAP) 1992–1999. Annali di Geofisica **42**, 280 pp.

Gregersen, S. & Schmidt, K. 2001: Tektonik i Danmark. Sorgenfrei–Tornquist Zonen. Geologisk Nyt **1**, 16–17. Aarhus: Aarhus Universitet.

Gregersen, S. & Voss, P. 2009: Stress change over short geological time: the case of Scandinavia over 9,000 years since the Ice Age. In: Reicherter, K., Michetti, A.M. & Silva Barroso, P.G. (eds): Palaeoseismology: historical and prehistorical records of earthquake ground effects for seismic hazard assessment. Geological Society Special Publications (London) **316**, 173–178.

Gregersen S. & Voss, P. 2010: Irregularities in Scandinavian postglacial uplift/subsidence in time scales tens, hundreds, thousands of years. Journal of Geodynamics **50**, 27–31.

Gregersen, S., Larsen, T.B. & Voss, P. 2011: Jordskælv i Sorgenfrei–Tornquist Zonen? Geoviden **1**, 18–19. København: Geocenter Danmark.

Hansen, J.M. 1977: Sedimentary history of the island Læsø, Denmark. Bulletin of the Geological Society of Denmark **26**, 217–236.

Hansen, J.M. 1980: Læsøs postglaciale udvikling i relation til den Fennoskandiske randzone. Dansk Geologisk Forening, Årsskrift for **1979**, 23–30.

Hansen, J.M. 1994: Læsøs tilblivelse og landskaber – om øen der rokker og hopper, 55 pp. København: Danmarks Geologiske Undersøgelse.

Hansen, J.M., Aagaard, T. & Binderup, M. 2011: Absolute sea levels and isostatic changes of the eastern North Sea to central Baltic region during the last 900 years. Boreas **41**, 180–208.

Jakobsen, P.R. & Pedersen S.A.S. 2009: Fracture valleys in central Jylland – a neotectonic feature. Geological Survey of Denmark and Greenland Bulletin **17**, 33–36.

Jensen, J.B., Petersen, K.S., Konradi, P., Kuijpers, A., Bennike, O., Lemke, W. & Endler, R. 2002: Neotectonics, sea-level changes and biological evolution in the Fennoscandian Border Zone of the southern Kattegat Sea. Boreas **31**, 133–150.

Khan, S., Knudsen, P. & Tscherning, C. 2005: Crustal deformations at permanent GPS sites in Denmark. In: Sansò, F. (ed.): A Window on the future of geodesy. Proceedings of the International Association of Geodesy Symposia **128**, 556–560.

Lagerbäck, R. 1991: Seismically deformed sediments in the Lansjärv area, northern Sweden. SKB Technical Report **91-17**, 58 pp. Stockholm: Svensk Kärnbränslehandtering AB.

Lykke-Andersen, H. & Borre, K. 2000: Aktiv tektonik i Danmark: der er liv i Sorgenfrei–Tornquist Zonen. Geologisk Nyt **6**, 12–13. Aarhus: Aarhus Universitet.

Mörner, N.-A. 2003: Paleoseismicity of Sweden, a novel paradigm, 320 pp. Stockholm: University of Stockholm.

Mörner, N.-A. 2009: Late Holocene earthquake geology in Sweden. In: Reicherter, K., Michetti, A.M. & Silva Barroso, P.G. (eds): Palaeoseismology: historical and prehistorical records of earthquake ground effects for seismic hazard assessment. Geological Society of Special Publications (London) **316**, 179–188.

Nielsen, L. & Thybo, H. 2004: Location of the Carlsberg Fault zone from seismic controlled-source fan recordings. Geophysical Research Letters **31**, L07621, *http://dx.doi.org/10.1029/2004GL019603*

Olesen, O., Blikra, L.H., Braathen, A., Dehls, J.F., Olsen, L., Rise, L., Roberts, D., Riis, F., Faleide, J.I. & Anda, E. 2004: Neotectonic deformation in Norway and its implications: a review. Norwegian Journal of Geology **84**, 3–34.

Ovesen, N.K., Blem, H., Gregersen, S., Møller, H.M.F. & Frederiksen, J.K. 2002: Recent terrain-movements in Copenhagen. Dansk Geoteknisk Forenings Bulletin **19**, 183–192.

Rosenkrantz, A. 1937: Bemærkninger om det østsjællandske Daniens stratigrafi og tektonik. Meddelelse fra Dansk Geologisk Forening **9**, 199–212.

Authors' address

Geological Survey of Denmark and Greenland, Øster Voldgade 10, DK-1350 Copenhagen K, Denmark. E-mail: *sg@geus.dk*

Results of monitoring groundwater above the natural gas underground storage at Stenlille, Denmark

Troels Laier

Groundwater in the Stenlille area is regularly analysed for light hydrocarbons after a natural gas underground storage facility was established there in 1989. The monitoring is carried out by the Geological Survey of Denmark and Greenland and is part of the authorities' requirements for the environmental approval of the natural gas storage run by the state-owned Danish Oil and Gas company DONG A/S. Groundwater from observation wells and water wells in the area was analysed every month during the first year of operation and four times a year in the following years. More frequent analyses are undertaken on special occasions.

Underground gas storage

Two underground storage facilities were established in Denmark in order to buffer the supply of gas from the North Sea, one in salt caverns in Jylland, the other in a deep aquifer at a depth of 1500 m near Stenlille (Fig. 1). Natural gas underground storage is possible in deep sealed geological formations with good reservoir quality and covered by tight caprock. These conditions are met by an anticlinal structure near Stenlille with a vertical closure of *c.* 35 m covering an area of 14 km². The Gassum Formation forms the reservoir where gas is stored by displacing formation water. The formation is of Late Triassic age and consits of cyclically interbedded sandstone and marine mudstone that were deposited as a result of changes in the depositional environment (Hamberg & Nielsen 2000). The overlying 300 m thick Lower Jurassic Fjerritslev Formation, which consists of claystone, serves as a caprock for the sandstone reservoir (Fig. 2). The total estimated storage capacity of the Stenlille structure equals three billion normal cubic metres, and due to reservoir heterogeneities, gas is stored in several separate zones (Fig. 1). The gas storage is operated by 14 wells for injection and withdrawal of gas and six wells used for observational purposes, most of them in the periphery of the structure.

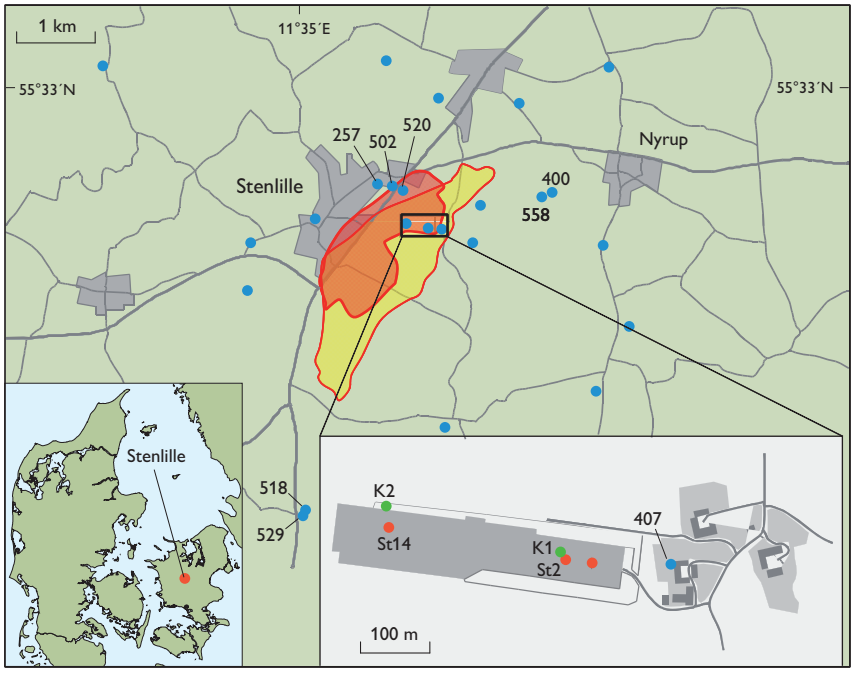

Fig. 1. Map of the Stenlille area showing the location of water wells (blue), observation wells for shallow aquifers (green, inset map) and deep wells (red). The extent of the underground gas storage is indicated by coloured areas, where yellow and red show different gas zones.

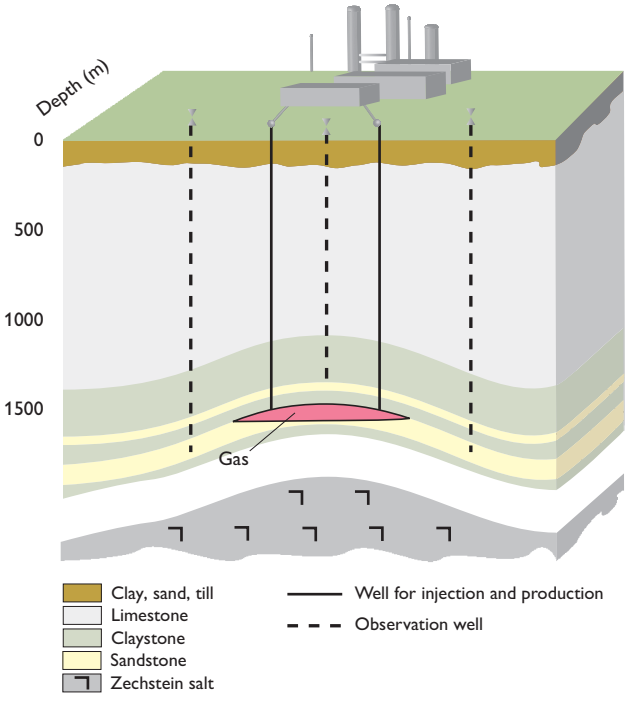

Fig. 2. Sketch of the natural gas underground storage facility at Stenlille. A Zechstein salt pillow is located below the surface. The development of the salt pillow has deformed the overlying beds into a dome. Sandstone: Gassum Formation sandstone (Late Triassic), claystone: Fjerritslev Formation (Early Jurassic).

Baseline study

As part of the pre-investigation of the Stenlille stucture, a baseline study was carried out in order to characterise the type and concentration of natural hydrocarbons present in the rocks within and above the future gas storage reservoir. Analyses of hundreds of drill cuttings from deep wells indicated no significant occurrence of hydrocarbons, although low concentrations of *in situ* generated hydrocarbons appeared to be present in the organic rich Fjerritslev Formation (Laier & Øbro 2009). A very low concentration of methane (30 mg/l), possibly of microbial origin, was observed in the saline formation water of the Gassum Formation (Laier & Øbro 2009).

Bacterial methane in groundwater

Methane is generally not analysed in groundwater unless its presence is suspected; therefore very few analyses existed prior to the baseline study. Groundwater from 21 water wells in the Stenlille area was sampled, and methane was found to occur in low concentrations (0.01–0.49 mg/l) in all of them except two (Laier 1989). No higher hydrocarbons were detected in any of the samples. Stable isotope analyses of nine of

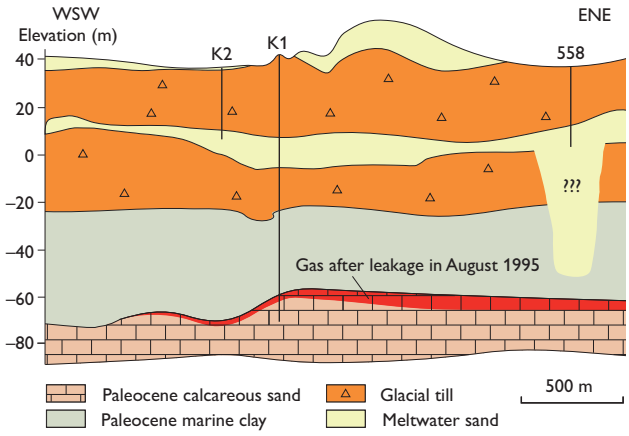

Fig. 3. Geological cross section of the upper layers of the Stenlille natural gas underground storage. The locations of wells K1, K2 and 558 are shown on Fig. 1. The red colour indicates the distribution of gas after the St14 leakage in August 1995 (for details see Laier 2010).

the samples showed that the methane was of bacterial origin ($\delta^{13}C_{CH4}$: –90 to –62‰; Laier 1989). The bacterial methane most likely comes from peat layers in the area. Most water wells in the area draw water from glacial meltwater sand found at depths of 20–30 m and overlain and underlain by glacial till (Fig. 3).

Bacterial methane (0.40 mg/l; $\delta^{13}C_1 = -64.5$‰) was also found in groundwater from the shallow filter of the K1 observation well located adjacent to the first injection well (St2; Fig. 1). The methane concentration in the brackish water from the deep filter (Fig. 3) was too low (0.02 mg/l) to permit analysis of its carbon isotope ratio.

Natural gas storage

Storage of natural gas from the Danish part of the North Sea began in July 1989. The gas is dominated by methane (91%) with a little ethane (5.5%) and propane (2.0%). The average $\delta^{13}C_{CH4}$ value of methane is –46.6‰. The composition of the natural gas stored in the Stenlille structure is markedly different from that of the gas dissolved in shallow groundwater (Fig. 4). This makes it fairly easy to distinguish between the two types of gas and identify even minor leaks from the deep gas storage reservoir at the near surface.

Groundwater methane

A fairly large variation in the concentration of methane from 0.4 to 3.7 mg/l was observed in water samples from a shallow filter of the K1 observation well in the early 1990s, but not in samples from a deeper filter, which had very low values (0.02 mg/l; Fig. 5). If the variation in methane concentra-

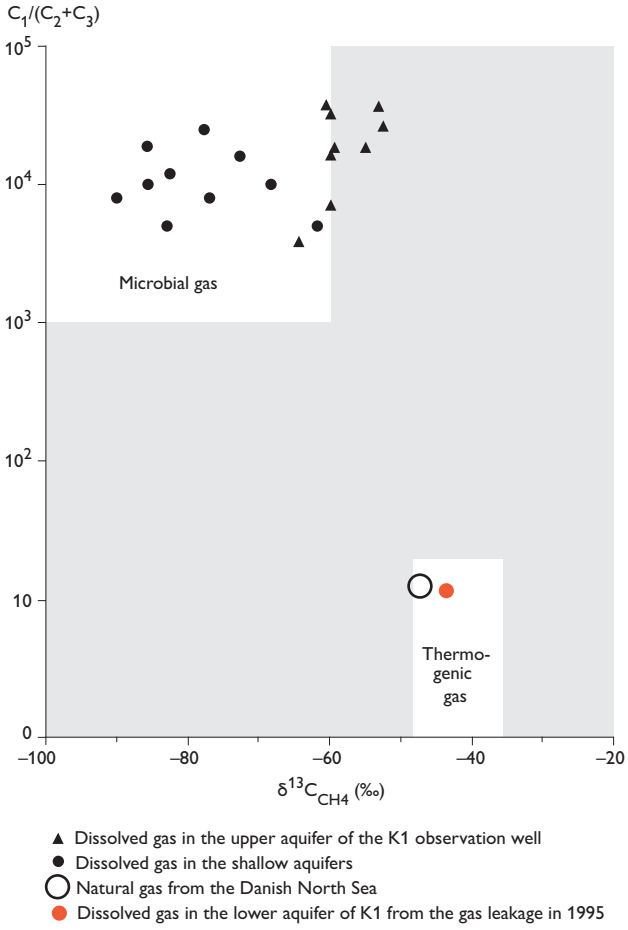

Fig. 4. Classification diagram showing the chemical and isotopic composition of natural gas from the Danish North Sea and dissolved gas in shallow aquifers. The $C_1/(C_2+C_3)$ ratio for the dissolved gas represents a minimum value as both ethane and propane were below detection limit for all dissolved gases. The white areas are typical of thermogenic and microbial gas and the grey area represents either mixtures of these gas types or gas of unknown origin. C_1: methane concentration, C_2: ethane concentration, C_3: propane concentration.

tion was due to a leakage around the nearby St2 well (Fig. 1), the opposite might be expected with an increase in methane at the deeper level first. In order to deduce the origin of the methane, isotope analyses were regularly performed during the first year of sampling. The isotope ratio of the methane ($\delta^{13}C_{CH4}$: −62 to −52‰) together with a lack of higher hydrocarbons indicate that the methane was bacterial in origin (Fig. 4), though its source remains unknown. Since the methane concentration was highest during the first years after drilling the K1 well, one may speculate whether hydrogen generated by anaerobic corrosion of iron filings from drilling may have led to methane formation as suggested by Daniels *et al.* (1987). Groundwater methane concentration in water from the Stenlille waterworks and from private water wells remained at the low levels measured prior to the storage of natural gas (Fig. 6).

Minor gas leakage

In September 1995, gas bubbles were observed at the terrain surface near the newly drilled St14 injection well (Fig. 1), and a sample of the gas was immediately collected and analysed. Its chemical and isotopic composition was similar to that of the gas being stored (Fig. 4), so there was little doubt that gas leaked from the new well. The leak was due to technical problems during gas injection (Laier & Øbro 2009) and was quickly stopped, but an estimated 5000 m³ of gas was lost to geological formations above the reservoir cap rock.

A week after the leak was observed at the surface, a significant increase in the dissolved gas concentration was measured in the deep filter of the K1 well, located 250 m from the St14 well. This gas had almost the same composition as the reservoir gas (Fig. 4). No free gas was observed during collection of water from this level, so it was concluded that all the gas was dissolved at this time. However, for the gas to migrate from St14 to K1 during a week, a free gas phase

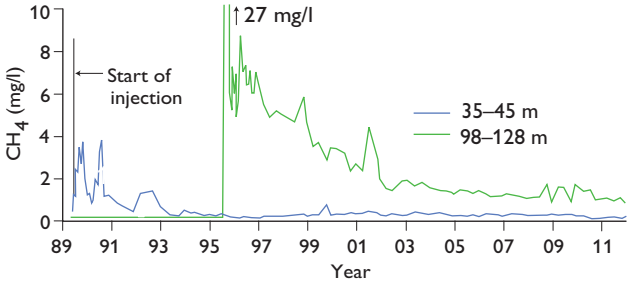

Fig 5. Methane concentration in groundwater from the K1 observation well. The sudden increase in dissolved methane was noted one week after the gas leakage at St14.

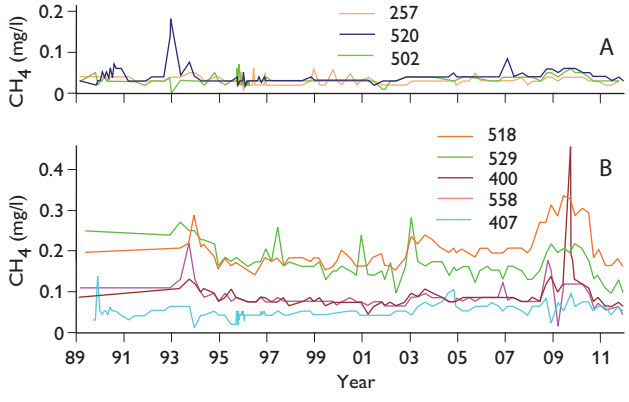

Fig. 6. Methane concentration in groundwater from wells supplying the Stenlille waterworks (**A**) and from private wells (**B**).

must have existed at some point, although free gas was never observed in the samples from any of the wells. The concentration of dissolved gas has decreased since the gas leakage occurred and is presently below 1 mg/l, and its composition has hardly changed.

Traces of natural gas in a water well near Nyrup

The regular groundwater survey revealed a significant increase in methane in October 2009, from 0.1 to over 0.4 mg/l, in water well 558 south-west of Nyrup (Figs 1, 6B). Traces of ethane and propane were also observed, indicating the presence of natural gas in low concentrations. An immediate follow-up investigation indicated a high proportion of old groundwater in the well due to a low pumping rate. When the normal pumping rate for the well was re-established, groundwater methane dropped below 0.1 mg/l and the higher hydrocarbons ethane and propane could no longer be detected. It was concluded that minor amounts of natural gas from the leak in 1995 had migrated into the Paleocene calcareous sand below Paleocene marine clay of low permeability and reached the water well near Nyrup (Fig. 3; Laier 2010). A buried valley at Nyrup may have allowed gas to migrate to shallower depths where it gradually dissolved in groundwater (Jørgensen & Sandersen 2009). The very low pumping rate in well 558 resulted in less infiltration of younger groundwater, which enabled the detection of natural gas in older groundwater (Laier 2010).

Conclusions

No leakage from the natural gas underground storage has occurred through the natural (geological) barriers. Regular analyses of dissolved hydrocarbons in shallow groundwater only showed the presence of bacterial methane, which was also present prior to the storage of natural gas. The traces of natural gas observed for a short period in one of the water wells in 2009 could be related to a minor leak from a newly drilled injection well in August 1995.

References

Daniels, L., Belay, N., Rajagopal, B.S. & Weimer, P.J. 1987: Bacterial methanogenesis and growth from CO_2 with elemental iron as the sole source of electrons. Science **237**, 509–511.

Hamberg, L. & Nielsen, L.H. 2000: Shingled, sharp-based shoreface sandstones: depositional response to stepwise forced regression in a shallow basin, Upper Triassic Gassum Formation, Denmark. In: Hunt, D. & Gawthorpe, R.L. (eds): Sedimentary reponses to forced regressions. Geological Society Special Publications (London) **172**, 69–89.

Jørgensen, F. & Sandersen, P. 2009: Kortlægning af begravede dale i Danmark. Opdatering 2007–2009, 374 pp. Copenhagen: Geological Survey of Denmark and Greenland. *http://www.begravededale.dk/PDF_2009/Rapport_Begravede_dale_2009_137mb.pdf*

Laier, T. 1989: Stenlille Gas Storage – study of naturally occurring hydrocarbon gases before injection. DGU Service Report **15**, 53 pp. Copenhagen: Geological Survey of Denmark.

Laier, T. 2010: Spor af naturgas i Nyrup vandværksboring oktober 2009. Danmarks og Grønlands Geologiske Undersøgelse Rapport **2010/1**, 30 pp.

Laier, T. & Øbro, H. 2009: Environmental and safety monitoring of the underground gas storage facility at Stenlille, Denmark. In: Evans, D.J. & Chadwick, R.A. (eds): Underground gas storage: worldwide experiences and future development in the UK and Europe. Geological Society Special Publications (London) **313**, 81–92.

Author's address

Geological Survey of Denmark and Greenland, Øster Voldgade 10, DK-1350 Copenhagen K, Denmark. E-mail: *tl@geus.dk*

Groundwater protection in Denmark and the role of water supply companies

Jacob Dyrby Petersen and Lisbeth Flindt Jørgensen

Denmark has a decentralised water supply structure with about 2500 water supply companies. Until recently, about 150 of these, especially the larger ones, were owned by local authorities; the rest are private, all run on an independent and not-for-profit basis. Recently, a new law, the Water Sector Law (Miljøministeriet 2009), was implemented. Its purpose is to privatise the water supply sector (although, as hitherto, into not-for-profit corporations), and statutory duties are separated from operations in order to make the supply of drinking water to consumers as efficient as possible. An important element of the Water Sector Law is the introduction of a new regulatory body, the Utility Secretariat. The role of this new institution under the Danish Competition and Consumer Authority is to enforce price ceilings on drinking water, based on a selection of benchmark parameters.

Danish policy is to base the drinking water supply on unpolluted groundwater. Nevertheless, in 2010, pesticides were detected in 25% of all tested, active abstraction wells, and the level for individual substances was exceeded in 4.5% of the wells (Thorling *et al*. 2011), a situation more or less unchanged over the last 20 years. This calls for further and continuous measures to strengthen groundwater protection. In addition, the range of protective activities implemented over the last decades may require reinforcement as groundwater monitoring data show that a high proportion of young groundwater is polluted with pesticides (Thorling *et al.* 2011).

A modern Danish waterwork from Østerby, eastern Jylland.

Our hypothesis is that during the last decades groundwater protection has changed from being a national responsibility to becoming a more locally embedded task. We also see a change towards the water supply companies being the major actors capable of initiating active groundwater protection. This transition also implies a change as regards economy, viz. from public authorities to consumers. The aim of this paper is to discuss how the Water Sector Law affects the frames for groundwater protection when an increasing part of the effort hinges on the water supply initiative taken by private companies.

Background

Denmark is one of the countries in the world most heavily reliant on groundwater as more than 99% of all water supplies are derived from this source (Jørgensen & Stockmarr 2009). Thus Denmark has a strong incentive to, and tradition for, knowledge-based groundwater management. The characteristics of the Danish hydrogeological conditions, combined with wide-ranging groundwater monitoring and a relatively advanced technological and administrative approach as well as a tradition for public involvement in administration, have shaped the present framework of groundwater protection in Denmark.

In Denmark, official groundwater protection began in the 1970s with the creation of the Ministry of the Environment. The ensuing environmental legislation and the establishment of 14 regional authorities prepared the path for regional groundwater management strategies based on national legislation for the protection of the environment, including groundwater. As a consequence of a statutory framework reform in 2007, abolishing the 14 regional authorities, groundwater protection was transferred to the 98 municipalities (kommuner).

Initially, mainly prospective activities were addressed, but a few years later remediation acts were enforced and resources allocated to manage the 'sins of the past' in terms of old polluted sites. Water supply and water demand manage-

Table 1. The interviewed institutions

Interviewed institution	Representing
Two large, urban water supply companies	Water supply
Two water supply associations	Professional body
One agricultural association	Professional body
Two municipalities (kommuner)	Public sector (local)
The Nature Agency (Ministry of the Environment)	Public sector (national)
The Utility Secretariat (Danish Competition and Consumer Authority)*	Public sector
One large, private contractor/consultant	Private sector

*The authority implementing the Water Sector Law

ment strategies emerged, e.g. by launching saving campaigns targeted at both industrial and private consumers. Appeals soon followed not to use pesticides in private gardens etc. to reduce groundwater contamination. These public campaigns were initiated and implemented by the state as well as the water supply companies. The latter were allowed a more operational role in groundwater protection by a change of the Water Act in 1999, financing activities through water levies (Miljøministeriet 1999). Thus groundwater protection was no longer solely dependent on initiatives by the state.

Methods

To analyse the past and present status of involvement in groundwater protection and to examine what is conceived as the overriding issues of the new Water Sector Law, two major sources are used: (1) a survey conducted in 2010 among the 75 largest Danish water supply companies (Pedersen 2010a) and (2) qualitative interviews in 2011 with key persons in the water sector (Table 1), combined with a concurrent study of the political and legislative process surrounding the implications of the water sector reform (Petersen 2011). Given the dynamic nature of the field of study, the interviews were conducted within a period of six months with follow-ups carried out as semi-structured interviews based on an iterative and adaptive approach (Kvale 1997). The interviews covered the views of informants on:

- the historical development of the water supply sector;
- the interplay between the authorities and the water supply companies;
- the efforts and players in the Danish groundwater protection regime and
- the legislative process and the implications for the economic and ecological aspects of future groundwater protection.

The theoretical frame was partly based on a theoretical network analysis adapted from Sørensen & Torfing (2005) and partly on a meta-analysis of the understanding of groundwater management from the definition of Market Environmentalism (Bakker 2005). The network approach was used to analyse the use of decision making and coordinating networks between actors instead of the two traditional management instruments: hierarchy (i.e. state control) and free market. This enables an assessment of how the Water Sector Law has changed the opportunities of the water supply sector to form and co-operate within networks.

Market environmentalism can be used as a theoretical tool to analyse the development of resource understanding and resource management based on market mechanisms, based on studies from the UK. From being a supply-led, state-owned and managed resource, groundwater in the UK is increasingly governed through the private sector and market-based instruments. As a country of comparison, the theoretical framework is used to analyse the development in Denmark.

Results

In 2010, 48% of the 75 largest Danish water supply companies were actively involved in groundwater protection activities, and were partly financing these (Pedersen 2010a). The companies reported that they had used between 1 and 25% of their annual turnover on groundwater protection (Pedersen 2010b). Although these estimates are highly uncertain, water supply companies have reported increasing expenditure on these protection activities (Fig. 1), and the figures indicate

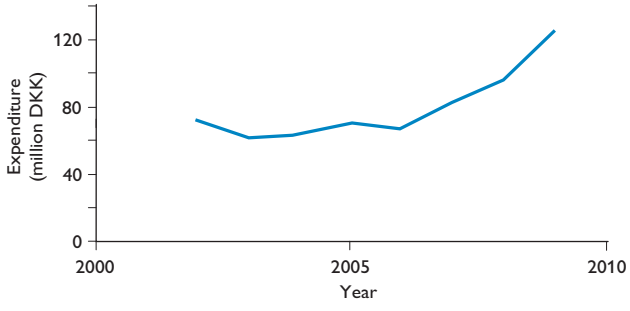

Fig. 1. Expenditure related to groundwater protective activities as reported by the water supply companies. Modified from Petersen (2011).

Before Water Sector Law

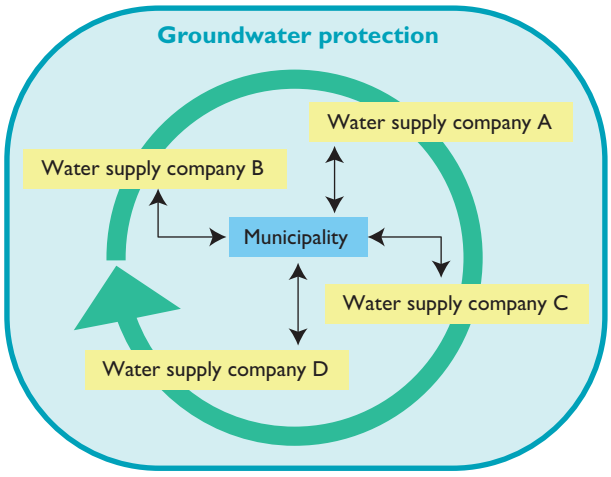

After Water Sector Law

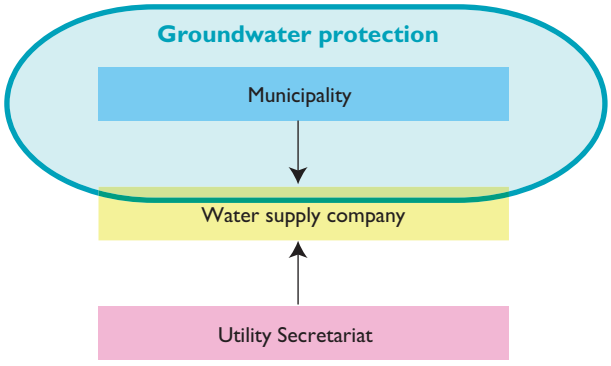

Fig. 2. The framework for groundwater protection before and after the implementation of the Water Sector Law. The networking is expected to decrease, and the water supply companies will change from being both operators, planners and decision makers to be operators only.

a total annual funding from the water supply sector of more than 100 million Danish kroner (Petersen 2011). More than half of the interviewed water supply companies expected expenditure to increase or at least remain at the same level in forthcoming years, and more than 60% expected necessary future activities (Pedersen 2010b).

The interviews conducted by Petersen (2011) reflect that the water supply companies have taken care of a range of different tasks connected with groundwater protection. They have often voluntarily entered networks (see Fig. 2) with each other and the relevant municipalities and thereby broadened the character of tasks to a degree that would otherwise have been impossible, based on individual water supply company economy and human resources. The tasks cover afforestation, volunteer farming agreements with landowners, groundwater resource and quality investigations, entry into action plans together with other water suppliers, stakeholders and local authorities, etc. These tasks were previously financed by adding an extra consumer levy on the water price, typically a groundwater protection tariff of less than 2% of the total water price per cubic metre. As a consequence of the Water Sector Law, the water supply companies fear that this will not be possible in the future as the law allows the Utility Secretariat to establish differentiated price ceilings for the individual water supply companies (Petersen 2011) based solely on production expenditure.

One of the two water supply organisations have expressed their concerns at this new development, expecting that the water supply companies will have to focus their activities only on economic issues and not, as previously, be able to perform groundwater protective activities for long-term consumer benefit (Petersen 2011).

The interviews revealed concerns regarding the capability of local authorities to set up groundwater protective activities at the same level as the former regional authorities, due to limited resources under the new statutory framework. These concerns are related to both spatial (arm's length) aspects (the water resource being managed at a local and not a regional level, giving local interests larger influence) and resource issues (the local authorities lacking possibilities of sustaining both economy and skills; Petersen 2011). Furthermore, there is fear among water associations that the local authorities will only have an active role in protecting the groundwater in quantitative terms, as qualitative aspects are now to be handled in national legislation and action plans, and not at a local level. Thus the municipalities may only be in a position to administer and outline the overall framework, and only perform limited actual groundwater protective activities. Accordingly, the interviewed municipalities expressed their expectations that the water supply companies are to be *the* active players in these activities, and that the economic resources are to be found through water levies (Petersen 2011). The capacities of the water supply companies should therefore include the practical implementation of future groundwater protection measures, at least as seen from the municipalities' point of view.

Discussion

Over the past two decades, the water supply companies have entered into different *networks.These* networks have been established for various reasons, which could be an experience of missing coordination in societal management, or a need for mutual action and sharing of knowledge and resources (Sørensen & Torfing 2005). The networks have been associated especially with groundwater protective activities such

as afforestation, voluntary agreements with landowners on non-pesticide cultivation, investigations and action plans (Petersen 2011).

How does the new Water Sector Law influence these networks and their associated activities? The law sets strict limits on how the water supply companies can use their financial resources. The first few trials have already shown that the Water Sector Law does not provide the framework necessary for continuation of former activities such as afforestation and networking, as the financial platform in terms of a water tax is not in accordance with the law. Both the water supply companies and the local authorities look upon this as a bottleneck in establishing and continuing effective groundwater protection (Petersen 2011).

The intension behind the Water Sector Law is to ensure economically efficient company operations and at the same time the law emphasises that the main objective of the companies is to abstract, treat and distribute drinking water (Petersen 2011). On the other hand, a central element is that the water supply companies are allowed – if not obliged – to perform groundwater protective activities if required by the local authorities as part of a public environmental action plan, dictated by the central authorities.

As the interviews revealed, the experience and financial capacity of the decentralised water supply companies have played an essential role in the protection of the Danish groundwater over the past decades, and there is considerable concern regarding the future fate of these activities (Petersen 2011).

The new regulatory paradigm is by Bakker (2005) described as Market Environmentalism, where market mechanisms are to ensure efficiency, competition and sustainability. Whereas the business aspects are beyond the scope of this paper, the environmental perspective implies a movement towards a capitalisation of the environment to include resource protection in water pricing, as attempted in the UK. From a quantitative perspective, the price can reflect most of the cost related to abstraction and distribution. Qualitative groundwater protection, however, has entrenched complexities. Due to the intertemporal aspect and imperfect, although ever increasing knowledge, the financing of qualitative protection may shift during the coming years as the water supply companies are encouraged to focus more narrowly on initiatives directly related to their resource.

Our study shows that combined with the recent structural reforms of the environmental management authorities, the Water Sector Law sets the stage for a shift in a formerly accepted managerial practice. This is mainly seen as a drawback as it reduces the possibilities of the water supply companies to undertake groundwater protective actions that are seen as necessary by the individual companies and leaves them in a role where they are only operators of actions dictated by the municipality. The benefits may, on the other hand, be a better coordinated and integrated water management policy, where the groundwater protection is seen in a more holistic approach that also calls for actions in areas where the water supply companies have not so far been active. However, this calls for a strong incorporated and active integrating governance strategy from the local authorities. Only the future can show how this will come out.

References

Bakker, K. 2005: Neoliberalizing nature? Market environmentalism in water supply in England and Wales. Annals of the Association of American Geographers **95**, 542–565.

Jørgensen, L.F. & Stockmarr, J. 2009: Groundwater monitoring in Denmark: characteristics, perspectives and comparison with other countries. Hydrogeology Journal **17**, 827–842.

Kvale, S. 1997: Interview. En introduktion til det kvalitative forskningsinterview, 318 pp. København: Hans Reitzels Forlag.

Miljøministeriet 1999: Lovbekendtgørelsen nr 130 af 26. februar 1999 om vandforsyning mv.

Miljøministeriet 2009: Lovbekendtgørelsen nr 469 af 12. juni 2009 om vandsektorens organisering og økonomiske forhold.

Pedersen, P.E. 2010a: Vandforsyninger under hårdt pres. Vækst **131**(2), 12–13.

Pedersen, P.E. 2010b: Et væld af metoder til grundvandsbeskyttelse. Vækst **131**(2). Only available online: *http://www.hedeselskabet.dk/page.6360.aspx?recordid6360=335*

Petersen, J.D. 2011: Dyrebare dråber. Vandforsyningernes rolle i grundvandsbeskyttelse, 86 pp. Unpublished Master thesis, Roskilde Universitet, Danmark.

Sørensen, E. & Torfing, J. 2005: Netværksstyring: fra government til governance, 218 pp. Frederiksberg: Roskilde Universitetsforlag.

Thorling, L., Hansen, B., Langtofte, C., Brüsch, W., Møller, R.R., Mielby, S. & Højberg, A.L. 2011: Grundvand. Status og udvikling 1989–2010, 139 pp. Særudgivelse. København: De Nationale Geologiske Undersøgelser for Danmark og Grønland. Only available online: *http://www.geus.dk/publications/grundvandsovervaagning/1989_2010.htm*

Authors' addresses

J.D.P., *Roskilde University, Department of Technological and Socio-Economic Planning, Universitetsvej 1, DK-4000 Roskilde, Denmark.*
E-mail: *dyrby@ruc.dk*

L.F.J., *Geological Survey of Denmark and Greenland, Øster Voldgade 10, DK-1350 Copenhagen K, Denmark.*

Anorthosites in Greenland: a possible raw material for aluminium?

Christian Knudsen, Jan Wanvik and Henrik Svahnberg

The famous Swiss-born, Norwegian geologist and geochemist Victor Goldschmidt suggested that anorthosite could be used as a source of aluminium replacing bauxite, and acid leaching of the anorthosite was his innovative idea. Anorthosite is a rock type consisting of more than 90% plagioclase which is an acid-soluble, aluminium-rich silicate mineral occurring in basement rocks of both Norway and Greenland (Fig. 1). Experiments conducted in Norway during the century after Goldschmidt's initial idea showed that it is technically possible to use anorthosite as a raw material in the production of aluminium metal. Goldschmidt mapped parts of the large anorthosite massifs along Sognefjord in the period 1916–1919. During the Second World War, sampling and core drilling were conducted in Norway, and an anorthosite mine was opened by Norsk Hydro where up to 400 men were employed and some 15 000 tonnes of rock were quarried before sabotage ended the work in 1945. There was renewed interest in anorthosite as an alternative raw material for aluminium in Norway in the years 1976–1982, but experiments conducted in this period did not lead to an economically viable concept. Recent developments at the Institute for Energy Technology in Norway have led to the discovery of a more promising process based on nitric acid that can yield additional products such as Precipitated Calcium Carbonate (PCC) for the paper industry, amorphous silica and ammonium nitrate fertiliser. The process can also be used as a sink for CO_2 by taking CO_2 from, for example, a power plant and binding it to PCC.

Solubility as a function of mineral chemistry

The mineral plagioclase covers a range of compositions from albite ($NaAlSi_3O_8$) to anorthite ($CaAl_2Si_2O_8$) and forms a solid solution series. The solubility of plagioclase, and therefore of anorthosite, increases with the calcium content, expressed as the anorthite content or An% in the plagioclase (Fig. 2). The higher solubility of the calcium-rich plagioclase makes it more attractive as a source of aluminium, as does the content of aluminium which increases with the anorthite content (calcium content; Fig. 2). Anorthosite bodies in the inner Sognefjord–Voss area in western Norway have a calcium-rich plagioclase composition (Fig. 2) with an anorthite content of 65–78%. The solubility and aluminium content determine the quality of anorthosite as a raw material for aluminium production. To provide an overview of

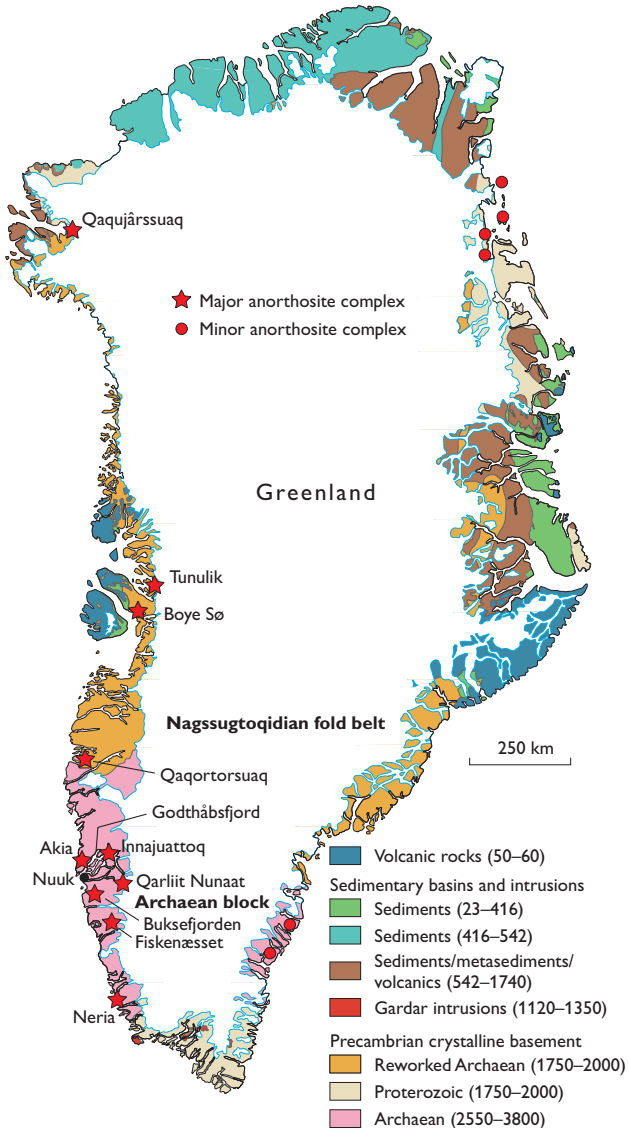

Fig. 1. Simplified geological map of Greenland showing anorthosite occurrences. Ages in million years.

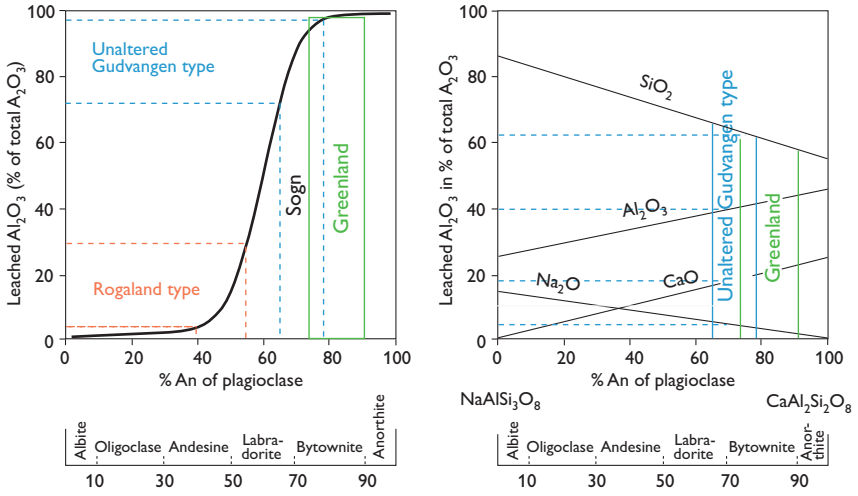

Fig. 2. Chemical composition (left) and solubility (right) of plagioclase. Modified from Wanvik (2000). Gudvangen, Rogaland and Sogn are anorthosite occurrences in Norway. Greenland is based on an average from Table 1.

the variation in these parameters and accordingly the value of anorthosite as a potential raw material in aluminium production, the Geological Survey of Denmark and Greenland conducted a survey of the compositional variation of anorthosite complexes in Greenland.

Anorthosites in Greenland

Anorthosite rock bodies are found in Archaean basement rocks in most parts of Greenland and constitute up to 5% of the bedrock in a region. They are easy to recognise in the field because of their very light weathering colour which also makes the rock very useful as a structural marker when mapping in deformed terranes. Anorthosite can be divided into several types including 'Archaean calcic anorthosite' (Ashwal 1993). The calcium content in the plagioclase of 'Archaean calcic anorthosite' is high (75–90% An). This feature distinguishes Archaean anorthosite from, for example, the 'Proterozoic (massif) type anorthosite' with 35–60% An. So far, only the Archaean type of anorthosite has been described from Greenland.

The Archaean anorthosite occurrences in Greenland are generally deformed and metamorphosed to such an extent that their genetic relationships are difficult to reveal. They often occur as decimetre- to metre-sized pods and inclusions in the country gneiss. However, there are a number of places where larger bodies of anorthosites are found with preserved primary textures and relationships. The most prominent occurrence is the Fiskenæsset complex consisting of anorthosite, leucogabbro, gabbro and ultramafic rocks. Here it has been demonstrated that anorthosite forms parts of large intrusions of basaltic composition and formed as cumulates by crystal fractionation (Windley *et al.* 1973; Myers 1975; Windley & Garde 2009).

Table 1. Average Al_2O_3, CaO, Fe_2O_3 and Na_2O compositions of anorthosites calculated from whole-rock analytical data

	N lat.	W long.	No of analyses	Al_2O_3	CaO	Fe_2O_3	Na_2O	CIPW % plag*	CIPW % An*
Fiskenæsset group 1†	63°15´	50°00´	13	30.6	16.3	2.5	1.8	90.1	83.8
Fiskenæsset group 2			3	32.5	16.3	1.9	1.8	94.1	83.6
Fiskenæsset group 3			3	30.5	12.5	1.5	4.0	92.4	65.7
Buksefjorden	63°55´	51°20´	6	29.3	14.1	1.5	2.2	90.7	73.7
Qarliit Nunaat (Godthåbsfjord)	64°04´	49°45´	1	28.5	11.9	0.9	4.1	93.0	61.0
Naajat Kuuat (Godthåbsfjord)	64°10´	50°03´	7	28.9	13.6	1.8	2.5	88.7	72.9
Storø (Godthåbsfjord)	64°23´	51°07´	1	32.3	16.0	0.6	2.1	96.6	81.3
Akia (Godthåbsfjord)	64°30´	52°06´	9	30.6	15.2	1.8	2.2	91.4	79.6
Ivisaartoq (Godthåbsfjord)	64°44´	49°42´	6	29.8	14.7	3.0	2.6	91.1	75.2
Innajuattoq (Godthåbsfjord)	64°45´	50°40´	1	31.8	16.0	1.5	2.0	91.6	84.4
Qaqortorsuaq	66°35´	52°12´	3	33.6	15.8	0.9	2.2	94.1	82.6
Tunulik	70°03´	51°15´	5	28.9	12.9	1.0	3.5	91.5	67.1
Qaqujârssuaq	77°35´	64°45´	2	29.9	14.9	1.2	1.7	91.6	77.3
Gudvangen (Norway)			8	30.1	14.1	0.8	2.9	94.6	72.0

* % plagioclase in rock and % An in plagioclase are based on CIPW norm calculations. † Fiskenæsset is grouped on the basis of its rare-earth element patterns following Polat *et al.* (2009).

Fig. 3. **A**: The anorthosite at Innajuattoq in the Archaean block northwest of Nuuk. The mountain is 1206 m high, and the cliff section is *c.* 1100 m high. **B**: Close-up view; length of hammer handle *c.* 60 cm.

The primary relationship to the surrounding rocks is often obscured by tectonic activity or intrusive contacts to younger granitoids. All the anorthosites studied here are assumed to belong to the calcic Archaean type but their composition varies, (1) among the different complexes, (2) within the complexes as a function of the stratigraphical position and (3) within the mineral grain – from core to rim, often due to recrystallisation during metamorphism.

Around 12 anorthosite complexes in Greenland have been mapped and described (Fig. 1). The northernmost one is the Qaqujârssuaq anorthosite, which is also the largest single anorthosite mass in Greenland covering *c.* 100 km² of Smithson Bjerge and an unknown area under the Inland Ice (Dawes 2006). It is a *c.* 500 m thick succession composed of *c.* 90% anorthosite, *c.* 10% leucogabbro and <1% gabbro which was emplaced *c.* 2700 Ma ago (Nutman 1984).

The Tunulik anorthosite is located in an area of Archaean rocks deformed and metamorphosed in Palaeoproterozoic time *c.* 1900 Ma ago. Generally, the anorthosite occurs as blocks and pods in the surrounding tonalitic to granodioritic gneisses (Andersen & Pulvertaft 1986). The anorthosite can be traced south to the *c.* 25 km² large Boye Sø anorthosite (Garde & Steenfelt 1989).

The first anorthosite body to be found in Greenland was the anorthosite at Qaqortorsuaq in the *c.* 1900 Ma old Palaeoproterozoic Nagssugtoqidian fold belt (Ellitsgaard-Rasmussen & Mouritsen 1954). This body is very large and the exploration company Kryolitselskabet Øresund A/S estimated that there are *c.* 100 million tonnes of anorthosite per vertical metre in the deposit and the mountain Qaqortorsuaq is *c.* 1300 m high (Gothenborg & Keto 1977). The highest concentration of anorthosite complexes in Greenland is found in the core of the Archaean block around Nuuk (Akia, Innajuattoq, Storø, Najaat Kuuat with Qarliit Nunaat, Nunatuasuk and Ivisaartoq; Fig. 1; Table 1). One of the anorthosite bodies is located at Innajuattoq (Fig. 3).

The Fiskenæsset anorthosite complex is one of the largest and best known Archaean anorthosite complexes worldwide. Parts of the complex have retained an igneous stratigraphy, cumulate textures, layering, grading and channel deposits (Windley *et al.* 1973; Windley & Smith 1974; Windley & Garde 2009; Myers 1975, 1976, 1985), showing that it is a sheet-like, layered basic intrusion. Based on *in*

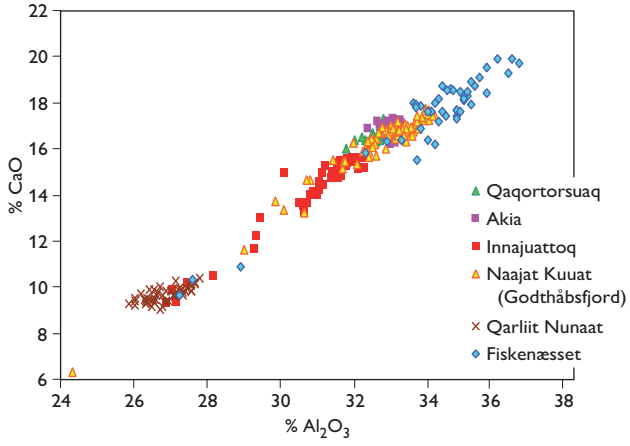

Fig. 4. Microprobe analyses of plagioclase from Greenland anorthosites showing CaO versus Al_2O_3 wt%. The range of plagioclase compositions is due to variations from core to rim in individual grains as well as to variations between different parts of the complexes. The linear relationship between CaO and Al_2O_3 is due to the coupled substitution of albite ($NaAlSi_3O_8$) by anorthite ($CaAl_2Si_2O_8$).

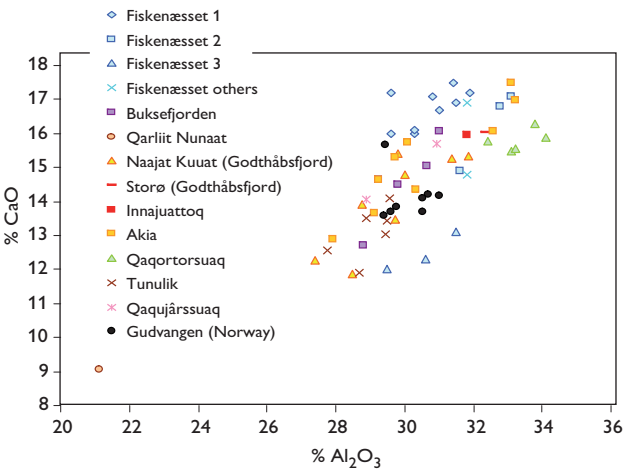

Fig. 5. Whole-rock analyses of anorthosites showing wt% CaO versus wt% Al_2O_3. Anorthosites in Greenland are compared to anorthosites from Gudvangen in Norway. Most of the Greenlandic occurrences have higher CaO content due to higher anorthite content. Hence their plagioclase is rich in both Ca and Al.

situ $^{207}Pb/^{206}Pb$ zircon ages of up to 2950 Ma, Keulen *et al.* (2010) concluded that the intrusion age is *c.* 2970 to 2950 Ma. The anorthosite unit is *c.* 250 m thick (Myers 1985). At localities where the anorthosite is least deformed, it typically appears as megacrystic with 1–10 cm equant, relict igneous plagioclase grains dispersed in 1–5 mm large metamorphic plagioclase. The main part of the anorthosite is deformed, and the plagioclase is metamorphic in a granular texture.

Anorthosite composition

There is a large range of plagioclase compositions among the anorthosite complexes in Greenland (Fig. 4) with the highest content of calcium found in the Fiskenæsset complex. Whole-rock analyses indicate that very calcium-rich plagioclase also occurs in the anorthosite at Akia (Fig. 5; Dymek & Owens 2001).

Most Greenland anorthosite rocks are more calcic than the Norwegian ones and according to the Norwegian experiences should be more soluble and hence more suitable as a raw material for aluminium production. A possible continuation of this project could be to collect samples from anorthosites in Greenland and conduct solubility tests using the Norwegian methods. The most promising occurrence is the Fiskenæsset complex which is the largest anorthosite in Greenland, has the highest bulk rock CaO content and contains the most calcic plagioclase in Greenland. The anorthosites at Akia, Innajuattoq and Qaqortorsuaq contain very calcic plagioclase and low contents of other minerals. These occurrences are located close to the sea and could be targeted in further studies.

Acknowledgement

The Bureau of Minerals and Petroleum in Nuuk is thanked for financial support.

References

Andersen, M.C. & Pulvertaft, T.C.R. 1986: Occurrences of anorthositic rocks in reworked Archaean basement in the Umanaq area, central West Greenland. Rapport Grønlands Geologiske Undersøgelse **129**, 18 pp.

Ashwal, L.D. 1993: Anorthosites, 422 pp. Berlin: Springer.

Dawes, P.R. 2006: Explanatory notes to the Geological map of Greenland, 1:500 000, Thule, sheet 5. Geological Survey of Denmark and Greenland Map Series **2**, 97 pp.

Dymek, R.F. & Owens, B.E. 2001: Chemical assembly of Archaean anorthosites from amphibolite- and granulite-facies terranes, West Greenland. Contributions to Mineralogy and Petrology **141**, 513–528.

Ellitsgaard-Rasmussen, K. & Mouritzen, M. 1954: An anorthosite occurrence from West Greenland. Meddelelser fra Dansk Geologisk Forening **12**, 436–442.

Garde, A.A. & Steenfelt, A. 1989: A new anorthosite/gabbro complex at Nûgssuaq, central West Greenland. Rapport Grønlands Geologiske Undersøgelse **145**, 16–20.

Gothenborg, J. & Keto, L. 1977: Report on the aerial reconnaissance between Sukkertoppen Ice Calot and Nordenskiölds Gletscher 1977, 84 pp. Unpublished report, Kryolitselskabet Øresund A/S, Copenhagen, Denmark (in archives of Geological Survey of Denmark and Greenland, GEUS Report File 20210).

Keulen, N., Næraa, T., Kokfelt, T.F., Schumacher J.C. & Scherstén A. 2010: Zircon record of the igneous and metamorphic history of the Fiskenæsset anorthosite complex in southern West Greenland. Geological Survey of Denmark and Greenland Bulletin **20**, 67–70.

Myers, J.S. 1975: Igneous stratigraphy of Archaean anorthosite at Majorqap qâva, near Fiskenæsset, South-west Greenland. Rapport Grønlands Geologiske Undersøgelse **74**, 27 pp.

Myers, J.S. 1976: Channel deposits of peridotite, gabbro and chromitite from turbidity currents in the stratiform Fiskenæsset anorthosite complex, southwest Greenland. Lithos **9**, 281–291.

Myers, J.S. 1985: Stratigraphy and structure of the Fiskenæsset complex, southern West Greenland. Bulletin Grønlands Geologiske Undersøgelse **150**, 72 pp.

Nutman, A. 1984: Precambrian gneisses and intrusive anorthosite of Smithson Bjerge, Thule district, North-West Greenland. Rapport Grønlands Geologiske Undersøgelse **119**, 31 pp.

Polat, A., Appel, P.W.U., Freyer, B., Windley, B., Frei, R., Samson, I.M. & Huang, H. 2009: Trace element systematics of the Neoarchaean Fiskenæsset anorthosite complex and associated meta-volcanic rocks, SW Greenland: evidence for a magmatic arc origin. Precambrian Research **175**, 87–115.

Wanvik, J.E. 2000: Norwegian anorthosites and their industrial uses, with emphasis on the massifs of the Inner Sogn–Voss area in western Norway. Norges Geologiske Undersøkelse Bulletin **436**, 103–112.

Windley, B.F. & Garde, A.A. 2009: Arc-generated blocks with crustal sections in the North Atlantic craton of West Greenland: crustal growth in the Archean with modern analogues. Earth-Science Reviews **93**, 1–30.

Windley, B.F. & Smith, J.V. 1974: The Fiskenæsset complex, West Greenland. Part II. General mineral chemistry from Qeqertarssuatsiaq. Bulletin Grønlands Geologiske Undersøgelse **108**, 54 pp.

Windley, B.F., Herd, R.K. & Bowden, A.A. 1973: The Fiskenæsset complex, West Greenland. Part I. A preliminary study of the stratigraphy, petrology and whole rock chemistry from Qeqertarssuatsiaq. Bulletin Grønlands Geologiske Undersøgelse **106**, 80 pp.

Authors' addresses

C.K., *Geological Survey of Denmark and Greenland, Øster Voldgade 10, DK-1350 Copenhagen K, Denmark.* E-mail: *ckn@geus.dk.*

J.W., *Geological Survey of Norway, Leiv Eirikssons vei 39, 7040 Trondheim, Norway.*

H.S., *Stockholm University, Svante Arrhenius väg 8, SE-106 91, Stockholm, Sweden.*

From 3D mapping to 3D modelling: a case study from the Skaergaard intrusion, southern East Greenland

Kristian Svennevig and Pierpaolo Guarnieri

The powerful 3D mapping tool at the photogrammetry laboratory of the Geological Survey of Denmark and Greenland (GEUS) is ideal for collecting high-quality 3D geological data in remote and inaccessible areas with a high degree of exposure such as Greenland (Vosgerau *et al.* 2010). So far this 3D mapping tool has been used to visualise and extract very precise geological data from aerial and oblique photographs. In the study reported on here, the 3D mapping tool was used to generate data for 3D geological modelling. The Skaergaard intrusion (Fig. 1) is a well-known Eocene layered gabbro. The study of the intrusion has had great importance for the understanding of magmatic petrology, magma differentiation and fractional crystallisation since the early studies by Wager & Deer (1939). It was chosen for 3D modelling because it is well studied from a petrological point of view and because the shape of the magma chamber was previously modelled in a network of 2D cross sections (Nielsen 2004). In this paper, it is modelled for the first time in 3D using a detailed 1:20 000 scale geological map (McBirney 1989), 1:27 000 scale aerial photographs from 1973, data from drill holes and geophysical data.

3D mapping

The 1:27 000 scale aerial photographs where scanned, triangulated and georeferenced with Socketset software. The geological map was digitised as well as georeferenced using 1:150 000 scale aerial photographs and finally draped on a high-resolution (10 × 10 m grid) digital elevation model derived from the 1:27 000 scale aerial photographs. Geological features were drawn as polylines from both the aerial photographs and the geological map. Visible parts of the outer boundary were collected using the 3D stereoplotter (Fig. 2A) with very high accuracy (Vosgerau *et al.* 2010). Oblique aerial photos were not used for 3D-mapping as the area is not sufficiently covered and the setting up of the few available photo lines is beyond the scope of this paper. Other boundaries defined from mineral parageneses and compositions (Wager & Brown 1968) were digitised from the 1:20 000 map in ArcGIS. The boundaries from the aerial photographs are much more accurate than those of the map (Fig. 3) because they represent directly observable geological features. Furthermore polylines from the aerial photographs have real 3D coordinates measured directly on the 3D stereo plotter, whereas polylines from the ArcGIS map have X-Y coordinates from the map and Z coordinates imported from the digital elevation model. This leads to additional uncertainty as elevations in the ArcGIS map and the digital elevation model are not generated from the same source and sometimes do not overlap in the entire area of interest.

Structural readings (dip direction and dip angle) for the geological boundaries were generated from polylines using the in-house-developed software tool GEUS Planes (Fig. 2B). This tool calculates strike, dip and standard deviations on strike and dip for each node (vertex) of a polyline, generating large amounts of strike-dip measurements from the 3D geometry of the geological boundaries.

3D modelling and discussion

The 3D modelling of the Skaergaard intrusion was carried out using the software tool Leapfrog-3D. This software can generate surfaces and volumes from structural readings,

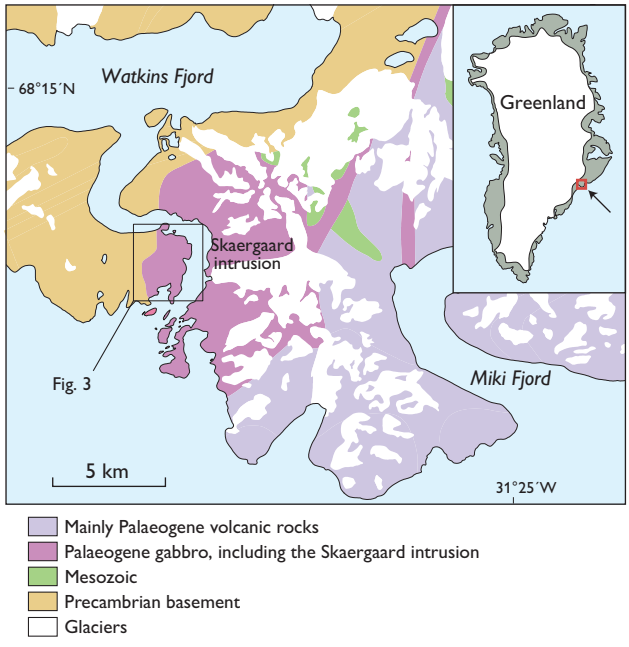

Fig. 1. The Skaergaard intrusion area, southern East Greenland.

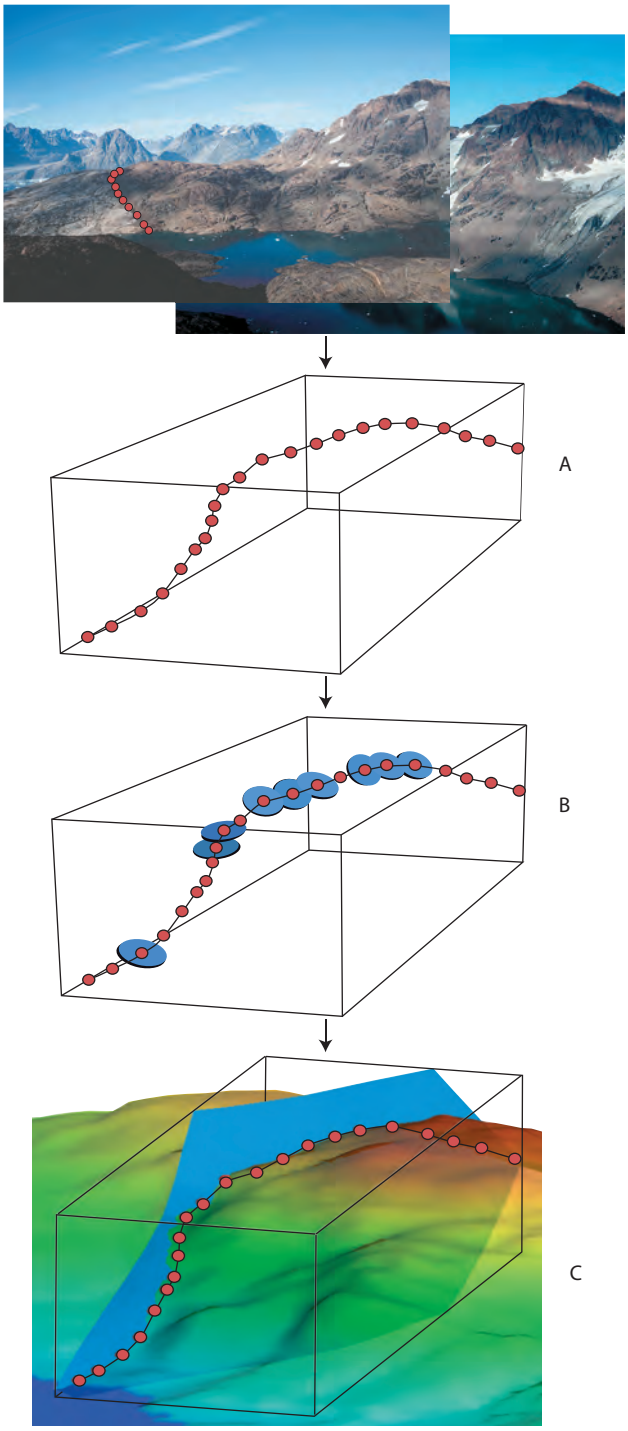

Fig. 2. Simplified workflow diagram describing the process of generating 3D data from photographs to 3D modelling. **A**: polylines representing geological boundaries or structures are extracted from a 3D stereo plotter. **B**: The nodes of the polylines are converted into structural readings (here shown as small blue discs) using the GEUS Planes tool. Measurements with a poorly defined plane (high standard deviation on either the dip, dip-azimuth or plane) are discarded. **C**: The structural readings are imported into a 3D modelling software (Leapfrog 3D) where surfaces and volumes can be generated and compiled to a 3D model of the geological object.

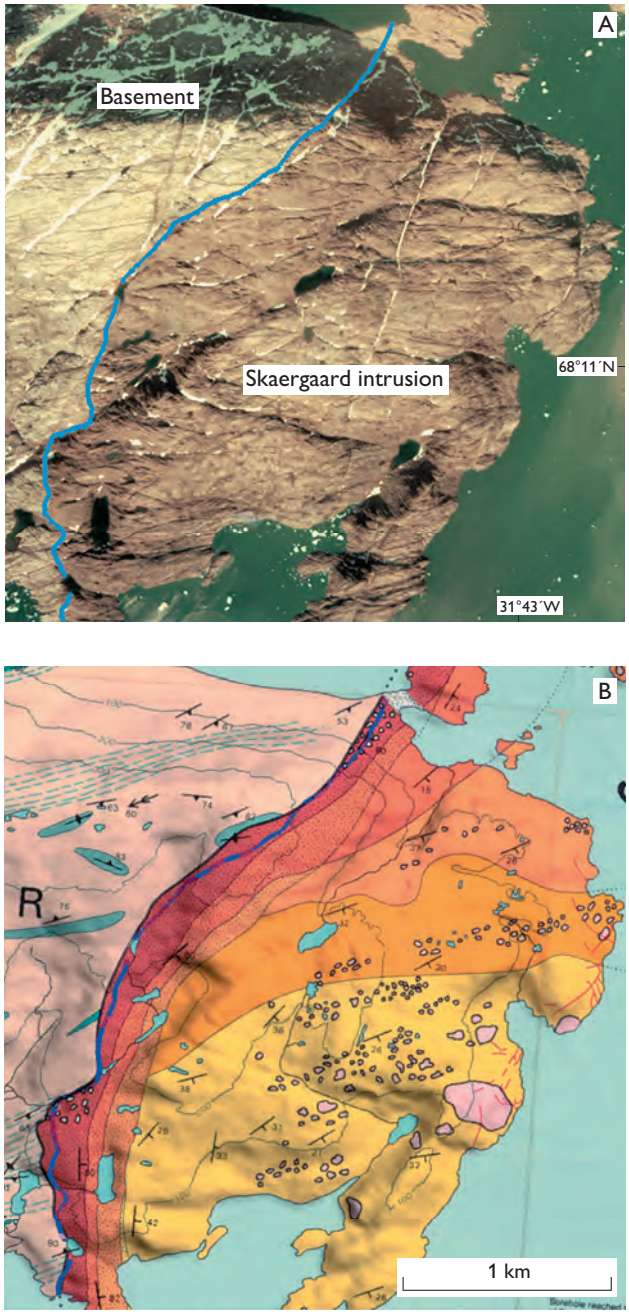

Fig. 3. Example of a polyline (blue) representing the boundary between the Skaergaard intrusion (dark grey in Fig. 3A, light yellow to red in Fig. 3B, representing different lithological units) and the basement (light grey in Fig. 3A, light skin tone in Fig. 3B). The same polyline is drawn on the 1:27 000 aerial photographs (**A**) and shown on the geological map of McBirney (1989) (**B**) for comparison. The difference between the locations of the two lines is up to 100 m.

points and polylines (Fig. 2C). In standard surface modelling, only a couple of structural readings are used for generating surfaces. The great number of structural readings produced by GEUS Planes present a problem to the modelling software making it necessary to manually select which strike-dip measurements to use for the construction of surfaces. This complication will be solved in a forthcoming upgrade of the GEUS Planes tool by changing the output and by using modelling software that can import the standard deviation as a parameter and use it to estimate the quality of the structural readings in the creation of surfaces.

In areas with no pre-Quaternary exposures, such as glaciated areas or water-covered areas, support points were introduced to guide the surfaces. Drill-hole data were also imported along with a geophysical gravity model of the floor of the intrusion (T.M. Rasmussen, personal communication 2011) to further improve the model. Due to erosion and lack of exposures the locations of the roof and northern boundary

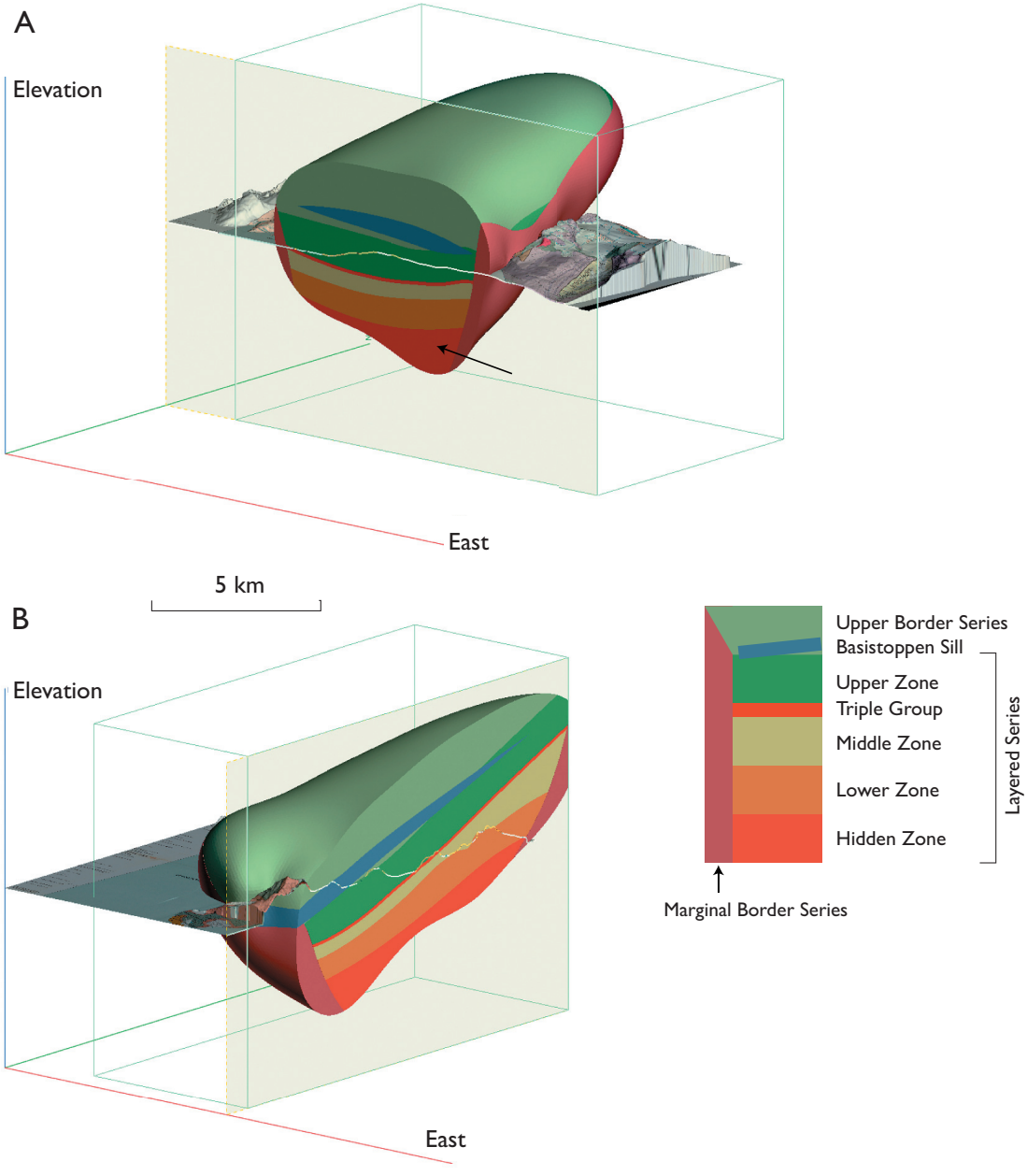

Fig. 4. 3D model of the Skaergaard intrusion in E–W (**A**) and N–S (**B**) sections. The view is towards 320° at a plunge of 15°. No vertical exaggeration. Notice the wedge-like shape of the Hidden Zone (black arrow in **A**).

of the intrusion are poorly constrained, and these were modelled with considerable uncertainty. Two structural readings (strike/dip, 180/20 S and 180/10 S) were constructed to guide the roof surface of the magma chamber. These orientations were estimated by extrapolating the roof boundary in the southern part of the intrusion (Wager & Deer 1939; Nielsen 2004) with the regional dip (10–20°S) of the Tertiary strata hosting the intrusion (Nielsen & Brooks 1981).

The geophysical model for the floor of the intrusion has the same dip as the regional strata of 10–20°S but also shows a dip of around 15° towards the east that is unexpected from the surface and drill-hole data used for generating the model. This is reflected in the wedge-like shaped of the Hidden Zone in the 3D model (Fig. 4A). Furthermore, the modelled floor of the intrusion near the northern boundary is located much more deeply than expected. Based on a single drill hole in the northern part of the intrusion that reaches the contact zone of the floor (Holness *et al.* 2007), unexposed gabbro of the intrusion is estimated to reach a depth of no more than 450 m (T.F.D. Nielsen, personal communication 2012), whereas the geophysical model predicts 1450 m. Several explanations can be suggested for this discrepancy: (1) The density of the gabbro at the northern margin may be underestimated, (2) uncertainty of the floor depth from drill-hole data or (3) rock types below the floor of the intrusion may have unexpected high densities. Irrespective of the various uncertainties, the preliminary estimate of the total volume of the intrusion is between 279 and 305 km^3 (depending on different estimates of the northern boundary). This is in good agreement with a previous estimate of 280 ± 23 km^3 (Nielsen 2004).

The Triple Group (Fig. 4), defined by three distinctive leucocratic layers in the uppermost part of the Middle Zone, is of particular interest as it is rich in palladium and gold (Bird *et al.* 1991; Nielsen *et al.* 2005). The degree of detail in the model presented here is too low for a thorough investigation of these levels, but our data reflect the concave nature of the layers (Fig. 4) also described by Nielsen (2004). Future expansion of the model with data from oblique photographs can greatly improve our understanding of the Triple Group, because it is clearly seen on photographs (fig. 11c in Brooks 2011), being well exposed on the steep mountain slopes.

Concluding remarks

The 3D mapping tool at the GEUS photogrammetry laboratory is ideal for generating high quality data for 3D modelling. It is, however, necessary to fine-tune the GEUS Planes tool and to conduct the modelling in a more advanced software such as GoCAD or Move in order to take full advantage of the high quality and quantity of the data. With these software tools, it is also possible to do advanced modelling and, for example, carry out balanced unfolding and backstripping of geological structures and units.

Acknowledgements

Max Nykjær Strunck is thanked for setting up the aerial photographs and for helping with the digital elevation model. Thorkild Maack Rasmussen is thanked for producing the geophysical model and Troels F.D. Nielsen is thanked for valuable discussion of the geology of the Skaergaard intrusion.

References

Bird, D.K., Brooks, C.K., Gannicott, R.A. & Turner, P.A. 1991: A gold-bearing horizon in the Skaergaard intrusion, East Greenland. Economic Geology **86**, 1083–1092.

Brooks, C.K. 2011: The East Greenland rifted volcanic margin. Geological Survey of Denmark and Greenland Bulletin **24**, 96 pp.

Holness, M.B., Nielsen, T.F.D. & Tegner, C. 2007: Textural maturity of cumulates: a record of chamber filling, liquidus assemblage, cooling rate and large-scale convection in mafic layered intrusions. Journal of Petrology **48**, 141–157.

McBirney, A.R. 1989: Geological map of the Skaergaard intrusion, East Greenland. Eugene, USA: University of Oregon (map sheet).

Nielsen, T.F.D. 2004: The shape and volume of the Skaergaard intrusion, Greenland: implications for mass balance and bulk composition. Journal of Petrology **45**, 507–530.

Nielsen, T.F.D. & Brooks, C.K. 1981: The East Greenland rifted continental margin: an examination of the coastal flexure. Journal of the Geological Society (London) **138**, 559–568.

Nielsen, T.F.D., Andersen, J.C.Ø. & Brooks, C.K. 2005: The Platinova Reef of the Skaergaard intrusion. In: Mungal, J.E. (ed.): Exploration for platinum group element deposits. Mineralogical Association of Canada Short Course Series **35**, 431–455.

Vosgerau H., Guarnieri P., Weibel R., Larsen M., Dennehy, C., Sørensen, E.V. & Knudsen, C. 2010: Study of a Palaeogene intrabasaltic sedimentary unit in southern East Greenland: from 3-D photogeology to micropetrography. Geological Survey of Denmark and Greenland Bulletin **20**, 75–78.

Wager, L.R. & Deer, W.A. 1939 (re-issued 1962): Geological investigations in East Greenland. Part III. The petrology of the Skaergaard intrusion, Kangerdlugssuaq, East Greenland. Meddelelser om Grønland **105**(4), 352 pp.

Wager, L. R. & Brown, G.M. 1968: Layered igneous rocks, 588 pp. Edinburgh: Oliver and Boyd.

Authors' address

Geological Survey of Denmark and Greenland, Øster Voldgade 10, DK-1350 Copenhagen K, Denmark. E-mail: *ksv@geus.dk*

Geological assessment of the East Greenland margin

Michael B.W. Fyhn, Thorkild M. Rasmussen, Trine Dahl-Jensen, Willy L. Weng, Jørgen A. Bojesen-Koefoed and Tove Nielsen

The East Greenland margin consists of a number of sedimentary basins, platforms and structural highs (Figs 1, 2). Due to the challenges imposed by the Arctic climate, the region is in an early stage of exploration, and knowledge of the geology and petroleum potential of the margin is limited. However, the significant prospectivity of the conjugated European North Atlantic margin and the nature of the North-East Greenland onshore geology prompt for future offshore exploration. The US Geological Survey thus highlighted the North-East Greenland margin in their latest assessment of the Arctic region (Gautier *et al*. 2011). With a mean estimate of undiscovered recoverable oil, gas, and natural gas liquids of approximately 31 billion barrels of oil equivalents, the US Geological Survey ranked the North-East Greenland margin fourth in the entire Arctic region, only superseded by known producing petroleum provinces.

In preparation for the initial East Greenland licence rounds in 2012 and 2013 the Geological Survey of Denmark and Greenland gathers geological information on the margin necessary for the decision process of the Greenland authorities regarding exploration. Geophysical analyses complemented by well-data, onshore geology and information from the conjugated Atlantic margin form the backbone of the study. The East Greenland margin is covered by an open seismic grid supplemented by gravimetric and magnetic data. All existing 2D seismic, gravimetric and magnetic data are included in the current study. Most of the data are confidential. Restricted by the general confidential nature of the project, this paper aims to summarise the geology of the East Greenland margin based on the current and previous studies and to briefly assess some of the implications for the regional petroleum prospectivity.

East Greenland offshore geology

The East Greenland margin stretches almost 3000 km from Kap Farvel in the south to Nordostrundingen in the north (Fig. 1). In the south it is narrow, but north of Liverpool Land it begins to widen to more than 300 km. The geology varies considerably along its length.

East Greenland margin south of Shannon

A continuous Paleocene–Eocene (61–53 Ma) pre- to post-break-up volcanic cover blankets almost the entire East Greenland margin between Kap Farvel and the island of Shannon (Fig. 1). Paleocene – Early Eocene magmatism re-

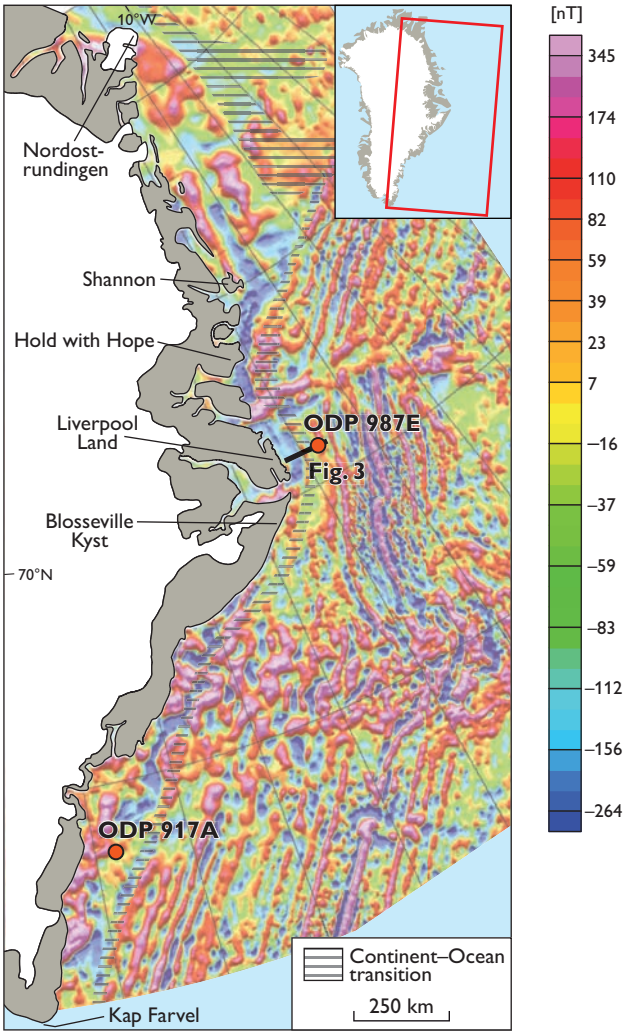

Fig. 1. The East Greenland margin from Kap Farvel to Nordostrundingen with offshore magnetic total field anomaly from the CAMP-GM compilation (Gaina *et al*. 2009).

cords the trace of the Icelandic hotspot that induced magmatism along most of the proto-North Atlantic margin and likely led to continental break-up between Europe and Greenland.

Thick seaward-dipping reflection packages interpreted as basalt flows exist near the continent–ocean transition indicating the presence of a very thick basalt-dominated succession below the distal part of the margin (Fig. 3). Basalt successions several hundred metres to kilometres thick exist onshore central East and North-East Greenland. It is likely that similar and thicker Paleocene – Lower Eocene basalt successions cover large parts of the offshore margin judging from seismic data, wells and onshore analogies (Fig. 2).

Only the ODP well 917A offshore South-East Greenland penetrates the entire basaltic cover (Fig. 1; Larsen & Saunders 1998). The well was drilled on the shoreward part of the margin and encountered 779.5 m of mainly basalts and

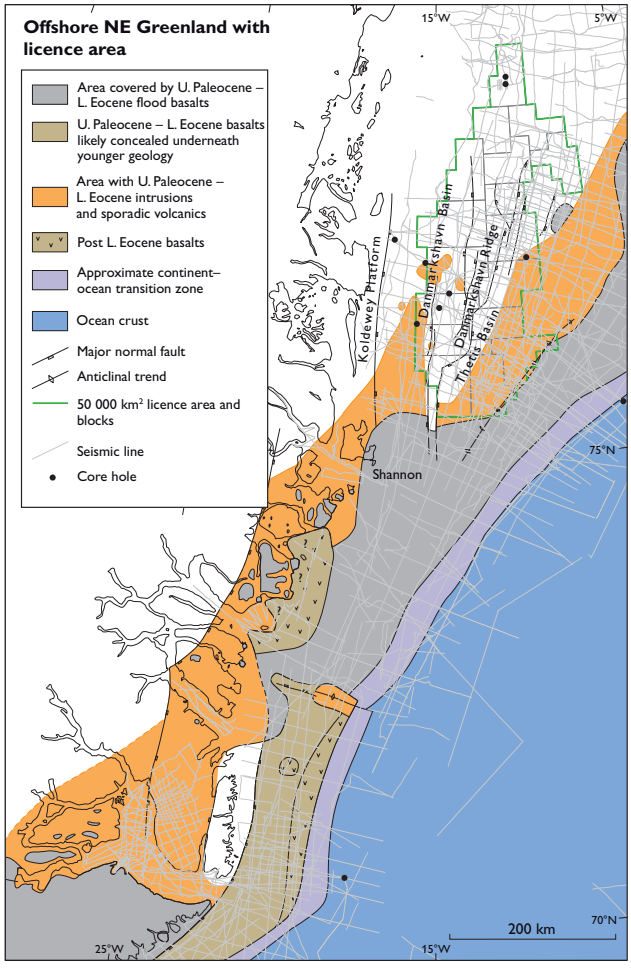

Fig. 2. The extent of massive volcanism along the North-East Greenland margin. Magmatism influenced areas up to 200 km north of the basalt cover as indicated by the heavily intruded part of the Thetis and Danmarkshavn Basins.

thus documents the presence of a thick volcanic cover in the shoreward part of the margin that, according to seismic evidence, significantly thickens seawards.

Offshore Liverpool Land, the Paleocene/Eocene top-basalt surface is not clearly discernable on all seismic transects. However, this is probably due to the deep burial of the basalt succession beneath a thick post-basaltic cover. In the area offshore Hold with Hope, the presence of volcanics younger than the regional Upper Paleocene – Lower Eocene flood basalts is interpreted from seismic data (Fig. 2). These are likely to be genetically related to Middle Eocene – earliest Miocene magmatism observed immediately onshore.

Sub-basalt sediments. The Tertiary basalt cover generally impedes seismic imaging of the deeper geology. Offshore South-East Greenland, sub-basaltic acoustic velocities derived from refraction seismic data generally range from 4.5 to 6 km/s increasing downwards (Hopper *et al.* 2003), which does not provide unequivocal evidence for regional, thick sub-basaltic sedimentary basins.

A sub-basaltic succession of deformed metasediments barren of fossils drilled in ODP well 917A was suggested to be Upper Cretaceous to Lower Paleocene in age, like onshore sediments farther north (Larsen & Saunders 1998). However, the succession could also represent much older Caledonian metasediments formed in a foreland setting, comparable to onshore metasediments farther to the north and lying beneath the conjugated British margin.

Offshore North-East Greenland, Upper Palaeozoic – Mesozoic deposits below the basalts are suggested by the presence of thick such deposits along the shore, immediately onshore and on the conjugated Norwegian North Atlantic margin. Moreover, a thick pre-basaltic sedimentary succession can be recognised offshore Shannon, continuing southwards below the basalts.

Post-Paleocene sediments. The Eocene and younger succession between Kap Farvel and Shannon attains thicknesses up to *c.* 3 sec two-way travel time (TWT). The succession is absent or very thin shoreward, and over large areas, break-up volcanics and Upper Palaeozoic and Caledonian basement crop out at the seafloor.

Farther offshore, an Eocene and younger shelf progradation along most of the margin resulted in the build-up of the prominent modern shelf-slope that generally straddles the continent–ocean transition. The Blosseville Kyst Fault Zone along the Blosseville Kyst and its northern continuation the Liverpool Land Fault Zone downfault the break-up volcanic cover with up to 2 sec TWT (Fig. 2). Rifting along Blosseville Kyst and Livepool Land Fault Zones was likely

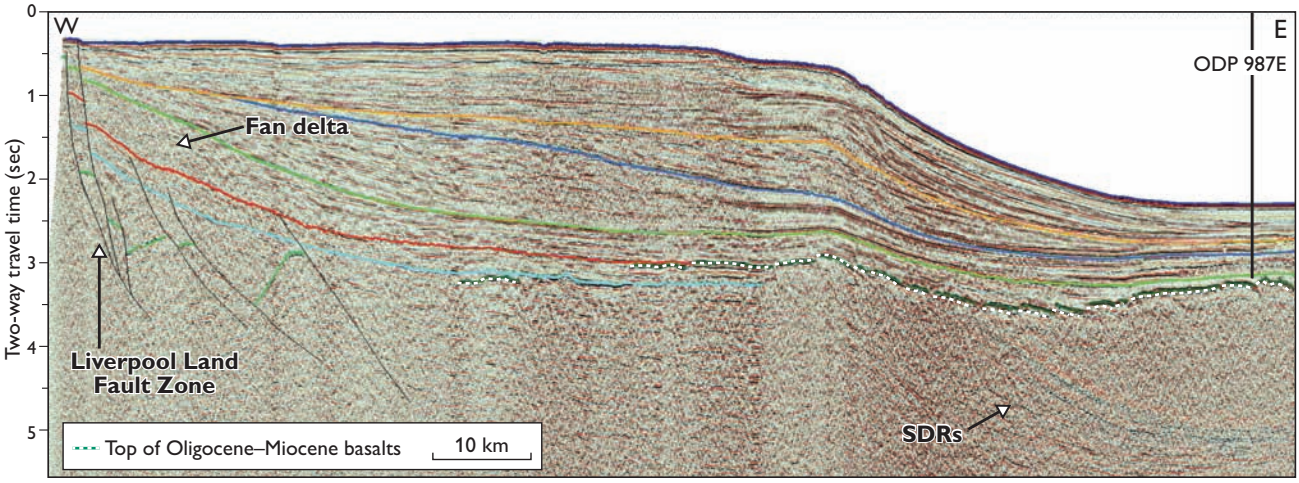

Fig. 3. An E–W seismic profile crossing the Liverpool Land Fault Zone and related syn-tectonic fan delta deposits and the continent–ocean transition indicated by seaward-dipping reflectors (SDRs). The ODP 987E well drilled Recent to Miocene strata and terminated slightly above the basalts.

associated with a westward jump of the spreading axis and the separation of the Jan Mayen microcontinent from central East Greenland during mid-Cenozoic time (Mjelde *et al*. 2008). Faulting mostly affected the lower part of the post-break-up succession, and a significant syn-tectonic fan delta flanks the fault zones suggesting (?)Late Eocene/Oligocene to *c.* Early Miocene faulting (Fig. 3). Faults only penetrate the seafloor near the coast where erosion and non-deposition have prevented fault burial.

East Greenland margin north of Shannon

North of the island of Shannon, the landward edge of the basalt cover curves to the east and continues farther seawards to the north where a wide basalt belt fringes the continent–ocean transition (Fig. 2). This leaves the shelf area north of Shannon virtually unaffected by Tertiary flood basalts and thus permits fair to good seismic imaging of Paleocene and older successions. As a result, up to *c.* 10 sec TWT several deep sediment-filled basins can be recognised north of Shannon that are likely to correspond to between 15 and 20 km of sedimentary infill.

The area can be structurally divided into the Danmarkshavn and Thetis Basins separated by the Danmarkshavn Ridge – a *c.* 300 km long rifted basement high (Fig. 2). The Danmarkshavn Basin is downfaulted relative to the Koldewey Platform to the west and the Danmarkshavn Ridge to the east. The Thetis Basin marks the oceanward part of the North-East Greenland margin that borders the North Atlantic oceanic crust. The depositional succession filling in the Thetis Basin may be of comparative thickness to that of the Danmarkshavn Basin, but there are significant differences in the geological development of the two basins.

The Koldewey Platform makes up an area of sediment-covered, more shallow basement bridging the Danmarkshavn Basin and the onshore basement province. The Danmarkshavn Ridge stands in marked contrast to the deeply downfaulted Thetis Basin farther east. As the high degrades into fault blocks to the north, the ridge plunges and the structural separation of the Thetis and Danmarkshavn Basins crumbles.

Structural and stratigraphic development. The deepest deposits in the Danmarkshavn Basin and on the Danmarkshavn Ridge form a prominent syn-rift succession interpreted to be Devonian and Carboniferous in age (Hamann *et al*. 2005). The unit is located in a rift system often confined by low-angle extensional faults, which may reflect extensional reactivation of Caledonian thrust faults.

The syn-rift succession is overlain by a unit in the central and southern part of the Danmarkshavn Basin that has in places been mobilised into diapiric and pillow-like structures interpreted as salt kinetic features. The succession is interpreted as Lower Carboniferous to Early Permian deposits comparable to coeval sediments in the western part of the Barents Sea (Hamann *et al*. 2005).

The Late Palaeozoic successions are buried beneath an up to a few kilometres thick unit only moderately affected by syn-depositional faulting and interpreted as Upper Permian – Jurassic deposits. By analogy to the conjugated Atlantic margin and onshore geology, the Upper Permian – Jurassic succession is likely to contain a number of prominent source rock intervals. Of these the Upper Jurassic equivalent to the Kimmeridge Clay Formation may be of particular importance to potential petroleum systems in the region.

The top of the Jurassic is marked by a pronounced angular unconformity associated with the onset of Cretaceous rifting

(Hamann *et al*. 2005). Cretaceous rifting resulted in several kilometres of downfaulting towards the Thetis Basin, and to a lesser extent also along the margins of the Danmarkshavn Basin. Consequently, the Danmarkshavn Ridge became an elevated rift-shoulder subject to erosion during most of the Cretaceous. In contrast, vast amounts of sediment were shed into the adjacent basins and kilometre-thick Cretaceous successions exist in the depocentres. Large fault- and anticlinal structures within Cretaceous and older successions formed in association with the Cretaceous extension. Many of these resemble structures hosting world-class oil and gas fields on the conjugate European Atlantic margin, thus boosting expectations for the North-East Greenland margin.

A change from fault-controlled subsidence concentrated along the basins to regional eastward tilting took place close to the Cretaceous/Tertiary boundary. The change resulted in flooding and burial of the Danmarkshavn Ridge during the Early Tertiary and instigated regional eastwards progradation across the basin areas.

Only modest volcanism, if any, took place across the basins north of Shannon. However, the southern Danmarkshavn and Thetis Basins were heavily intruded far north of the edge of the East Greenland basalt province, which degrades seismic imaging of the deepest stratigraphy over large areas. During mid-Tertiary time, sediment supply increased resulting in build-up and eastward progradation of a steep shelf-slope. This was likely caused by denudation of the East Greenland margin and the inner basin areas. As a result, the Lower Tertiary and Mesozoic deposits lie beneath the Plio/Pleistocene sediments along the inner half of the North-East Greenland shelf.

Implications for the petroleum prospectivity offshore East Greenland

Assessment of the petroleum prospectivity along the South-East and central East Greenland margin is associated with considerable uncertainties. A sub-basaltic source rock seems to be a prerequisite for a working petroleum system along the margin, but the thick volcanic cover complicates analysis of the deeper geology. Regional presence of sub-basaltic basins is at present uncertain offshore South-East Greenland, which also makes the prediction of an effective petroleum system along this part of the margin uncertain. Farther north between Liverpool Land and Shannon the chances of sub-basaltic basins containing significant source-rock intervals are high. However, interpretation of the sub-basaltic structural style is problematic at present and the maturation history of potential source-rock intervals is uncertain, which complicates the prospectivity assesment.

Farther north, extreme sea-ice conditions are a major impediment to future exploration. In addition, Tertiary uplift and erosion as well as past glacial advances across the shelf may have affected the regional petroleum potential. However, the presence of large structures and the good chance of adequately matured source-rock intervals urge for further investigation. The highest density of structures is located along the flanks of the basins and across the Danmarkshavn Ridge, which are also the areas covered in the coming licence rounds (Fig. 2). Many of these structures are associated with significant potential direct hydrocarbon indicators, which may reflect the presence of significant petroleum accumulations offshore North-East Greenland. This is highly encouraging for further exploration in one of the last frontier areas on Earth.

Acknowledgement

The Bureau of Minerals and Petroleum, Nuuk, is acknowledged for funding.

References

Gaina, C., Werner, S.C. & the CAMP-GM group 2009: Circum-Arctic mapping project – gravity and magnetic maps. Report **2009.010**, 21 pp. Trondheim: Geological Survey of Norway.

Gautier, D.L. *et al*. 2011: Assessment of NE Greenland: prototype for development of Circum-Arctic resource appraisal methodology. In: Spencer, A.M. *et al*. (eds): Arctic petroleum geology. Geological Society Memoirs (London) **35**, 663–672.

Hamann, N.E., Whittaker, R.C. & Stemmerik, L. 2005: Geological development of the Northeast Greenland shelf. In: Doré, A.G. & Vining, B.A. (eds): Petroleum geology: North-West Europe and global perspectives. Proceedings of the 6th Petroleum Geology Conference, 887–902. London: Geological Society.

Hopper, J.R., Dahl-Jensen, T., Holbrook, W.S., Larsen, H.C., Lizarralde, D., Korenaga, J., Kent, G.M. & Kelemen, P.B. 2003: Structure of the SE Greenland margin from seismic reflection and refraction data: Implications for nascent spreading center subsidence and asymmetric crustal accretion during North Atlantic opening. Journal of Geophysical research **108**, 2269, *http://dx.doi.org/10.1029/2002JB001996*

Larsen, H.C. & Saunders, A.D. 1998: Tectonism and volcanism at the southeast Greenland rifted margin: a record of plume impact and later continental rupture. In: Saunders, A.D., Larsen, H.C. & Wise, S.W. (eds): Proceedings of the Ocean Drilling Program Scientific results **152**, 503–533.

Mjelde, R., Raum, T., Breivik, A.J. & Faleide, J.I. 2008: Crustal transect across the North Atlantic. Marine Geophysical Research **29**, 73–87.

Authors' address

Geological Survey of Denmark and Greenland, Øster Voldgade 10, DK-1350 Copenhagen K, Denmark. E-mail: *mbwf@geus.dk*

New evidence for possible generation of oil off south-western Greenland

Troels Laier and Hans Peter Nytoft

In 2011, traces of bitumen in the 1160 Ma old Ilímaussaq intrusion in South Greenland have been examined in order to determine their origin. The investigation was prompted by the recent interest in hydrocarbon exploration off western Greenland, an interest expressed in the form of four new licences in the region (Christiansen 2011). The hydrocarbon potential in the region was realised after reinterpretation of seismic profiles across the Labrador Sea, and this indicates the presence of a sedimentary basin off south-western Greenland (Fig. 1; Chalmers & Pulvertaft 2001). However, the main problem in petroleum exploration off south-western Greenland is that no prolific marine source rocks have been demonstrated (Christiansen 2011). Therefore, any trace of hydrocarbons, however small that may help demonstrate the occurrence of source rocks in the region, deserves careful examination.

Recently, bitumen biomarkers have been used to question the presumed abiogenic origin of hydrocarbons in crystalline rocks of the Ilímaussaq intrusion (Laier & Nytoft 2012). In this paper, we focus on the origin of the bitumen and compare it with previous finds in central West Greenland. The presence of hydrocarbons in the Ilímaussaq intrusion has been known since 1970 (Petersilie & Sørensen 1970) but unlike the discovery of oil seeps in the Nuussuaq region in central West Greenland twenty years later, which had a positive impact on petroleum exploration (Christiansen 2011), the hydrocarbons in the Ilímaussaq intrusion were largely ignored in the context of offshore exploration. The reason for this is twofold: (1) hydrocarbons in the Ilímaussaq intrusion are much more difficult to recognise than on Nuussuaq, and (2) analytical results are confusing with respect to the origin of the hydrocarbons. Discrete millimetre-size hydrocarbon accumulations have only been observed twice, and samples of this material were unfortunately not available for analysis in the present investigation. The material, which is a waxy paraffinic hydrocarbon of $C_{28}H_{56}$, was located in vugs of pegmatite veins and labelled as an evenkite-like mineral by Konnerup-Madsen *et al.* (1979). Otherwise hydrocarbons in the Ilímaussaq intrusion only exist in fluid inclusions, mainly as C_1–C_5, and as dispersed bitumen invisible to the naked eye. The stable carbon isotopic ratio of methane ($\delta^{13}C = -7‰$) released from the inclusions by crushing (Petersilie & Sørensen 1970) differed from that of associated methane in most oil and gas reservoirs, which has $\delta^{13}C$ values of –30 to –50‰. The ratio was closer to the isotopic ratio of primodial carbon of the Earth's mantle, which has $\delta^{13}C$ values around –5‰. The paraffinic hydrocarbons of 'evenkite' on the other hand had a $\delta^{13}C$ value of –29‰, which is within the expected range for hydrocarbons generated by thermal maturation of organic matter (Konnerup-Madsen *et al.* 1988).

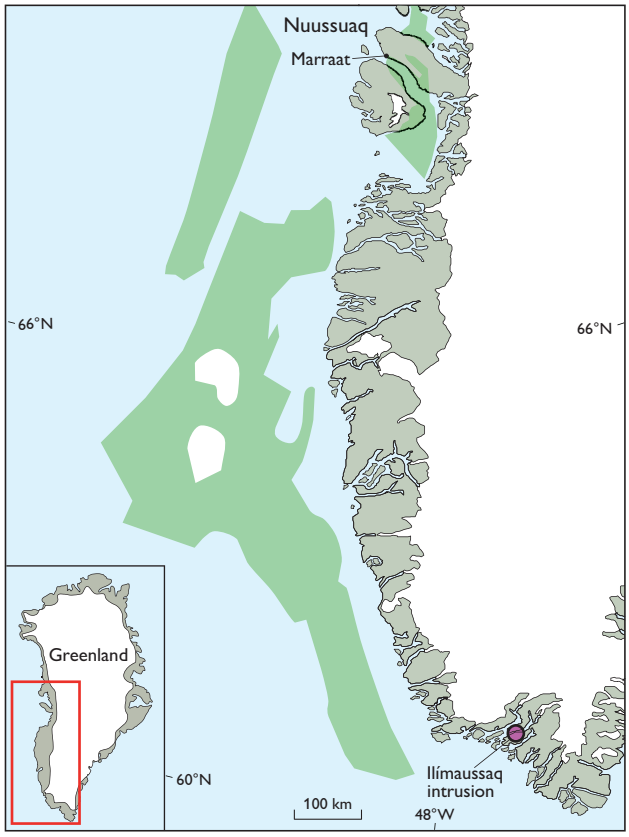

Fig. 1. Map of south-western Greenland showing the distribution of Mesozoic/Cenozoic rift basins offshore (green). Modified from Chalmers & Pulvertaft (2001). Oil seeps occur on Nuussuaq.

 Geological Survey of Denmark and Greenland Bulletin 26, 65–68. Open access: www.geus.dk/publications/bull

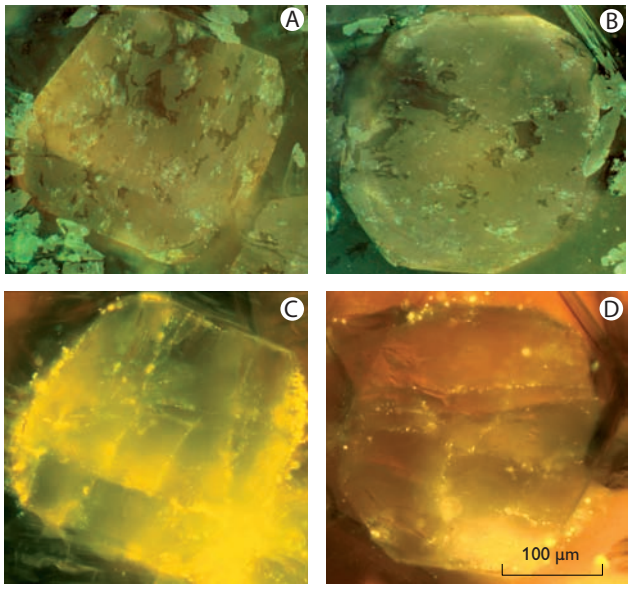

Fig. 2. Photomicrographs of lujavrite (GGU 57033) viewed under visible light (**A, B**) and in ultraviolet light (**C, D**) showing hydrocarbons along the edges of eudialyte crystals and as traces of tiny inclusions within the crystals.

Dispersed bitumen in crystalline rocks

The distribution of bitumen was examined by microscopy using ultraviolet light, which causes the aromatic constituents of bitumen to fluoresce. Unfortunately, a number of the rather common minerals, e.g. sodalite, in different rock types of the Ilímaussaq intrusion also fluoresce strongly making it almost impossible to indentify traces of bitumen with certainty in some samples. Lujavrite contains only little sodalite and offers the best possibility to study the distribution of bitumen (Fig. 2). The bitumen occurs along crystal edges and as trails of tiny inclusions within single crystals of, for example, eudialyte. Trails of tiny inclusions are usually taken as evidence of a secondary origin formed in healed fractures. Thus hydrocarbons probably migrated through the rock and were trapped in certain minerals.

Bitumen content and composition

It was possible to extract bitumen from naujaite, kakortokite and lujavrite, which are the three major rock types in the Ilímaussaq intrusion, by using a 7:1 mixture of dichloromethane and methanol. The bitumen content varied from 110 to 300 mg per kg rock and consisted of paraffins (20%), aromates (20%), NSO compounds (compounds with nitrogen, sulphur and oxygen; 50%) and asphaltenes (10%). The non-polar fraction from the different rock extracts was analysed by gas chromatography with a flame-ionisation detector for total composition and mass spectrometry for biomarker

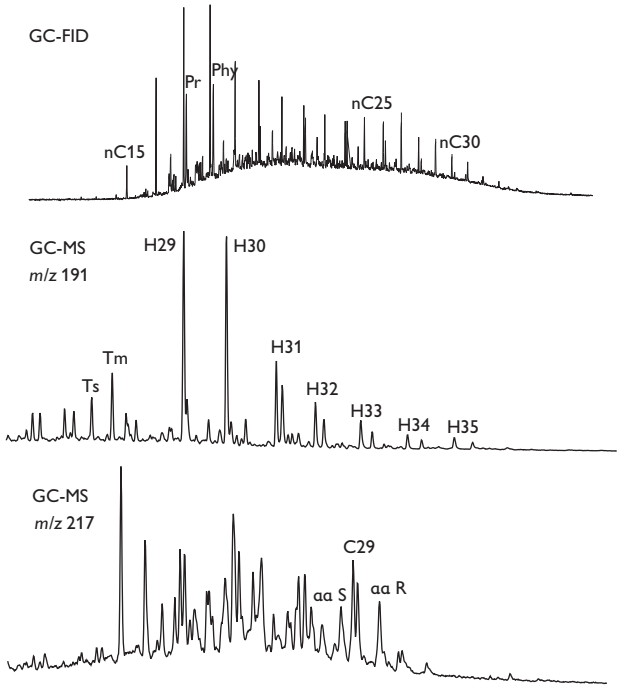

Fig. 3. Chromatograms of the aliphatic fraction of extract from Ilímaussaq kakortokite *m/z* 191 (hopanes+tricyclic) and *m/z* 217 (steranes). **FID**: flame ionisation detector, **GC-MS**: gas chromatography - mass spectrometry.

characterisation (Fig. 3). All samples gave very similar *m/z* 217 chromatograms showing a typical marine sterane distribution, although the presence of oleananes in the *m/z* 191 chromatogram suggests some input from land plants. Oleananes are derived from angiosperms, which appeared in the Late Cretaceous, and hence the presence of oleananes provides a maximum age for the source of the bitumen. Since other triterpanes are known to co-elute with oleananes, gas chromatograph mass spectrometry (GC-MS-MS) was also conducted to confirm their presence (Fig. 4). The GC-MS-MS analysis not only confirmed the presence of oleananes but also showed the existence of bicadinanes, which is a less common group of biomarkers from land plants from Late Cretaceous or Tertiary. Oleananes and bicadinanes were also observed in oil seeps from the Nuussuaq region (Fig. 4; Bojesen-Koefoed *et al.* 1999; Nytoft *et al.* 2002).

Migration and entrapment of hydrocarbons

Not only is bitumen much more difficult to recognise in rocks from the Ilímaussaq intrusion than in basalts from Nuussuaq, but the migration route of hydrocarbons to the Ilímaussaq intrusion is also less evident. In Nuussuaq the oil seeps are found in Tertiary plateau basalts overlying Cretaceous and Tertiary sediments, some of which are potential

source rocks. In the Ilímaussaq intrusion, the bitumen is found in Proterozoic crystalline rocks which are much older than the source rock, which is not older than Late Cretaceous as shown by the presence of oleanes and bicadinanes. In contrast to the Nuussuaq region, no potential source rock for hydrocarbons has been reported in South Greenland, where Proterozoic gneisses and granites, igneous and sedimentary rocks are found. The youngest rocks in South Greenland are those of the Gardar Province (*c.* 1300–1100 Ma), which is dominated by continental sandstones and lavas with numerous dykes and large intrusions (Poulsen 1964), one of which is the Ilímaussaq peralkaline intrusion. The Ilímaussaq intrusion solidified 3–4 km below the surface but is now exposed as a result of erosion. The latest uplift and erosion started *c.* 35 Ma ago according to thermo-chronometric investigations (Japsen *et al.* 2006). However, the latest uplift phase was preceded by subsidence during Late Cretaceous to Eocene. During this subsidence phase the region was prob-

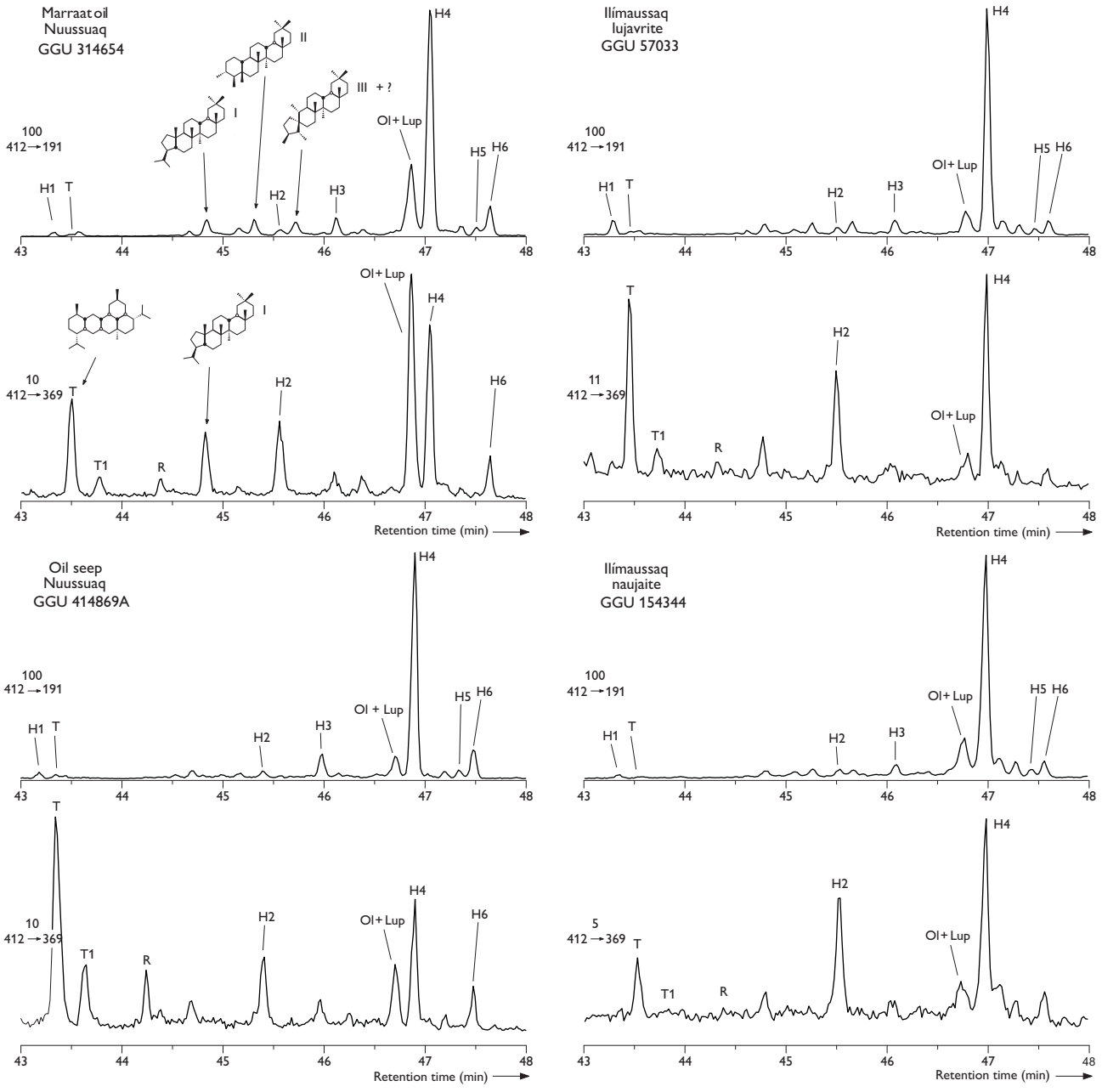

Fig. 4. Pentacyclic C_{30} triterpanes in an Ilímaussaq bitumen (412 → 191 and 412 → 369). Numbered peaks: oleananes (**Ol** + **Lup**) and similar land-plant components (**I** – **III**). Peaks **H1**–**H6**: hopanoids. Peaks **T**, **T1** and **R**: bicadinanes.

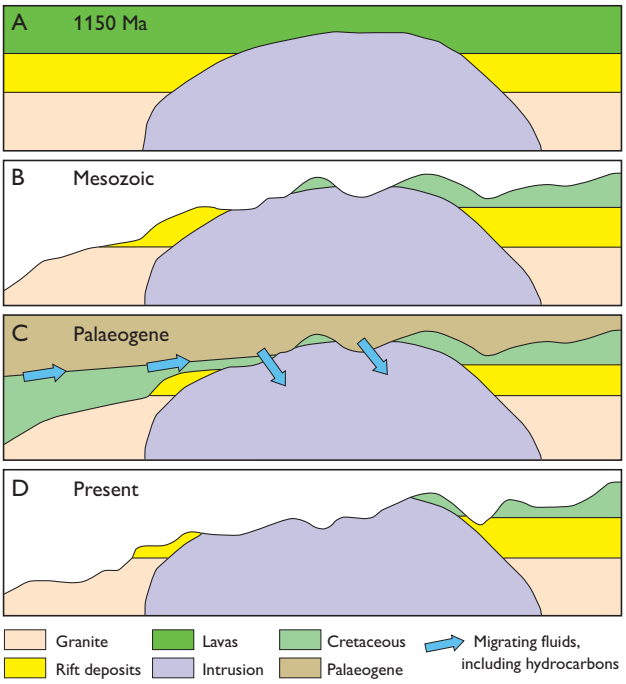

Fig. 5. Sketch of the geological evolution of the Ilímaussaq area.

ably covered by up to 2 km of marine sediments (Chalmers & Pulvertaft 2001; Japsen *et al.* 2006). The reburial and uplift history in South Greenland was probably similar to that of West Greenland, including the Nuussuaq region (Bonow *et al.* 2007). Thus it is likely that hydrocarbons migrated from marine sediments into the rocks of the Ilímaussaq intrusion during the period of reburial (Fig. 5).

Hydrocarbons have only been reported from the Ilímaussaq intrusion and not from other rocks in South Greenland. There may be two reasons for this: (1) rocks from the Ilímaussaq intrusion have been studied in much more detail than other rocks due to the occurrence of rare minerals, some of which have economic potential, and (2) the Ilímaussaq intrusion may be more deeply weathered than other rocks in the region because it contains water-soluble minerals (Rose-Hansen & Sørensen 2002).

From the biomarkers found in the bitumen, there is little doubt that the hydrocarbons were generated by thermal maturation of a marine source rock and migrated into the rocks of the Ilímaussaq intrusion at a later stage. It is unlikely that the bitumen formed by condensation of lighter hydrocarbons of abiogenic origin as hypothesised by Petersilie & Sørensen (1970). Hydrocarbon gases in fluid inclusions in rocks from the Ilímaussaq intrusion were considered to be abiogenic in origin on the basis of the heavy isotopic value of methane (Petersilie & Sørensen 1970; Konnerup-Madsen *et al.* 1988). However, they may also be of organic origin if the isotopic ratio of the gases was altered by fractionation due to diffusion of gases from the rocks (Laier & Nytoft 2012).

References

Bojesen-Koefoed, J.A., Christiansen, F.G., Nytoft, H.P. & Pedersen, A.K. 1999: Oil seepage onshore West Greenland: evidence of multiple source rocks and oil mixing. In: Fleet, A.J. & Boldy, S.A.R. (eds): Petroleum geology of Northwest Europe. Proceedings of the 5th Conference. Petroleum Geology Conference Series **5**, 305–314. London: Geological Society.

Bonow, J.M., Japsen, P., Green, P.F., Wilson, R.F., Chalmers, J.A., Klint, K.E., van Gool, J.A.M., Lidmar-Bergström, K. & Pedersen, A.K. 2007: A multi-disciplinary study of Phanerozoic landscape development in West Greenland. Geological Survey of Denmark and Greenland Bulletin **13**, 41–44.

Chalmers, J.A. & Pulvertaft, T.C.R. 2001: Development of the continental margins of the Labrador Sea – a review. In: Wilson, R.C.L. *et al.* (eds): Non-volcanic rifting of continental margins: a comparison of evidence from land and sea. Geological Society Special Publications (London) **187**, 79–107.

Christiansen, F.G. 2011: Greenland petroleum exploration: history, breakthroughs in understanding and future challenges. In: Spencer, A.M. *et al.* (eds): Arctic petroleum geology. Geological Society Memoirs (London) **35**, 647–661.

Japsen, P., Bonow, J.M., Peulvast, J.-P. &Wilson, R.W. 2006: Uplift, erosion and fault reactivation in Southwest Greenland. Field report summer 2006. Danmarks og Grønlands Geologiske Undersøgelse Rapport **2006/63**, 77 pp.

Konnerup-Madsen, J., Larsen, E. & Rose-Hansen, J. 1979: Hydrocarbon-rich fluid inclusions in minerals from the alkaline Ilímaussaq intrusion, South Greenland. Bulletin de Minéralogie **102**, 642–653.

Konnerup-Madsen J., Kreulen R. & Rose-Hansen J. 1988: Stable isotopic characteristics of hydrocarbon gases in the alkaline Ilímaussaq complex, South Greenland. Bulletin de Minéralogie **111,** 567–576.

Laier, T. & Nytoft, H.P. 2012: Bitumen biomarkers in the mid-Proterozoic Ilímaussaq intrusion, Southwest Greenland – a challenge to the mantle gas theory. Marine and Petroleum Geology **30**, 50–65.

Nytoft, H.P., Bojesen-Koefoed, J.A., Christiansen, F.G. & Fowler, M.G. 2002: Oleanane or lupane? Reappraisal of the presence of oleanane in Cretaceous–Tertiary oils and sediments. Organic Geochemistry **33**, 1225–1240.

Poulsen, V. 1964: The sandstones of the Precambrian Eriksfjord Formation in South Greenland. Rapport Grønlands Geologiske Undersøgelse **2**, 16 pp.

Petersilie, I.A. & Sørensen, H. 1970: Hydrocarbon gases and bituminous substances in rocks from the Ilímaussaq alkaline intrusion, South Greenland. Lithos **3**, 59–76.

Rose-Hansen, J. & Sørensen, H. 2002: Geology of the lujavrites from the Ilímaussaq alkaline complex, South Greenland, with information from seven bore holes. Meddelelser om Grønland, Geoscience **40**, 58 pp.

Authors' address

Geological Survey of Denmark and Greenland, Øster Voldgade 10, DK-1350 Copenhagen K, Denmark. E-mail: *tl@geus.dk*

Methane and possible gas hydrates in the Disko Bugt region, central West Greenland

Naja Mikkelsen, Troels Laier, Tove Nielsen, Antoon Kuijpers and Niels Nørgaard-Pedersen

Current climate models predict an annual temperature increase in the Arctic between 4° and 6°C by the end of the 21st century with widespread impact on the Arctic environment. Warming will lead to thawing of the widespread, permanently frozen, high-latitude peat-lands and to degradation of marine gas hydrates, both of which may increase the rate of methane release to the atmosphere. This will influence global climate as methane is a potent greenhouse gas with a large global warming potential. Marine gas hydrates are found worldwide on continental margins and frequently occur in the Arctic. Interpretation of seismic profiles has also indicated their presence in the Disko Bugt region in western Greenland.

In June 2011 a scientific cruise was undertaken in the Disko Bugt region (Fig. 1) to investigate the occurrence of methane and possible gas hydrates in the region. The cruise was part of a multidisciplinary scientific project *Impact on permafrost, gas hydrates and periglacial processes following climate changes in Greenland (Permagas)*. The project studies the impact of global climate warming on permafrost and gas hydrates in the Disko Bugt region. The aim of the project is to link marine and terrestrial occurrences of gas emissions.

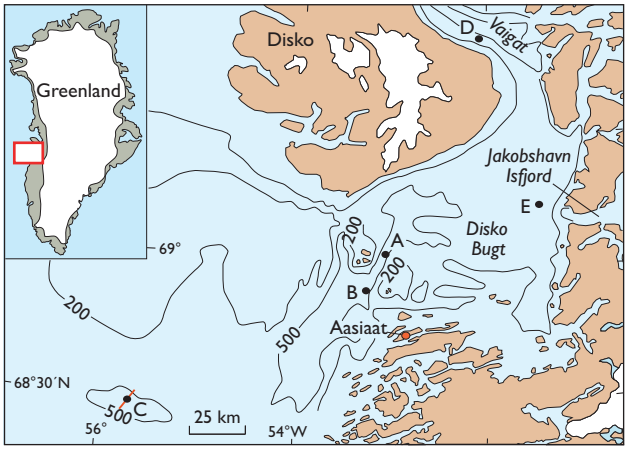

Fig. 1. Map of the Disko Bugt region. The black dots show core sites in Egedesminde Dyb (A, B), on the shelf off Aasiaat (C), in southern Vaigat (D) and off Jakobshavn Isfjord (E). Methane was encountered at sediment sites A and B, and traces of methane occurred at site C. At sites D and E, where pockmarks have been mapped during previous surveys, evidence of upwelling freshwater was found. Contours: 100, 200 and 500 m. The red line that crosses the core location at site C shows the position of the seismic profile in Fig. 3.

Marine gas hydrates

Gas hydrate is a crystalline solid consisting of gas molecules, usually methane, with each gas molecule surrounded by a frame of water molecules. Marine gas hydrates form under high pressure and low temperature in sediments below the seabed (Fig. 2). Depending on the bottom water temperature methane hydrate is typically stable in sea-floor sediments on the continental slope, but in high-latitude regions with low bottom water temperatures, the top of the gas hydrate stability zone may occur at shallower depths.

Gas hydrates are a potential energy resource as well as a potential risk for geohazards and the safe exploitation of sea bed resources (Kvenvolden & Rogers 2005). The worldwide amount of carbon bound in gas hydrates is conservatively estimated to total twice the amount of carbon found in all

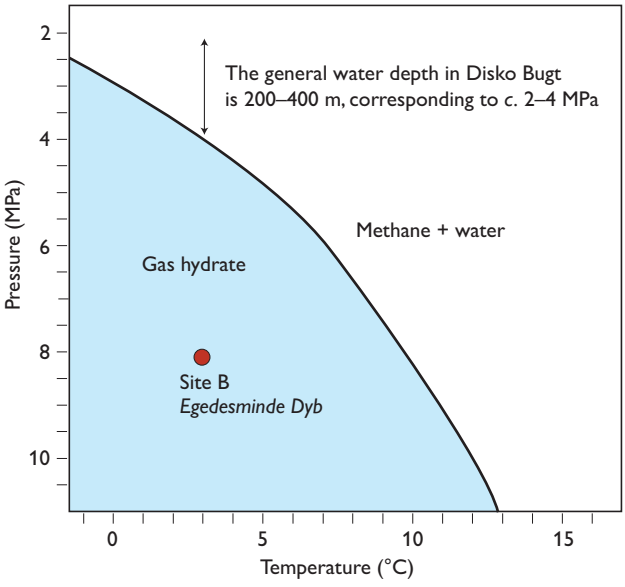

Fig. 2. Phase diagram showing the boundary between free methane (no colour) and gas hydrate (blue).

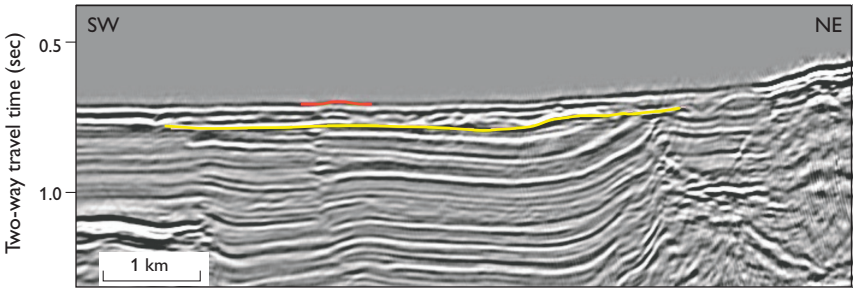

Fig. 3. Reflection seismic profile from site C (Fig. 1). The bottom-simulating reflector (yellow) at 75 msec two-way travel time below the seabed may indicate the occurrence of an up to 70 m thick gas hydrate zone. Pockmarks and seabed mounds (red) overlying faults in the shallow sub-seabed unit may be caused by seepage of free gas from beneath the gas hydrate zone. The seismic profile is part of released data acquired for the company Nunaoil in 1998.

known fossil fuels on Earth, and methane bound in hydrates amounts to approximately 3000 times the volume of methane in the atmosphere. In a warming world, methane from the dissociation of large and dynamic gas hydrate reservoirs therefore has the potential to influence oceanic and atmospheric carbon pools and thus influence global climate.

Gas hydrate may be recognised on seismic profiles by the presence of a so-called bottom-simulating reflector that marks the base of the gas hydrate stability zone (MacKay *et al.* 1994). The reflector is caused by the impedance contrast between the solid gas hydrate layer and free gas accumulations beneath. However, bottom-simulating reflectors are also found in areas without gas hydrates.

The Disko Bugt region

Since the discovery of extensive oil seeps north of Disko in 1992 (Christiansen *et al.* 1996), marine geologists' interest in the Disko Bugt region has increased significantly. However, little is known about the possible existence of gas hydrates on the continental margin, offshore West Greenland. The presence of pockmarks in Disko Bugt (Weinrebe *et al.* 2008) provides evidence of upwelling gas or fluid from the sea bottom. The bottom water temperature is *c.* 3°C in the Disko Bugt region and gas hydrates can be expected to occur at water depths exceeding 400 m, provided that methane occurs in high concentrations. During collection of a piston core in central Disko Bugt high gas content was demonstrated by the sudden escape of large amounts of strongly expanding gas that disrupted the sediment (Kuijpers *et al.* 2001). In addition, bottom-simulating reflectors have been observed on a number of seismic profiles from the area (Fig. 3).

Material and methods

During the cruise, up to 6 m long gravity cores and up to 2 m long cores, taken with a Max Planck Institute Rumohr Lot corer, were retrieved from five sites above and within the gas hydrate stability zone. The cores were sub-sampled for analysis of sediments and pore fluids (Fig. 4; Nielsen *et al.* 2011). The sediment cores were subjected to a number of geochemi-

Fig. 4. Plastic liners with 10 cm diameter cores sampled for pore water. The samples were analysed during the cruise for concentrations of methane, sulphate and dissolved sulphide. The Rhizon samplers were inserted into pre-drilled holes in the gravity core sections and pore water extracted by applying vacuum to the sampler when pulling the syringe piston.

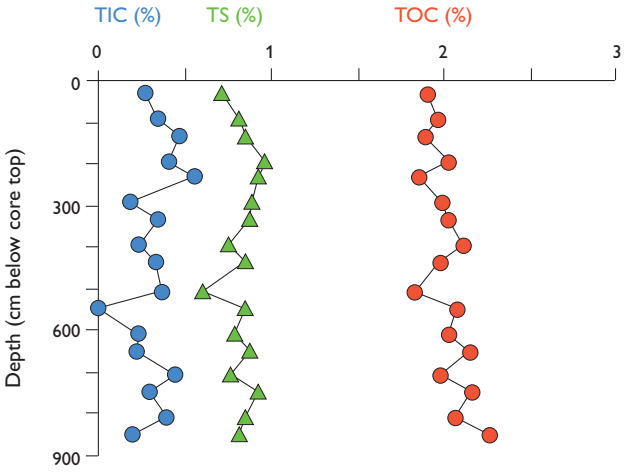

Fig. 5. Total inorganic carbon (TIC), total sulphur (TS) and total organic carbon (TOC) in a sediment core from site B in Egedesminde Dyb (after Kuijpers *et al.* 2001).

cal analyses, including measurements of methane concentrations and concentration of pore-water solutes (particularly sulphate), which aimed at providing data that could confirm the presence of gas hydrates.

Geochemical results and discussion

In the cores collected in Egedesminde Dyb at sites A and B (Fig. 1), which are situated within the gas hydrate stability zone, high pore-water methane concentrations were noted. However, the maximum methane concentration measured (*c.* 16 mM) is much below what is expected for methane saturation at 800 m depth in the Egedesminde Dyb (147 mM; Yamamoto *et al.* 1976). This is probably due to partial degassing during core retrieval. A pressure core barrel was not available during the cruise and the large drop in pressure during retrieval of the sediment cores would inevitably lead to loss of methane. Therefore it was not possible to prove the existence of small amounts of methane hydrate that may have formed as a result of *in situ* methane supersaturation. We did not observe any diagnostic features of hydrates either, such as trends in the chloride concentration or soupy sediment textures.

The methane is most likely microbial in origin and formed *in situ* as a result of organic matter degradation below the sulphate zone *c.* 0.5 m below the sea floor. This assumption is supported by the high content of organic matter in the sediment (total organic carbon = 1.9–2.3%; Fig. 5). Methane production is also promoted by the relatively high sedimentation rate in the area, 0.4–0.5 cm/year at site B (Moros *et al.*

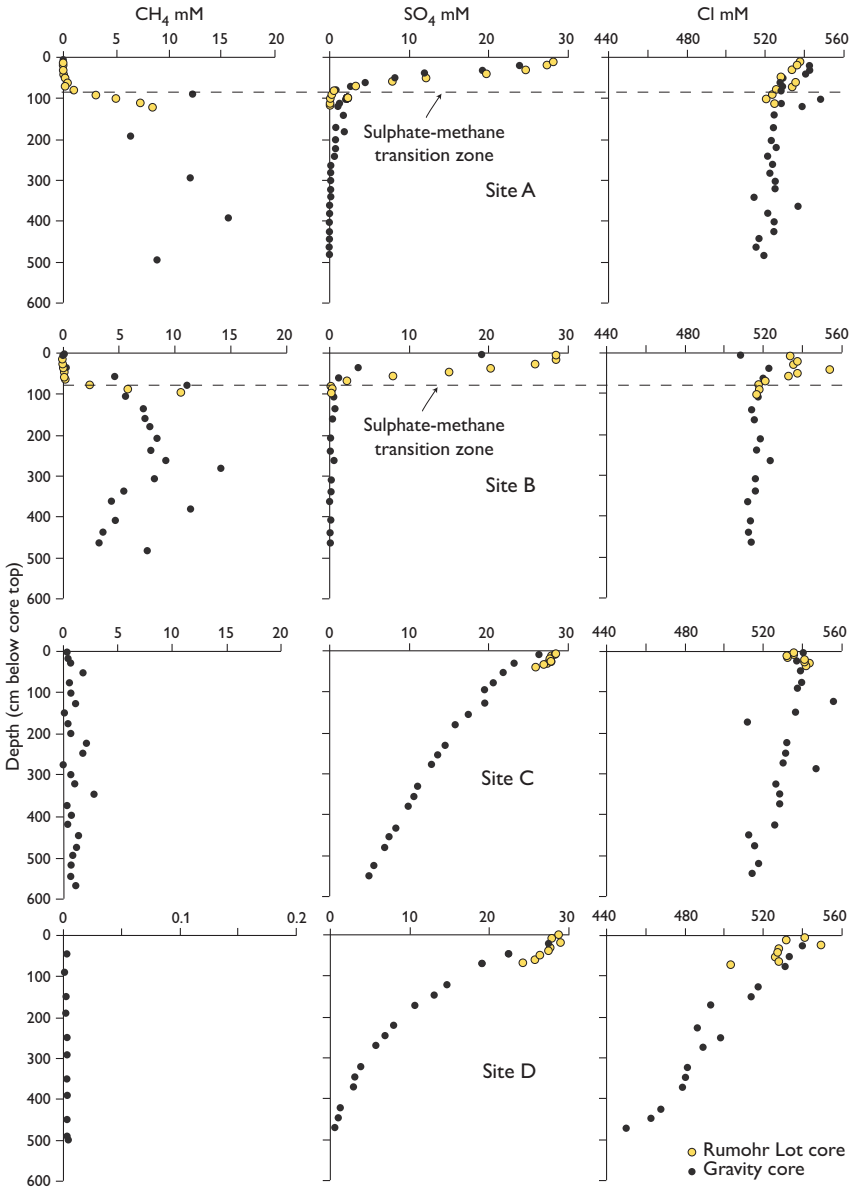

Fig. 6. Pore-water concentration profiles of dissolved methane, sulphate and chloride from sediment cores retrieved from Egedesminde Dyb (sites A (842 m) and B (865 m)), off Aasiaat (site C, 544 m) and from Vaigat (site D, 469 m). Yellow symbols: short Rumohr Lot cores, black symbols: gravity cores. Concentrations are in mM (millimoles per litre).

2006) that allows for a high proportion of easily degradable organic matter to enter the zone of methanogenesis (Henrichs & Reeburgh 1987).

At site C in the area west of Aasiaat the much lower methane concentration than at sites A and B may be explained by the high sulphate concentration (Figs 1, 6), which generally excludes the presence of methane (Iversen & Jørgensen 1985). Still the concentration of methane is significantly above background values for other sulphate pore-water concentrations in the Disko Bugt region. This may suggest upward migration of methane from gas hydrates as indicated by seismic data from the area (Fig. 3). The slight decrease in pore-water chloride concentrations with depth (Fig. 6) may further sustain the assumption of an upward migration of fluids depleted in chloride from below.

Pore-water sulphate in sediment cores from site D located in the southern end of the strait Vaigat is almost exhausted at approximately 5 m below the sea floor (Figs 1, 6). However, the low sulphate concentration is presumably not entirely due to *in situ* microbial sulphate reduction, as the decrease in pore-water chloride concentration with depth indicates a considerable contribution of freshwater from submarine groundwater discharge (Fig. 6).

Additional field work was conducted during the cruise in an area off the mouth of Jakobshavn Isfjord (site E). Pockmarks observed during an earlier multibeam survey in that area (Weinrebe *et al.* 2008) were suspected to have formed due to upward gas migration (Hovland & Svendsen 2006). However, the absence of methane together with the sediment texture observed in sediment cores from the area indicate that the pockmarks form from upwelling water and not from gas seepage.

Concluding remarks

The geochemical data obtained as a result of the 2011 cruise to the Disko Bugt region indicate that gas hydrates may occur in the region. Further investigation of the possible gas hydrates will continue during a new cruise in the area in 2012.

Acknowledgements

The 2011 cruise was supported by a grant from Geocenter Denmark to the project *Permagas*. The success of the cruise depended very much on the operational skills of the captain and crew of the R/V *Paamiut* and the smooth co-operation during the cruise with a scientific team from the Greenland Institute of Natural Resources.

References

Christiansen, F. G., Bate, K.J., Dam, G., Marcussen, C. & Pulvertaft, T.C.R. 1996: Continued geophysical and petroleum geological activities in West Greenland in 1995 and the start of onshore exploration. Bulletin Grønlands Geologiske Undersøgelse **172**, 15–21.

Henrichs, S.M. & Reeburgh, W.S. 1987: Anaerobic mineralization of marine sediments organic matter: rates and role of anaerobic processes in the oceanic carbon economy. Geomicrobiology Journal **5**, 191–237.

Hovland, M. & Svendsen, H. 2006: Submarine pingoes: indicators of shallow gas hydrates in a pockmark at Nyegga, Norwegian Sea. Marine Geology **228**, 15–23.

Iversen, N. & Jørgensen, B.B. 1985: Anaerobic methane oxidation rates at the sulphate–methane transition in marine sediments from Kattegat and Skagerrak (Denmark). Limnology Oceanography **30**, 944–955.

Kvenvolden K.A. & Rogers B.W. 2005: Gaia's breath – global methane exhalations. Marine and Petroleum Geology **22**, 579–590.

Kuijpers, A., Lloyd, J.M., Jensen, J.B., Endler, R., Moros, M., Park, L.A., Schulz, B., Jensen, K.G. & Laier, T. 2001: Late Quaternary circulation changes and sedimentation in Disko Bugt and adjacent fjords, central West Greenland. Geology of Greenland Survey Bulletin **189**, 41–47.

MacKay, M.E., Jarrard, R.D., Westbrook, G.K. & Hyndman, R.D. 1994: Origin of bottom-simulating reflectors: geophysical evidence from the Cascadia accretionary prism. Geology **22**, 459–462, *http://dx.doi.org/10.1130/0091-7613(1994)022%3C0459:OOBSRG%3E2.3.CO;2*

Moros, M., Jensen, K.G. & Kuijpers, A. 2006: Mid- to late-Holocene hydrological and climatic variability in Disko Bugt, Central West Greenland. The Holocene **16**, 357–367.

Nielsen, T., Laier, T., Mikkelsen, N. & Kristensen, J.B. 2011: Permagas project: Sampling gas hydrates in the Disko Bay area. Cruise Report – R/V Paamiut 20 to 26 June 2011. Danmarks og Grønlands Geologiske Undersøgelser Rapport **2011/105**, 40 pp.

Weinrebe, W., Kuijpers, A., Klaucke, I., Fink, M., Jensen, J.B. & Mikkelsen, N. 2008: High-resolution bathymetry of Disko Bay and Ilulissat Icefjord, West Greenland. American Geophysical Union fall meeting, San Fransisco, California, 15–19 December 2008 (Abstract C31E-0563).

Yamamoto, S., Alcauskas, J.B. & Crozier, T.E. 1976: Solubility of methane in distilled water and seawater. Journal of Chemical and Engineering Data **21**, 78–80.

Authors' address

Geological Survey of Denmark and Greenland, Øster Voldgade 10, DK-1350 Copenhagen K, Denmark. E-mail: *nm@geus.dk*

Ablation observations for 2008–2011 from the Programme for Monitoring of the Greenland Ice Sheet (PROMICE)

Robert S. Fausto, Dirk van As and the PROMICE project team*

Recent estimates from the glaciological community agree that the Greenland ice sheet is losing mass at an accelerated pace due to climate change (Velicogna 2009; Khan *et al.* 2010; Rignot *et al.* 2011). This has caught the attention of the public and policy makers due to the potential impact on sea-level rise (Dahl-Jensen *et al.* 2009). The mass loss can be attributed approximately equally to increases in meltwater runoff from surface melt and iceberg production (van den Broeke *et al.* 2009).

The robustness of mass-balance predictions relies heavily on observational data from the Greenland ice sheet and in recent years the need for frequent, reliable surface mass-balance measurements has increased (IPCC 2007; Dahl-Jensen *et al.* 2009). In anticipation of this need, the Programme for Monitoring of the Greenland Ice Sheet (PROMICE) was initiated in 2007, delivering *in situ* data from a network of automatic weather stations (AWS) covering eight different regions of the ice sheet (Fig. 1; van As *et al.* 2011). Apart from the direct insight into the surface mass balance provided by these stations, the *in situ* data are also valuable for calibrating and validating melt estimates from remote sensors and surface mass-balance models (Dahl-Jensen *et al.* 2009). In this paper, we present the ablation records for the PROMICE AWSs for 2008–2011, and the impact of the extraordinary atmospheric conditions on ablation in 2010 (Tedesco *et al.* 2011) are compared to the other years.

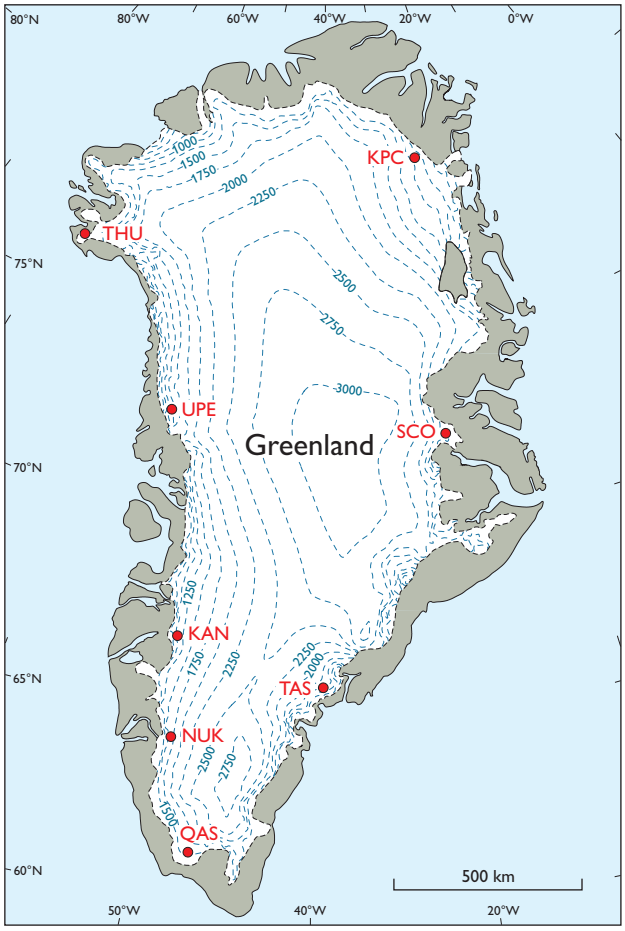

Fig. 1. Map of Greenland showing the locations of the PROMICE automatic weather stations. Each dot represents two or three stations. Station names are found in Table 1. Dashed lines: elevation contours.

PROMICE automatic weather stations

The PROMICE network in Greenland currently consists of eight sites with two (or three) AWSs placed at different elevations (Fig. 1; Table 1; Ahlstrøm *et al.* 2008) with a total of 18 stations. At each site, one station is typically located in the lower ablation zone close to the margin and the other in the upper ablation zone. Exceptions are station KAN_U, which is placed in the lower part of the accumulation zone, and station TAS_U, which is placed well below the equilibrium-line altitude for reasons of accessibility. Each station measures all relevant meteorological parameters and ice and snow ablation (Fig. 2). It measures and stores data every ten minutes

* Andreas P. Ahlstrøm, Signe B. Andersen, Morten L. Andersen, Michele Citterio, Karen Edelvang, Signe H. Larsen, Horst Machguth, Søren Nielsen and Anker Weidick.

Table 1. PROMICE automatic weather station metadata (status 2011)

Station name	Latitude (°N)	Longitude (°W)	Elevation (m a.s.l.)	Start date
KPC_L*	79°55′	24°05′	380	17 July 2008
KPC_U	79°50′	25°10′	870	17 July 2008
SCO_L	72°14′	26°49′	470	21 July 2008
SCO_U	72°24′	27°15′	1000	21 July 2008
TAS_L	65°38′	38°54′	270	23 August 2007
TAS_U	65°42′	38°52′	580	15 August 2007
QAS_L	61°02′	46°51′	310	24 August 2007
QAS_U	61°11′	46°49′	890	7 August 2008
NUK_L	64°29′	49°32′	560	20 August 2007
NUK_U	64°30′	49°16′	1140	20 August 2007
NUK_N	64°57′	49°53′	930	26 July 2010
KAN_L	67°60′	50°70′	670	1 September 2008
KAN_M	67°40′	48°49′	1280	1 September 2008
KAN_U	67°00′	47°10′	1830	4 April 2009
UPE_L	72°54′	54°18′	230	17 August 2009
UPE_U	72°53′	53°32′	980	17 August 2009
THU_L	76°24′	68°16′	570	9 August 2010
THU_U	76°25′	68°09′	770	9 August 2010

*L: Lower station, M: Middle station, U: Upper station, N: New station.

with the exception of the wind-speed observations that give the mean wind speed since the last measurement cycle, and the GPS measurements, which follow the transmission schedule. During winter (day 301 to day 99 of the year) the acquired data are transmitted once a day at midnight to limit power consumption when solar power is not available. During summer (day 100 to day 300) the data are transmitted hourly. The transmissions consist of daily or hourly average values of the more variable quantities such as temperature or radiation. Values of less variable quantities, such as surface height and station tilt are appended once every six hours in summer and once a day in winter for all daily transmissions.

Instrumentation and accuracy

The PROMICE AWSs are equipped with an Ørum & Jensen NT1400 pressure transducer assembly and two Campbell Scientific SR50A sonic rangers that monitor surface-height change caused by accumulation and ablation. The pressure transducer assembly consists of a (non-freezing) liquid-filled hose with a pressure transducer located at its end/bottom. The hose is drilled into the ice. The pressure signal registered by the transducer is that of the vertical liquid column over the sensor, which can be scaled to depth using the density of the liquid. The free-standing AWS tripod (Fig. 2) moves down with the ablating surface and the hose melts out of the ice, reducing the hydrostatic pressure from the vertical liquid column in the hose. The reduction in pressure provides the ablation totals. The assembly was first constructed and implemented by Bøggild *et al.* (2004). Since the first successful

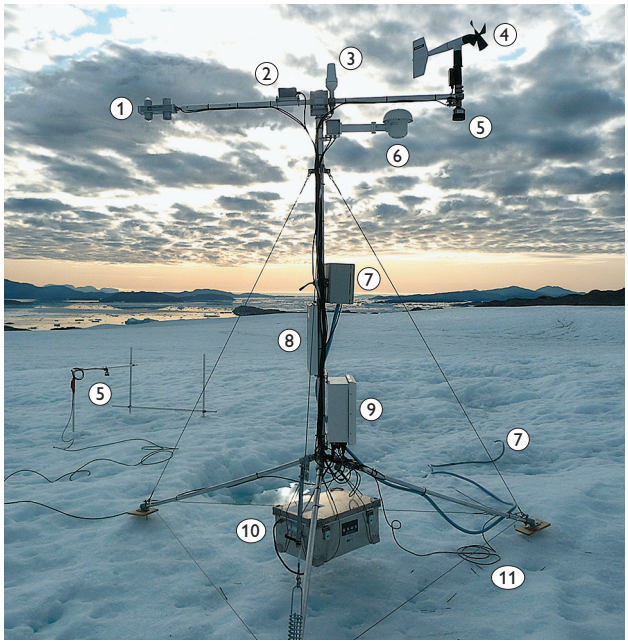

Fig. 2. The PROMICE automatic weather station UPE_L photographed on 17 August 2009. **1**: radiometer. **2**: inclinometer. **3**: satellite antenna. **4**: anemometer. **5**: sonic rangers. **6**: thermometer and hygrometer. **7**: pressure transducer. **8**: solar panel. **9**: data logger, barometer and GPS. **10**: battery box with 4 × 28 Ah batteries. **11**: 8-level thermistor string.

tests in 2001, we have developed the system and now use a larger diameter hose and have changed from relative to absolute pressure transducers. We also use an ethylene-glycol solution, instead of alcohol and secure the upper reference level of the assembly (in the form of a bladder) to the mast instead of leaving it exposed on the ice surface.

By measuring on a (sub-)daily timescale, the pressure transducer assembly is well suited to monitor ice ablation in remote regions, with clear advantages over other well-established methods. For instance, the stake readings providing information about surface-height change are done at every maintenance visit, so the records are limited to the visits. The accuracy of the SR50A sonic ranger is given by the manufacturer (Campbell Scientific) to be ±1 cm or ±0.4% of the measuring height after temperature correction. This was confirmed over 2.3 months of a virtually accumulation-free wintertime period at SCO_U, during which time standard deviations of 1.7 cm and 0.6 cm were found (after spike removal), corresponding to 0.7% and 0.6% of the distance measured by the two sonic rangers, respectively. However, the precision of the readings from these sensors may reduce over time as the sensors degrade due to continuous cycles of moisture freezing on and melting off them. A major problem with sonic rangers in surface-mass balance studies is that they need to be mounted on the stake assemblies drilled into

the ice. During a single melt season, these stake assemblies can melt out several metres, often causing them to move or even collapse during strong winds. In comparison, the pressure transducer assembly is operational until it has melted out of the ice, which can take several years depending on drill depth and the local ablation rate. This reduces the need for annual station visits, and thereby the considerable expenses associated with logistics in Greenland. The measurement uncertainty of the pressure transducer sensor given by the manufacturer is 2.5 cm. The mean standard deviation of the UPE and SCO pressure transducer readings outside the ablation season is found to be ±1 cm, indicating a small random error comparable to that of the sonic ranger. The precision of the pressure transducer readings falls over time as the transducer degrades due to the continuous pressure on the sensor.

Sensitivity drift defines the amount by which an instrument's sensitivity varies as ambient conditions change. Calibration tests of the pressure transducer show that the sensor sensitivity drift amounts to 1.6% on average for a four-year measuring period (0.4% per year), suggesting that drift is not a large source of error. The pressure transducer is especially suitable for high ablation areas of >3 m per year because it is independent of the stakes drilled into the ice (Fig. 2).

Ablation records for 2008–2011

The PROMICE ablation records presented in Table 2 are based on measurements by sonic rangers and pressure transducers, supplemented by stake readings. The net ablation values are calculated as the height difference between the end-of-melt-season surface level in the given year and the year before. The geographical distribution and annual net ablation records in Table 2 show that for all station pairs, the lower stations measure larger ablation totals than the upper ones, because the temperature decreases with elevation and the seasonal averaged surface albedo decreases towards the ice margin. There are considerable latitudinal differences as well, as the Greenland ice sheet is more than 2000 km long. Ablation totals in the southern part of Greenland typically amount to 3–7 m (at the lower TAS, QAS and NUK stations), whereas ablation totals at the more northerly SCO_L and UPE_L stations only amount to 2–3 m at low altitudes (<500 m a.s.l.). The ablation totals (negative value is net accumulation) from the upper stations (>500 m a.s.l.) typically amount to –0.3 to 4 m in the south (TAS, QAS, NUK, KAN) and –0.1 to 3 m in the north (KPC, SCO, UPE).

The record-warm year 2010 (in most regions of Greenland) showed the largest ablation at most AWS sites, followed by 2008, 2011, and lastly 2009 in the four-year PROMICE record. The 2010 ablation year was characterised by relatively low winter accumulation and a long period of positive air temperatures, which are both important for net ablation (Tedesco *et al.* 2011; van As *et al.* 2012). However, as the energy from solar radiation is the main contributor to the melting of snow and ice, the direct impact on ablation of inter-annual variability of temperature may be small. It was the combination of low winter accumulation and high temperatures, causing low albedo in large sections of the Greenland ice sheet in 2010, that resulted in large net ablation records (Tedesco *et al.* 2011; van As *et al.* 2012). The southern (QAS) and south-western (NUK and KAN) parts of Greenland experienced a particularly anomalous ablation season, with ablation totals of up to 3 m more than in other years. Even more significant was the melt response at stations close to the equilibrium-line altitude (zero net ablation) in the south and west; QAS_U went from a 0.3 m surface rise in 2009 to a 3.4 m surface lowering in 2010, and at KAN_M ablation increased from 0.3 m to 2.6 m during the same years. Even in normal years, the KAN_U station, which is placed in the accumulation zone, showed a surface lowering due to melt over the year 2010. On the other hand, the northern KPC_U station did not show anomalous ablation, as temperatures did not exceed their normal summer values (Table 2). North-East Greenland did not experience the anomalous circulation pattern that, in particular, southern and western Greenland experienced (Tedesco *et al.* 2011). Fifteen out of 18 PROMICE stations were successful in obtaining ablation

Table 2. Yearly ablation totals, given as the difference between the surface height at end of the melt season and that of the previous years, in metres snow/ice equivalent per year

Station\year	2008	2009	2010	2011
KPC_L	–*	–†	–†	–†
KPC_U	–*	–0.1‡	0.1‡	0.2‡
SCO_L	–*	2.6	3.5	3.1
SCO_U	–*	1.4	2.5	2.1
TAS_L	3.6	7.4**		3.4‡
TAS_U	3.3	1.5‡	3.9$	2.9
QAS_L	7.3	–	9.3	5.5
QAS_U	–*	–0.3‡	3.4	0.8
NUK_L	5.3	4.8	7.2	–
NUK_U	2.2	1.5	2.5	2.3
NUK_N	–	–	–*	5.1
KAN_L	–*	3.5	5.4	4.0
KAN_M	–*	0.3‡	2.6‡	1.7‡
KAN_U	–	–*	–	–0.2‡
UPE_L	–	–*	3.2	2.9
UPE_U	–	–*	2.7	2.6
THU_L	–	–	–*†	–†
THU_U	–	–	–*†	–†

* Partial data coverage due to station establishment that year. † Data may become available after the next maintenance visit. ‡ Sonic ranger measurement. $ Sonic ranger and stake measurements. ** Sonic ranger and stake measurements for both 2009 and 2010.

totals up until 2011. The remaining three stations (KPC_L, THU_L, and THU_U) did not transmit any data, but data may become available during the next maintenance visit. We obtained 42 interannual ablation totals for all the stations out of 50 possible totals. When disregarding the three stations that did not transmit, the number would be 45. This gives a success rate of 84% for all 18 stations, or 93% when disregarding the 3 non-transmitting stations.

Conclusions

Ablation totals at low altitudes (<500 m a.s.l.) typically amount to 3–7 m in the southern part of Greenland, with an ablation total at the more northerly stations of 2–3 m. The ablation totals from the upper stations above 500 m a.s.l., typically amount to −0.3 to 4 m in the south (TAS, QAS, NUK, KAN) and −0.1 to 3 m in the north (KPC, SCO, UPE). The interannual ablation totals show that 2010 was a year with large melt when compared to the other years. The 2010 season showed record-setting ablation totals for the southern (QAS) and south-western stations (NUK and KAN), however, a longer time series is needed to quantify the anomalous 2010 ablation totals (van As *et al.* 2012). The PROMICE station network has successfully obtained ablation totals at the end of 2011 for 15 out 18 stations. The interannual success rate was 84% for all 18 stations and 93% if the three non-transmitting stations (KPC_L, THU_L, and THU_U) are omitted.

Acknowledgements

The Programme for Monitoring of the Greenland Ice Sheet (PROMICE) is funded by the Geological Survey of Denmark and Greenland (GEUS) and the Danish Ministry of Climate, Energy and Building under Danish Cooperation for Environment in the Arctic (DANCEA), and is conducted in collaboration with the National Space Institute (DTU Space) and Asiaq (Greenland Survey). The NUK and KAN stations are (co-)funded by the Greenland Climate Research Centre (GCRC) and the Greenland Analogue project (GAP), respectively.

References

Ahlstrøm, A.P. & PROMICE project team 2008: A new programme for monitoring the mass loss of the Greenland ice sheet. Geological Survey of Denmark and Greenland Bulletin **15**, 61–64.

Bøggild, C.E., Olesen, O.B., Ahlstrøm, A.P. & Jørgensen, P. 2004: Automatic glacier ablation measurements using pressure transducers. Journal of Glaciology **50**(169), 303–304.

Dahl-Jensen, D. *et al*. 2009: The Greenland ice sheet in a changing climate: snow, water, ice and permafrost in the Arctic (SWIPA), 115 pp. Oslo: Arctic Monitoring and Assessment Programme (AMAP).

IPCC 2007: Intergovernmental Panel on Climate Change (IPCC) Fourth Assessment Report (AR4), Climate Change 2007. 4 volumes. Cambridge: Cambridge University Press.

Khan, S.A., Wahr, J., Bevis, M., Velicogna, I. & Kendrick, E. 2010: Spread of ice mass loss into northwest Greenland observed by GRACE and GPS. Geophysical Research Letters **37**, L06501, *http://dx.doi.org/10.1029/2010GL042460*

Rignot, E., Velicogna, I., van den Broeke, M.R., Monaghan, A. & Lenaerts, J. 2011: Acceleration of the contribution of the Greenland and Antarctic ice sheets to sea level rise. Geophysical Research Letters **38**, L05503, *http://dx.doi.org/10.1029/2011GL046583*

Tedesco, M., Fettweis, X., van den Broeke, M.R., van de Wal, R.S.W., Smeets, C.J.P.P., van de Berg, W.J., Serreze, M.C. & Box, J.E. 2011: The role of albedo and accumulation in the 2010 melting record in Greenland. Environmental Research Letters **6**, 014005, *http://dx.doi.org/10.1088/1748-9326/6/1/014005*

van As, D., Fausto, R.S. and the PROMICE project team 2011: Programme for Monitoring of the Greenland Ice Sheet (PROMICE): first temperature and ablation records. Geological Survey of Denmark and Greenland Bulletin **23**, 73–76.

van As, D., Hubbard, A.L., Hasholt, B., Mikkelsen, A.B., van den Broeke, M.R. & Fausto, R.S. 2012: Large surface meltwater discharge from the Kangerlussuaq sector of the Greenland ice sheet during the record-warm year 2010 explained by detailed energy balance observations. The Cryosphere **6**, 199–209.

van den Broeke, M., Bamber, J., Ettema, J., Rignot, E., Schrama, E., van de Berg, W.J., van Meijgaard, E., Velicogna, I. & Wouters, B. 2009: Partitioning recent Greenland mass loss. Science **326**, 984–986.

Velicogna, I. 2009: Increasing rates of ice mass loss from the Greenland and Antarctic ice sheets revealed by GRACE. Geophysical Research Letters **36**, L19503, *http://dx.doi.org/10.1029/2009GL040222*

Authors' address

Geological Survey of Denmark and Greenland, Øster Voldgade 10, DK-1350 Copenhagen K, Denmark. E-mail: *rsf@geus.dk*

Testing of an automatic earthquake detection method on data from Station Nord, Greenland

Nasim Karamzadeh, Peter H. Voss and Gholam D. Javan

Earthquakes are continuously monitored by a global network of several thousand seismic stations equipped with highly sensitive digital seismometers. The Geological Survey of Denmark and Greenland (GEUS) takes part in it by operating five seismic stations in Denmark and 18 in Greenland, some of the latter in collaboration with international partners. There are two main ways of detecting earthquakes from digital recordings of seismometers: (1) by a manual review of the data by an expert in processing seismic earthquake signals and (2) by an automatic method that uses a computerised algorithm to analyse the recordings.

Since the beginning of earthquake recording, earthquake detection at GEUS has been based on the manual review method. There are several reasons why an automatic detection procedure has not yet been implemented at GEUS: (1) historically, the staff at GEUS have conducted high-quality manual detection of earthquakes, based on a long tradition of manual seismogram analysis (Lehmann 1954), (2) the ambient noise level in Denmark is generally too high for small local earthquakes to be detected automatically and (3) in Greenland, the distance between the seismometers is too long for automatic methods. Previous tests on GEUS data showed that automatic detection using the so-called standard method resulted in a very high number of false detections, and the effort needed to distinguish real earthquake signals from noise signals was much greater than that needed in the manual method. In addition, the automatic method detected fewer earthquakes than the manual analysis. Therefore, new automatic methods are needed to extract real earthquake signals from the background noise.

In this article, we present results from testing a newly developed automatic detection method based on analysis of the frequency content of seismic signals. The aim of the study was to investigate whether the automated method can be used in Greenland or whether the manual procedure is still superior. The new method was tested on seismic data from Station Nord, which was selected because it is located in a region with many earthquakes, and because there are no nearby seismograph stations to support the measurements. The closest station is located at Danmarkshavn *c.* 540 km to the south. Therefore, the majority of earthquakes that occur in this region are only registered at Station Nord.

Earthquakes in the Station Nord region

Station Nord is located in eastern North Greenland, in a region where a major tectonic factor is the spreading that occurs along the rift zones in the northern North Atlantic and the Arctic Ocean (Døssing *et al.* 2010), and which gives rise to high seismic activity (Fig. 1). Another tectonic factor is postglacial isostatic rebound that was the source of three major earthquakes in 1971, 1987 and 1993 (Chung 2002), with magnitudes of 5.1, 5.5 and 5.4 on the Richter scale. Apart from the seismicity observed at the rift zone, most of the earthquakes in the region occur to the south and west of Station Nord (Fig. 1; Gregersen 1982). The earthquake hazard in the region is low, but represents the highest in Greenland (Voss *et al.* 2007). The hazard was illustrated by a strong tremor felt at Station Nord on 30 August 2005, caused by a magnitude 4.2 earthquake with an epicentre only 20 km away.

Automatic earthquake detection

The standard automatic earthquake detection method is known as the Short Term Average versus Long Term Average (STA/LTA) method (Havskov & Alguacil 2010). The basis of this method is two running time windows that both compute the average amplitude of the signal, one with a short

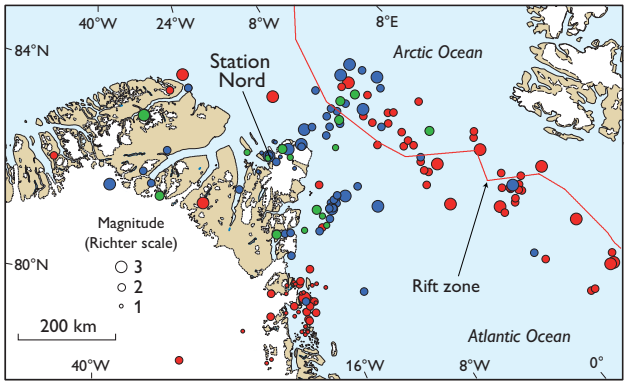

Fig. 1. Map of the region between north-eastern Greenland and Svalbard. Red dots: Epicentres located by GEUS using manual detection methods. Blue dots: Epicentres located using automatic detection method. Green dots: Located by both methods.

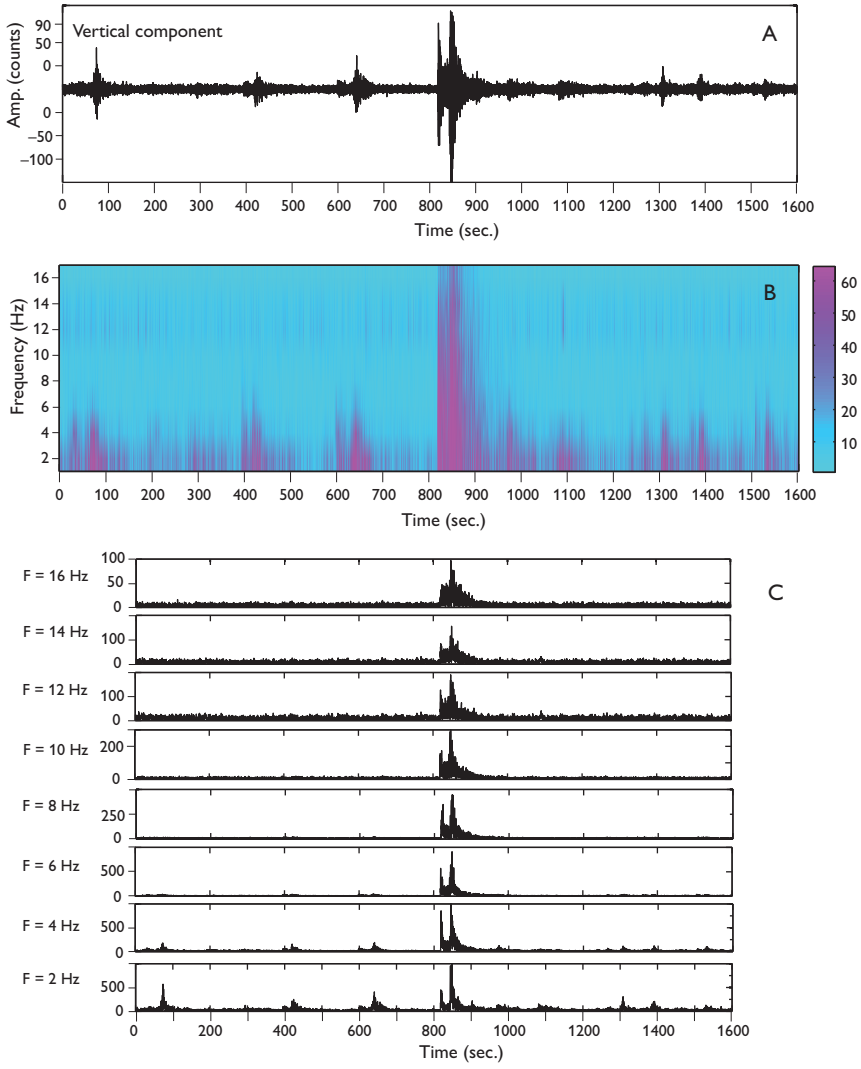

Fig. 2. **A**: Vertical component of a continuous seismogram, which included a signal from an earthquake and several short-duration, high-energy perturbations. **B**: Normalised spectrogram produced by short-time Fourier transformation for frequencies of 2–16 Hz with 2 Hz steps. The colours (scaled to use full colour spectrum) represent an estimate of the energy contained at the given frequency, within a short window (about 0.6 s). At 800–900 s, when an earthquake signal appears in the seismogram, the colours on the spectrogram change, which indicates an order of magnitude increase in the seismic energy over all frequencies. The detection of changes in energy over a proper range of frequencies, corresponding to the frequency content of the earthquake signals, led to the detection of an earthquake. Other increases in the energy level are seen at several other times, for example at 600–700 s. These peaks are only seen at low frequencies. **C**: Another representation of the same spectrogram showing the variation of local spectral energy for each frequency band over time. A sharp increase is seen at the onset of the earthquake signal, whereas the perturbation of energy in the background noise has disappeared at higher frequency bands.

duration (STA) and the other with a long duration (LTA). The LTA represents the stable background noise level of the seismic signal, whereas the STA will increase rapidly at the onset of a seismic signal. The signal is often band pass filtered to lower the ambient noise. The earthquake is detected when the STA/LTA exceeds a predefined threshold level (e.g. 10). The basic parameters required for this method are (1) the band pass filter, (2) the duration of STA and LTA and (3) the STA/LTA threshold level. The disadvantage of this method is that it triggers with all ground shaking that exceeds the threshold level. So, if the STA/LTA threshold level is set low to detect small earthquakes, many detections that are nothing but noise or bogus events lead to much additional manual post-processing. A high number of noise detections can be avoided by setting the STA/LTA at a higher threshold level, but then important earthquakes may not be detected.

In many seismic networks, automatic detection is operated with a low STA/LTA threshold level, but to avoid a lot of manual post-processing of detected signals, an additional criterion is applied before they are forwarded to manual processing. It states that the detection is only valid if the signal is also detected by a number of other seismic stations (e.g. 3) within a predefined time window; otherwise the detection is disregarded as being seismic noise. However, in order to use this criterion in the detection of small earthquakes, the network must include a large number of seismic stations located less than 100 km from each other. This is not the case in Greenland where the distance between the stations is around 300 km in western Greenland and around 600 km in eastern Greenland. Alternative methods are therefore required, and we have chosen an automatic method based on analysis of the short-time Fourier transform of the data. In addition to event detection, the automatic method also provides phase picks, magnitude measurements and azimuth estimates, but the primary aim of this study was to test the performance of the automatic event detections.

A spectrogram produced by short-time Fourier transform is a very useful tool in seismology because it can provide an image indicating the time at which a burst of energy occurs on a seismogram, in addition to the spectral composition of the signal (Gibbons *et al.* 2008). The event detection algorithm used in this study inspects the temporal variation of the signal spectrogram calculated in frequency bands corresponding to the frequency content of local and regional earthquakes (e.g. 2–16 Hz). For detected events, the *P*- and *S*-phases are picked. An example of a recorded seismogram with an earthquake signal and corresponding spectrogram is shown in Fig. 2 where an earthquake is observed on a seismogram at an approximate time of 800 s. Obvious changes in the colour of the spectrogram take place over a wide range of frequencies along the time axis, which indicate the arrivals of earthquake energy (Fig. 2B). Accordingly, the detection of a change in energy pattern over a pre-defined range of frequencies, corresponding to the frequency content of the earthquake signals, leads to the detection of an earthquake. The plots presented in Fig. 2C show the variation of energy for each frequency band, corresponding to the above spectrogram. These plots provide another representation of the spectrogram. The problem of detecting an earthquake on seismograms is now reduced to detecting sharp increases in the individual time series representing spectral energy versus time (the plot shown in Fig. 2C). To avoid false detections due to seismic noise with a frequency content overlapping the analysed frequencies, only detections made in most of the frequency bands are accepted. For instance, detections should be made at about the same time in at least five out of eight frequency sub-bands for a given spectrogram (Fig. 2B). Three missing detections are allowed, because this may happen for small events and noisy backgrounds, or low signal to noise ratio in some frequency bands. To reduce the false detection rate, all three components (vertical, N–S and E–W) of the seismograms are used in the event detection procedure.

Results

To test the automatic detection method, Station Nord data from 6 July 2010 to 6 March 2011 were used. Prior to this period, the digitising unit of the seismometer had been upgraded to sample at 100 Hz. Earlier, the instrument had sampled at 20 Hz; this limits earthquake analysis to frequencies below 10 Hz, which the automatic method was not prepared for. Station Nord is equipped with a Streckeisen STS-2 sensor and a Quanterra Q330 digitiser. The automatic method analyses data from all three components of the sensor, using 24 hour data files. The data are band pass filtered between 0.95 and 20 Hz before the detection algorithm is applied. The

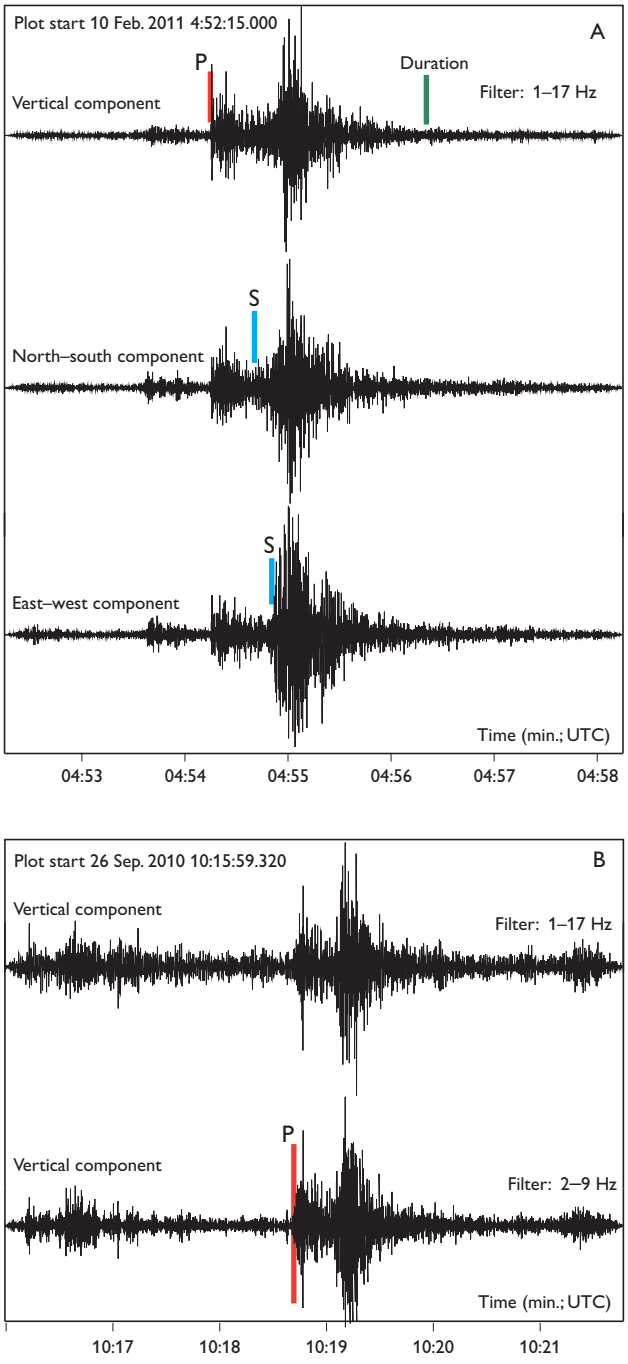

Fig. 3. **A**: Seismogram of a magnitude 2.2 earthquake filtered with a 1–17 Hz band pass filter containing the frequencies used for the automatic detection. The epicentre was located 354 km south-south-east of Station Nord. The automatic *P*-phase (**P**) was kept in the review, but the automatic *S*-phase (**S**) was repicked moving the epicentre 118 km. Automatic *S* pick is seen on the north–south channel, manual *S* pick is seen on the east–west channel and the automatic tremor duration is seen on the vertical channel. **B**: Vertical component of an earthquake not detected by the automatic method. Top trace: data with the 1–17 Hz filter used by the automatic method. Bottom trace: data with the 2–9 Hz filter used by the manual method. The earthquake had a magnitude of 1.1 and was located 234 km east-south-east of Station Nord. **UTC**: Universal Time, Coordinated.

detections are stored in the international SEISAN format. During the test period, 156 detections were recorded with the automatic method. A review of these detections showed that 13 were due to sensor calibrations or sensor noise, and 52 were caused by other noise signals such as man-made noise. The remaining 91 events were identified as earthquakes.

To test the performance of the automatic method, the data were also analysed with the Rasmussen method, where data are manually scanned using predefined time windows and filters (Rasmussen & Voss 2011). During this manual scanning, the z-channel was checked in two-hourly windows using a 2–9 Hz band pass filter, the same filter that is used to analyse the data from the seismometer at Danmarkshavn in the daily processing at GEUS. The scanning found 229 earthquakes in the study period, approximately two and a half times more earthquakes than found by the automatic method. An example of an earthquake that was not detected by the automatic method is shown in Fig. 3B. Comparison of the lists of earthquakes detected by the two methods shows that the automatic detections do not give a full subset of the manual detections, as the automatic method detected 26 events that were not found by the manual method. A review of these 26 earthquakes showed that 23 had a low signal to noise ratio in the frequency range of the band pass filter (2–9 Hz) used and three earthquakes were missed during the analysis.

After the detection procedure, we processed the detected events. In this process, the arrival times of the *P*- and *S*-phases were picked and the magnitude of the signal determined. The automatic method picks *P*- and *S*-phases and uses the duration of the signal tremor to estimate the magnitude. We reviewed the 91 earthquakes detected and found that the automatic pick of the *P*- and *S*-phases should be adjusted for all earthquakes. Most of the adjustments were within a few seconds, but for seven of the events the automatic pick errors were several seconds. In many cases, the duration of the automatic signal located the end of the event in the last part of the *S* wave, but in some instances the end of the duration was in the end of the *P* wave. A similar approach was used by Agius & Galea (2011) with good results, but further improvement of the processing is required. Examples of the performance of the automatic method are shown on seismograms in Fig 3.

Discussion and conclusions

The manual detection method found two and a half times more events than the automatic detection method. Replacement of the manual method with the automatic detection of earthquakes in Greenland will therefore result in a significantly lower number of earthquake detections. The quality of earthquake risk evaluation depends on a high detection level; thus a lower number of detections will lead to a lower quality of an earthquake risk evaluation. The automatic method contributed with 26 (11%) additional events to the manual detections, and hence a combination of the two methods may increase the number of earthquakes detected in the region. In addition, the automatic method was effective in avoiding false detections.

The automatic method gives earthquake locations and magnitude estimates, based on automatic phase picks, phase polarisation and signal duration, but the quality of this information is poorer than that obtained by manual processing. A manual review of the data will still be an important part of the quality control.

Acknowledgements

This study is part of a PhD project funded by the International Institute of Earthquake Engineering and Seismology for the first author, who was a visiting PhD student at GEUS in 2011. The Greenland Ice Sheet Monitoring Network is thanked for upgrading Station Nord.

References

Agius, M.R. & Galea, P. 2011: A single-station automated earthquake location system at Wied Dalam Station, Malta. Seismological Research Letters **82**, 545–559.

Chung, W.-Y. 2002: Earthquakes along the passive margin of Greenland: evidence for postglacial rebound control. Pure and Applied Geophysics **159**, 2567–2584.

Døssing, A., Stemmerik, L., Dahl-Jensen, T. & Schlindwein, V. 2010: Segmentation of the eastern North Greenland oblique-shear margin – regional plate tectonic implications. Earth and Planetary Science Letters **292**, 239–253.

Gibbons, S. J., Ringdal, F. & Kværna, T. 2008: Detection and characterization of seismic phases using continuous spectral estimation on incoherent and partially coherent arrays. Geophysical Journal International **172**, 405–421.

Gregersen, S. 1982: Seismicity and observations of Lg wave attenuation in Greenland. Tectonophysics **89**, 77–93.

Havskov, J. & Alguacil, G. 2010: Instrumentation in earthquake seismology. Modern Approaches in Geophysics **22**, 360 pp.

Lehmann, I. 1954: Characteristic earthquake records. Geodætisk Instituts Skrifter III. Række **18**, 33 pp.

Rasmussen, H.P. & Voss, P.H. 2011: Detection of earthquakes at the Geological Survey of Denmark and Greenland – GEUS. 42nd Nordic Seminar on Detection Seismology, Reykjavik, 5–7 October 2011. Icelandic Meteorological Office, programme and abstracts, 41 only.

Voss, P., Poulsen, S.K., Simonson, S.B. & Gregersen, S. 2007: Seismic hazard assessment of Greenland. Geological Survey of Denmark and Greenland Bulletin **13**, 57–60.

Authors' addresses

N.K. & G.D.J., *International Institute of Earthquake Engineering and Seismology, Arghavan St. 21, North Dibajee, Farmanieh Tehran 3913/19395 Islamic Republic of Iran*. E-mail: *n.karamzadeh@iiees.ac.ir*

P.H.V., *Geological Survey of Denmark and Greenland, Øster Voldgade 10, DK-1350 Copenhagen K, Denmark.*

The Cenozoic Song Hong and Beibuwan Basins, Vietnam

Michael B.W. Fyhn, Henrik I. Petersen, Lars Henrik Nielsen, Tran C. Giang, Le H. Nga, Nguyen T.M. Hong, Nguyen D. Nguyen and Ioannis Abatzis

The Vietnamese offshore margin holds a substantially underexplored petroleum potential. The key to unravelling this potential lies in understanding the tectono-stratigraphic framework of the region including the Cenozoic mechanisms governing syn-rift and source rock deposition. This is essential for prediction of, for instance the presence and nature of source rocks in South-East Asia and possible reservoir intervals in the syn-rift packages. The Vietnamese part of the Song Hong and Beibuwan Basins (Fig. 1) differs from other basins along the western margin of the South China Sea in that the Palaeogene syn-rift succession is sporadically exposed due to uplift and inversion. These exposures provide a unique glimpse into the Cenozoic syn-rift succession of the basin.

Considerable oil and condensate discoveries have recently been made in the Vietnamese part of the Song Hong Basin. This emphasises the need for improved geological models of the basin in order to unravel the local petroleum systems.

Since 1995, the Geological Survey of Denmark and Greenland and the Vietnam Petroleum Institute have conducted exploration-related, foreign development aid projects in Vietnam funded by the Danish Ministry of Foreign Affairs. The ongoing Danish–Vietnamese research cooperation operates through an ENhanced REsearch CApacity (ENRECA) project. The ENRECA group consists of both Danish and Vietnamese researchers who, through the project, have become the established experts in the region. The ongoing ENRECA work focuses on the geological development of the greater Song Hong Basin (including the Vietnamese part of the Beibuwan Basin). As part of the project activities, the ENRECA group has recently drilled a fully cored well into the syn-rift succession of the basin and is carrying out a comprehensive regional study combining seismic, well and outcrop information.

Evolution of the the Song Hong Basin and the greater Vietnamese margin

South-East Asia is tectonically one of the most complex regions in the world, shaped by continental collisions and the creation and subduction of oceanic basins. A large portion of the deformation associated with the Indian–Eurasian plate collision was likely accommodated in the neighbouring part of South-East Asia during the Cenozoic (e.g. Leloup *et al.* 2001). Indochina deformed in response to the collision and may have been squeezed hundreds of kilometres south-east-

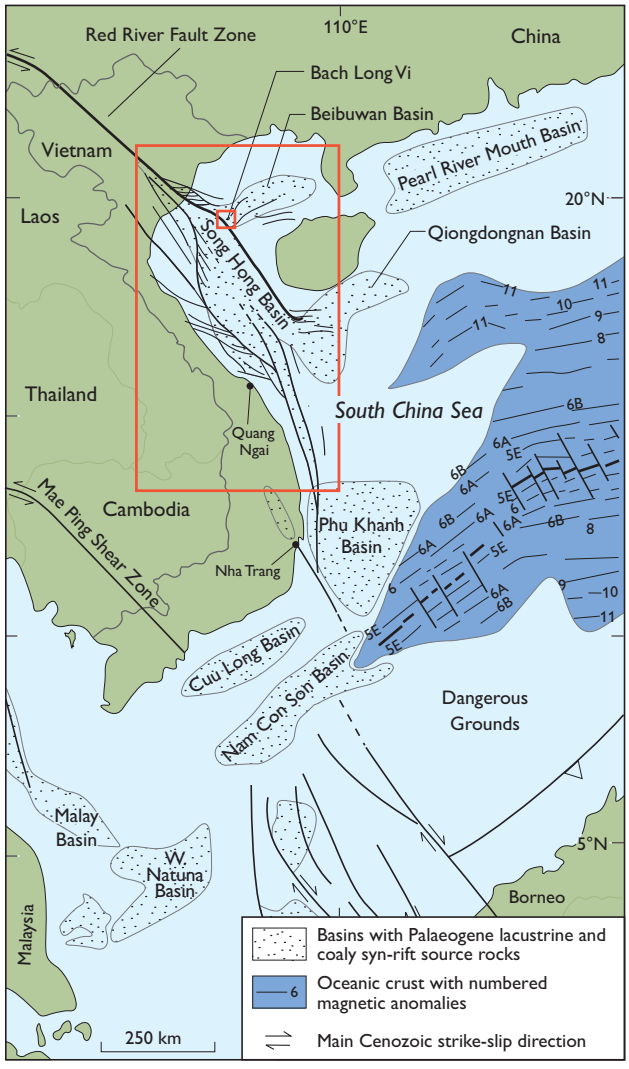

Fig. 1. Map of Indochina and the western part of the South China Sea showing the outline of the main Cenozoic structures and basins with lacustrine and coaly source rocks. The large red rectangle shows the study area, and the small rectangle shows the location of Fig. 3.

 Geological Survey of Denmark and Greenland Bulletin 26, 81–84. Open access: www.geus.dk/publications/bull

wards from the Himalayan collision front along enormous strike-slip fault zones (Fig. 1).

The Song Hong Basin is the largest Vietnamese sedimentary basin and covers close to one third of the western margin of the South China Sea. Its formation has been attributed to large-scale, left-lateral movements along the Vietnamese margin (e.g. Leloup *et al*. 2001), whereas a pull-apart model for the basin remains controversial (e.g. Hall & Morley 2004). Understanding the basic mechanism behind the formation of the Song Hong Basin is crucial for understanding the overall establishment of the western half of the South China Sea. The Song Hong Basin is likely to hold important information on the opening mechanism of the South China Sea.

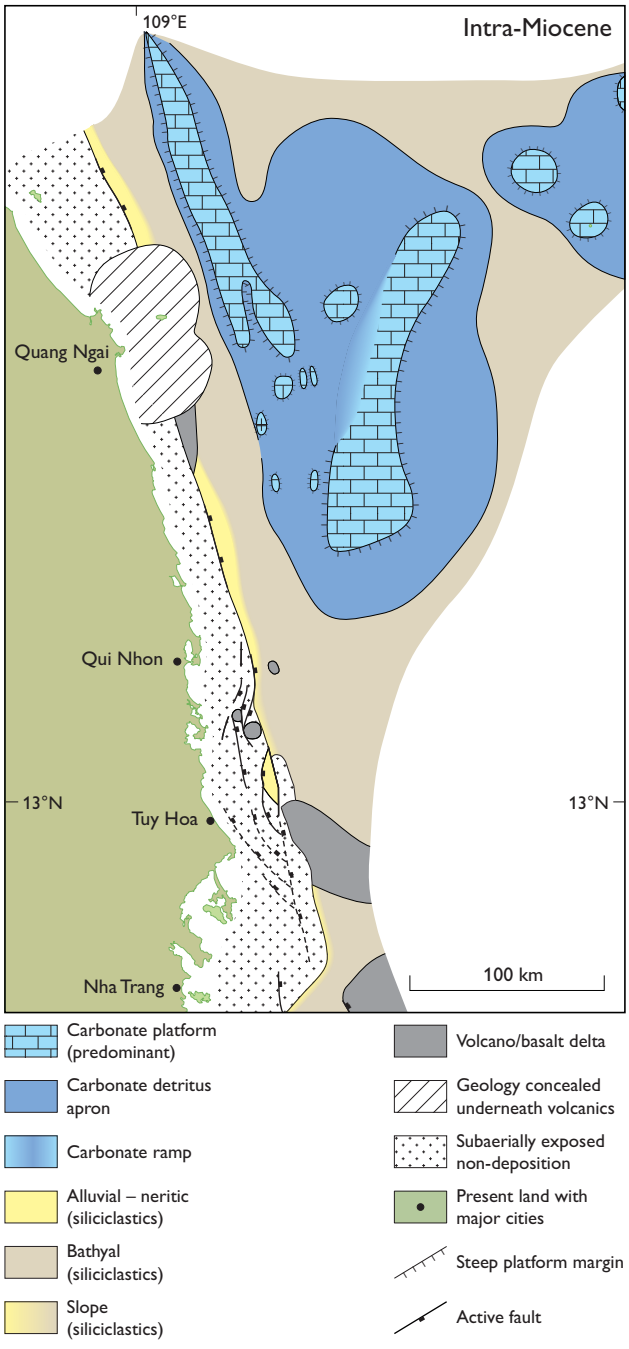

Fig. 2. Intra-Miocene depositional map for the southern part of the Song Hong and the Phu Khanh Basins. Carbonate deposition took place on structural highs, but was affected by siliciclastic input sourced from onshore uplift and local volcanism.

Whether the greater Vietnamese margin constitutes a transform margin or a more classic oblique rift margin is fundamental to the structural concepts applied when interpreting geophysical data across basins along the margin. So far it has not been possible to evaluate this satisfactorily due to the scarcity of seismic data tied to a limited number of wells offshore Vietnam. However, recent studies of relatively densely spaced seismic profiles tied to wells offshore central and southern Vietnam have led to an increased understanding of the tectonic evolution of the margin (Fyhn *et al*. 2009). It is clear from these studies that the Song Hong Basin is crucial for reconstructing the overall tectonic development of the western South China Sea.

The current ENRECA study is based on a comprehensive geoscientific database of the Vietnamese portion of the basin and aims to unravel the tectonic and depositional evolution of the basin in a regional context. This will allow a detailed stratigraphic understanding of the basin fill and a comprehensive structural analysis of the basin and the adjacent areas.

The Song Hong Basin forms a depocentre in the northwestern part of the South China Sea and is filled with up to 15–20 km of sediments. Sediment dispersal to the northwestern part of the South China Sea has largely occurred as spill from the Song Hong Basin. The distribution and style of sediments in the surrounding basins are therefore closely linked to the depositional pattern in the Song Hong Basin. Deposition evolved rapidly in the basin and varied in time and space from lacustrine and fluvial to marine sedimentation. Sedimentary environments ranged from carbonate platform, siliciclastic and lava deltas to shelf, slope and basin floor and were subject to relative sea-level changes. Combined with high sedimentation rates this makes the basin well suited for studies of Cenozoic depositional trends along the western South China Sea.

The depositional development in the basin is investigated through seismic stratigraphic and facies analyses, and well data are closely integrated in the analysis in order to extract age and lithologic information. Palaeogeographic reconstructions illustrate the gross-sedimentary evolution of the basin and form a primary result of this part of the study (Fig. 2). Information on the regional geological evolution can be obtained from the depositional style of the basin in addition to information on the establishment of the South

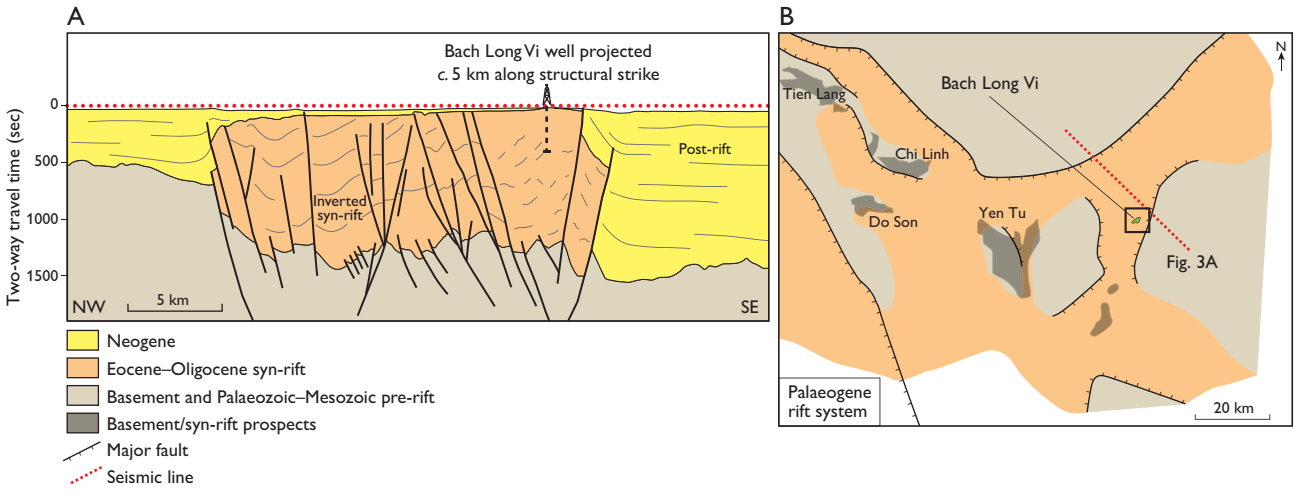

Fig. 3. **A**: Geotransect across the inverted Palaeogene graben, which is exposed on the island of Bach Long Vi a few kilometres from the profile. The approximate well trajectory is projected onto the section. The transect is based on the seismic line 89-1-103 (partly shown on Fig. 3B, red, dotted line). **B**: Map showing the outline of the primary Paleogene syn-rift depocentre and syn-rift structural highs in the north-eastern Song Hong Basin. Oil and condensate discoveries in the area are sourced from lacustrine and coaly syn-rift source rocks. Bach Long Vi forms a window to a graben directly linked with the syn-rift kitchen areas of the recent discoveries made in fractured and karstified Palaeozoic carbonates in the area.

China Sea, regional uplift history, sediment transport and Cenozoic climate.

Neogene basalt volcanism affected large parts of the Vietnamese margin from the Nam Con Son Basin in the south to the Song Hong Basin in the north, and acted coeval with widespread carbonate platform growth along the margin (Fig. 2). Magmatism was associated with regional onshore uplift and denudation, which seems to have had a significant derivative effect on contemporary deposition (Fyhn *et al*. 2009). Increased siliciclastic input to the offshore basins and elevated inorganic nutrient concentrations in platform areas associated with onshore uplift and denudation led to a lowering of long-term carbonate production and deposition. As a result, carbonate platforms drowned and became buried underneath kilometre-thick, prograding siliciclastic sediment wedges during the Late Neogene. In the southern Song Hong Basin, volcanics and carbonate platforms are nicely revealed by seismic data and are drilled and dated in wells (Fig. 2).

Syn-rift and source-rock deposition

Cretaceous and Cenozoic organic-rich lacustrine mudstones and humic coals, which were deposited during periods of rifting, form world-class source-rock intervals in South-East Asia (Fig.1). These source rocks frequently occur adjacent to coarse-grained, reservoir-quality sedimentary bodies derived from nearby elevated hinterland areas. Moreover, source-rock intervals are often located adjacent to fractured basement or pre-rift successions with effective reservoir characteristics. Understanding these rift systems, including the occurrence and genesis of lake systems and the sedimentary successions capable of generating and storing hydrocarbons, is critical when evaluating local petroleum systems over larger parts of South-East Asia.

It has long been recognised that stratigraphic wells through syn-rift successions are useful to unravel the deeper depositional systems including source-rock units (e.g. Sladen 1997). This is particularly true offshore northern Vietnam, where syn-rift lacustrine and coaly-sourced petroleum mainly occur in fractured and karstified pre-rift carbonates. Even so, little is known about the source-rock system, and deep wells drilled into the syn-rift succession have not provided information on the source rocks of the area. To address this problem, the ENRECA group drilled a 500 m fully cored well into the inverted syn-rift succession on the island of Bach Long Vi (Figs 1, 3) where highly oil-prone source-rock intervals are widespread. The core demonstrates a thick lacustrine succession within the area. At the time of writing, cores are transported to a core depository to be analysed in detail. Bach Long Vi has low relief and dense vegetation, and hence well-exposed outcrops on the island are limited to locations along the shore, and a satisfactory study of syn-rift sedimentation and source-rock quality is not possible based on outcrops alone. However, combined with the cored stratigraphic well, the geology of Bach Long Vi provides a unique opportunity to study syn-rift deposition and source-rock composition. The core provides a regional type section of

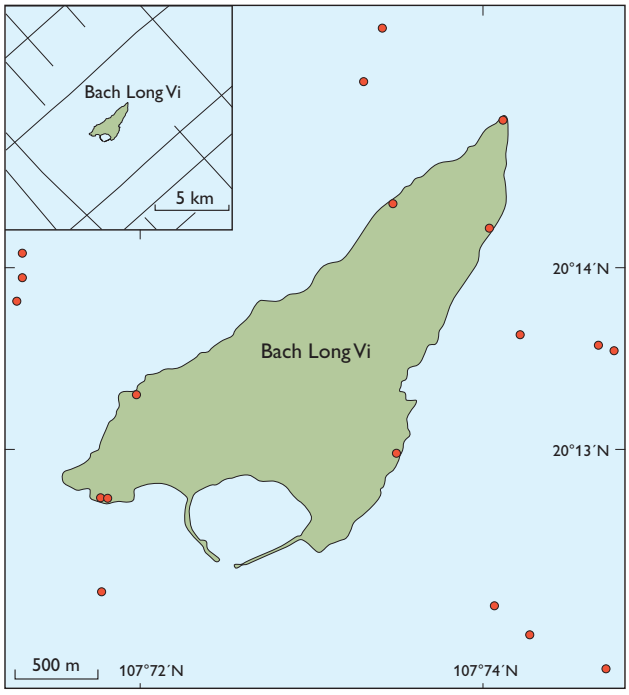

Fig. 4. Map of the island of Bach Long Vi. Red dots show sites of source-rock samples. The inset map shows the nearest industrial seismic lines in the area. For location see Figs 1 and 3.

the Palaeogene syn-rift succession. Sampled source-rock intervals are studied through general source rock screening and biomarker analysis combined with more advanced analysis of selected source-rock intervals.

Situated at the intersection of the Beibuwan and the Song Hong Basin, Bach Long Vi occurs in the centre of a newly discovered petroleum province offshore Vietnam (Fig. 3). Bach Long Vi sits at the top of a prominent structure associated with inversion of a Palaeogene graben. The island therefore provides a window into the nature of the Palaeogene syn-rift succession of the area. Highly oil-prone lacustrine mudstones with an organic content ranging from *c.* 2 to 7 wt.% total organic carbon were sampled from scattered outcrops on Bach Long Vi and from sub-sea outcrops around the island (Fig. 4). ENRECA analyses of these excellent source rocks confirm that petroleum-prone mudstones occur at various stratigraphic levels that crop out over the entire area (e.g. Petersen *et al*. 2004 and new unpublished data).

A dense net of seismic data cover the area offshore Bach Long Vi and reveals a N–S to NE–SW-trending, inverted Eocene–Oligocene graben. The graben fill sub-crops at and closely beneath the seafloor and forms the core of Bach Long Vi (Fig. 3A). The graben is part of a larger rift system that actively subsided during Palaeogene time (Fig. 3B). The deposits, including the sampled source rocks on and around Bach Long Vi, therefore form part of a regional syn-rift system, which is directly continuous with the syn-rift kitchen areas sourcing the recent oil and condensate discoveries in the region (Fig. 3). The preliminary results suggest that rich source-rock intervals could be present throughout much of the syn-rift succession in the basin, highly encouraging for further exploration.

Acknowledgements

The ENRECA project is funded by the Danish Ministry of Foreign Affairs via Danida. PetroVietnam co-funded the ENRECA 3 well and is thanked for providing data and for permitting publication of this paper.

References

Fyhn, M.B.W., Boldreel, L.O. & Nielsen, L.H. 2009: Geological development of the central and south Vietnamese margin: Implications for the establishment of the South China Sea, Indochinese escape tectonics and Cenozoic volcanism. Tectonophysics **478**, 184–214.

Hall, R. & Morley, C.K. 2004: Sundaland Basins. In: Clift, P. *et al*. (eds): Continent–ocean interactions within the East Asian marginal seas. Geophysical Monograph Series **149**, 55–85. Washington D.C.: American Geophysical *Union.Leloup*, P.H., Arnaud, N., Lacassin, R., Kienast, J.R., Harrison, T.M., Trong, T.T.P., Replumaz, A. & Tapponnier, P. 2001: New constraints on the structure, thermochronology and timing of the Ailao Shan-Red River shear zone, SE Asia. Journal of Geophysical Research **106**, B4, 6683–6732.

Petersen, H.I., Nytoft, H.P. & Nielsen, L.H. 2004: Characterisation of oil and potential source rocks in the northeastern Song Hong Basin, Vietnam: indications of a lacustrine–coal sourced petroleum system. Organic Geochemistry **35**, 493–515.

Sladen, C. 1997: Exploring the lake basins of east and Southeast Asia. In: Fraser, A.J., Matthews, S.J. & Murphy, R.W. (eds): Petroleum geology of Southeast Asia. Geological Society Special Publications (London) **126**, 49–76.

Authors' addresses

M.B.W.F., H.I.P., L.H.N. & I.A., *Geological Survey of Denmark and Greenland, Øster Voldgade 10, DK-1350 Copenhagen K, Denmark.*

E-mail: *mbwf@geus.dk*

T.C.G. & *L.H.Ng.*, Vietnam Petroleum Institute, 173 Trung Kinh Str., Yen Hoa Wrd., Cau Giay Dist., Hanoi, Vietnam.

N.T.M.H., Hanoi University of Mining and Geology, Dong Ngac, Tu Liem, Hanoi, Vietnam.

N.D.N., Hanoi University of Science, 334 Nguyen Trai-Thanh Xuan-Hanoi, Vietnam.

Rock phosphate and lime for small-scale farming in Tanzania, East Africa

Per Kalvig, Niels Fold, Jesper Bosse Jønsson and Elisante Elisaimon Mshiu

Poor soils are a major cause of poverty in sub-Saharan Africa, and thus restoration of soil fertility is a significant challenge for sustainable agriculture. Some of the main resources required, e.g. phosphate and lime, are present in many African countries and can be used by smallholder farmers in a relatively unprocessed form instead of expensive commercial fertilisers. Here we present a small study of the Mbeya region in Tanzania, which locally has both phosphate and lime.

Most soils in sub-Saharan Africa are losing nutrients necessary for sustainable agriculture. This is mainly due to intensive farming and the fact that the nutrients are not replaced adequately. Further reasons for nutrient losses are leaching, soil erosion and fixation by iron and aluminium oxides. Vast areas experience moderate to acute phosphorus deficiency (Vanlauwe & Giller 2006).

The Mbeya region in south-western Tanzania (Fig. 1) is characterised by intensive smallholder plots along with several local sources of phosphate-bearing rocks and limestone. The former were examined in the 1980s (Chesworth *et al.* 1988, 1989), but have never been utilised (Kalvig *et al.* 2010).

Phosphates and lime – opportunities and constraints

Soils may become acid for many reasons and high rainfall may lead to washing out the nutrients needed for healthy plant growth. Thus phosphorus and calcium deficiencies are common factors that restrict plant growth in highly leached tropical soils. The majority of smallholders cannot afford to use adequate quantities of commercial fertilisers and lime, resulting in low yields. An alternative is to use local sources, which can improve agricultural productivity by slowly releasing essential elements and raising the pH value of the soil. Phosphates, lime, potassium-rich minerals, clay, zeolite and mica are common locally, but lacking awareness of their effects, very few smallholders use them. If such an awareness could be fostered and local resources made available at affordable prices, it would give farmers an opportunity to improve their crop yields (van Straaten 2002; Mitchell 2005). The phosphate potential in Tanzania was outlined twenty years ago by Mchihiyo (1991). The study presented here shows that local phosphate can be made available at affordable costs.

Phosphate minerals. Natural fertilisers are available and can be used untreated. They comprise organic fertilisers such as manure, leaf litter and sludge, and rock fertilisers such as marl, rock phosphate, volcanic rock and mica. In contrast to natural fertilisers, artificial fertilisers are readily soluble and contain guaranteed total, active nutrient concentrations.

The practical challenges and potential benefits involved in the use of rock phosphate have been widely discussed (Mchihiyo 1991; Appleton 2002; van Straaten 2002, 2006; Vanaluwe & Giller 2006). The general view is that the use of rock phosphate for local agriculture is justified, provided its addition is managed in accordance with the type of crop and the conditions of the soil. Usually, crop yields only show a slow response over 2–3 years after the addition of rock phosphates, which makes it difficult to generate interest among local farmers.

The solubility of phosphate-bearing rocks differs widely depending on the mineralogy and chemistry of the rock

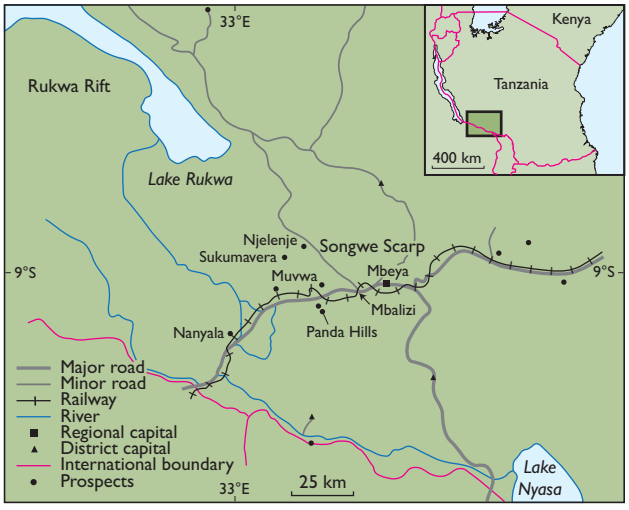

Fig. 1. Map of south-western Tanzania showing the Mbeya region with its main towns, roads and railway. The prospects indicated are known carbonatite occurrences which were considered potential phosphate resources by previous studies.

type, and not all of them are therefore effective when applied directly to the soil. Some important factors for the successful use of rock phosphate are: (1) the type of phosphatic rock, with apatite as the most common phosphate mineral containing 34–42% P_2O_5, (2) the reactivity of the phosphate rock, (3) the soil, where in particular pH, cation exchange capacity, phosphorus and calcium concentration, and phosphorus-fixing capacity of the soil play important roles, (4) the type of crop, because the ability to use H_2PO_4, which dominates at low pH, differs from crop species to crop species, and (5) fertiliser management (van Straaten 2002).

Lime. The primary reason for increasing the soil pH by liming is to reduce the aluminium toxicity to plants, and to ensure that Ca, Mg, K and P are available to the plant. Raising the pH value to 5.2–5.5 is adequate for increasing crop yields, whereas higher values reduce the breakdown of rock phosphate (Mitchell 2005).

Phosphate and lime resources in the Mbeya region

Geological setting. In Tanzania, a central Archaean craton is surrounded by Proterozoic fold belts (Fig. 2). The Mbeya region lies south-west of the Archaean craton in the NW–SE-striking 2000–1800 Ma old Ubendian fold belt. This fold belt is dominated by gneisses and amphibolitic rocks, intruded by 730 Ma old syenite-gabbro complexes, all of which have been intruded by carbonatite complexes of Cretaceous to late Palaeogene age. During the late Phanerozoic, rifting and faulting occurred in connection with the formation of the East African Rift Valley. The occurrence of Neogene sediments such as conglomerate, clay and chert as well as volcanic rocks is related to the rift valley.

Phosphate in the Mbeya region. The most promising phosphate occurrence is the Songwe Scarp carbonatite, which is a 20 km long, 50 m wide, NW–SE-striking, 100 ± 10 Ma old ferrocarbonatite (Miller & Brown 1963; Brown 1964). Mchihiyo *et al.* (1992) provide an overview of the exploration history of this carbonatite, which took place in the 1950s. The exploration focussed on uranium and comprised geological mapping of anomalous zones of the carbonatite some 2 km north-west of the village Njelenje (Fig. 1; Brown 1964). In the 1990s, the phosphate was assessed as a potential source of fertiliser (van Straaten 2002).

The exploration led to the recognition that several parts of the Songwe Scarp carbonatite are relatively rich in apatite. It was also discovered that areas with elevated concentrations of radioactive elements, yttrium and other rare-earth elements occur near Njelenje (Fig. 3). The highest phosphate concentrations were found in limonitic residual soils overlying the carbonatite, with up to 20% P_2O_5 and 6% K_2O. These soils can be used as phosphate fertilisers (Chesworth *et al.* 1989; Appletorn 2002; van Straten 2002).

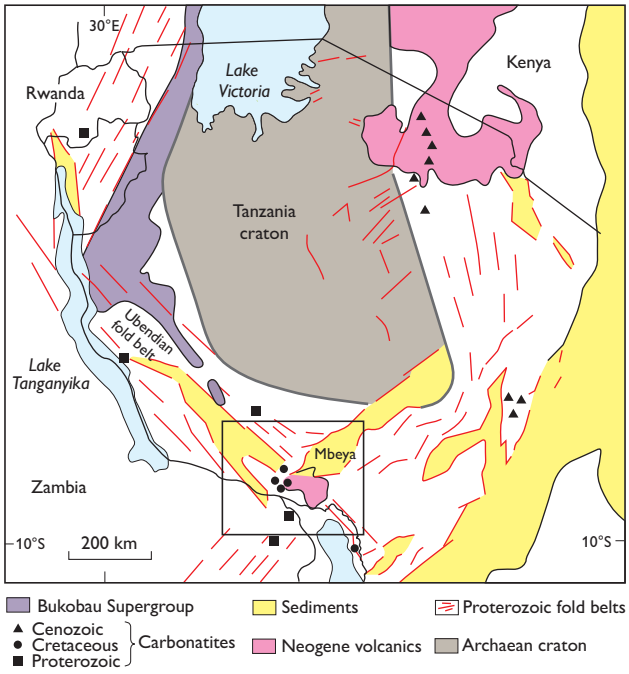

Fig. 2. Simplified geological map of Tanzania (based on van Straaten 2002). The Mbeya region (framed) is located in south-western Tanzania.

In addition to the Songwe Scarp carbonatite, the region holds several other occurrences of phosphate. One is the Panda Hills carbonatite where *c.* 1 Mt of residual phosphates with a P_2O_5 concentration up to 10.3% have been mapped (van Straaten 2002). Another is the Mbalizi carbonatite where weathered parts locally form a 0.5 m thick limonitic crust with up to 30% P_2O_5 (Mchihiyo 1991; Mchihiyo *et al.* 1992). This phosphate is under exploration as a potential source of niobium and other rare-earth elements. A third possibility of phosphate is guano from bats around Sukumavera, but the amount is far too small to play any role, even for smallholders (van Straaten 2002).

Limestone in the Mbeya region. Calcareous sedimentary rocks, mainly travertine in the Songwe valley, are mined for (1) dimension stones using a yellowish travertine near Nanyala in the Mbozi district, (2) carbonate for calcination and (3) cement production. Hochstein *et al.* (2000) and Roberts *et al.* (2004) provided geological details of this limestone unit and estimated that it covers an area of *c.* 13 km² with a thickness of 5–70 m, equivalent to >150 000 000 m³. An example of a weathered occurrence is shown in Fig. 4.

Fig. 3. Landscape around the village of Njelenje in the Songwe valley, looking east and showing the Songwe Scarp carbonatite.

Proposals for feasibility studies

Small-scale phosphate operation to supply local smallholders. The Songwe valley area holds two potential sources for the production of local rock phosphate: carbonatite and apatite-rich residuals of carbonatite. Given that previous studies indicate that enrichment of phosphorus has taken place in the residual apatite-rich soil (Mchihiyo *et al.* 1992) and that a production based on such soil is technically relatively straightforward, the present study only considers this source. In the vicinity of the village of Njelenje, the P_2O_5 concentration reaches 18–20% and the K_2O concentration 6% (Mchihiyo *et al.* 1992).

A pilot study was conducted in March 2010. The purpose was to learn from smallholding farmers what their local cultivation practices are and get their views on requirements on and limits to the use of locally produced phosphate fertilisers. The study also aimed at clarifying the availability of local labour for small-scale phosphate extraction. The village of Muvwa, located in the Mbeya region, was chosen due to its proximity to the phosphate resources of the Songwe Scarp carbonatite (Fig. 3). The study area encompassed 420 households corresponding to 1768 inhabitants of whom 331 persons were capable of working. Twenty-one households were interviewed in order to learn about the general pattern of cultivation practices. The low number means that the results are only indicative (Kalvig *et al.* 2010). As no geological data on the survey area are available, the data from Njelenje, situated *c.* 5 km to the north of the interview area, may serve to indicate the total available phosphorus content of the soils in the survey area.

A feasibility study of a potential rock phosphate production is warranted and, based on a labour intensive concept producing rock fertiliser for local consumption, should (1) assess the phosphate resource (grade and tonnage estimates – and the potential content of harmful elements), (2) propose a suitable set-up for the production and (3) assess the distribution and market prospects.

At this stage, no calculations of the required amount of local rock phosphate per hectare can be made, because a number of technical data are not yet available: the actual fertility of the soils of the trial area; depletion rate of phosphorus; fixation rate of phosphorus; identification of the most phos-

Fig. 4. Small section of limestone in the Nanyala area of the Mbeya region showing the boundary between topsoil and weathered rock.

phorus demanding crops; the average phosphorus content of the potential rock phosphate.

Small-scale extraction of lime to supply local smallholders. In the village of Nanyala, some hundred people are involved in small-scale mining of a weathered, whitish travertine accompanied by a semi-mechanised production of hydrated lime. More than ten mining licences cover the lime producing area.

The limestone resource in the Songwe valley consists of various grades of Quaternary to Recent travertine deposits. It is dominated by poorly consolidated, partly weathered, whitish rock, of which neither the quantity nor the quality has ever been thoroughly investigated as regards lime for agricultural use. The ideal agricultural lime is a ground dolomite or dolomitic limestone with a particle size <2 mm; 60% <400 μm and up to 50% <150 μm (Mitchell *et al.* 1997). Labour intensive production of agricultural lime is a relatively straightforward process (Mitchell & Mwanza 2005).

The March 2010 survey included interviews with some of the operators in the neighbouring Nanyala area (Kalvig *et al*. 2010). Hydrolime has been produced for several years in this area. There is a potential for diversifying the existing hydrolime production to include lime products for local use and particularly for sale to local smallholders cultivating coffee. In Tanzania, agricultural lime is mainly produced in the Tanga District located *c.* 800 km from the Mbeya region.

A feasibility study on how to extend the on-going production of hydrolime to include lime for agricultural use seems warranted. It should include all steps from quarrying and marketing to testing the products and should be based on a labour intensive concept.

Acknowledgements

Geocenter Denmark is thanked for financial support, and the Tanzania Commission for Science and Technology for permission to conduct field work.

References

Appleton, J.J. 2002: Local phosphate resources for sustainable development in sub-Saharan Africa. British Geological Survey Report **CR/02/121/n**, 134 pp.

Brown, P.E. 1964: The Songwe scarp carbonatite and associated feldspathization in the Mbeya Range, Tanganyika. Quarterly Journal of the Geological Society **120**, 223–240.

Chesworth, W., Semoka, J.M.R., van Straaten P., Mnkeni, P.M.S., Kamasho, J.A.M. & Mchihiyo, E.P. 1988: Tanzania–Canada agrogeology project: report on completion of the first phase, 93 pp. Ontario, Canada: University of Guelph.

Chesworth, W., van Straaten, P. & Semoka, J.M.R. 1989: Agrogeology in East Africa: the Tanzania–Canada project. Journal of African Earth Sciences **9**, 357–362.

Hochstein, M.P., Temu, E.P. & Moshy C.M.A. 2000: Geothermal resources of Tanzania. World Geothermal Congress 2000, Kyushu–Tohoku, Japan, 28 May to 10 June 2000. Proceedings 1233–1238.

Kalvig, P., Fold, N., Jønsson, J.B. & Mshiu, E.E. 2010: Local use of agrominerals. Untapped resources for farming communities in sub-Saharan Africa. Appraisal study on the agromineral potential in the Mbeya area, Tanzania. Danmarks og Grønlands Geologiske Undersøgelse Rapport **2010/107**, 58 pp.

Mchihiyo, E.P. 1991: Phosphate potential in Tanzania. Fertilizer Research **30**, 177–180.

Mchihiyo, E.P., Kiranga, O.W. & Mbasha, M.Z. 1992: Tanzania–Canada agromineral project. Report on completion of second phase (Madini Group). Unpublished report, Madini Group, Tanzania.

Miller, J.A. & Brown, P.E. 1963: The age of some carbonatite activity in south-west Tanganyika. Geological Magazine **100**, 276–279.

Mitchell, C.J. 2005: Farm lime: low cost lime for small-scale farming. British Geological Survey Technical Report **CR/03/066N**, 138 pp.

Mitchell, C.J. & Mwanza, M. 2005: Manual for small-scale production of agricultural lime. British Geological Survey Commissioned Report **CR/05/092N**, 31 pp.

Mitchell, C.J., Inglethorpe, S.D.J., Tawodzera, P., Bradwell, S. & Evans, E.J.M. 1997: Local development of affordable lime in southern Africa. British Geological Survey Technical Report **WC/94/20**, 120 pp.

Roberts, E.M., O'Connor, P.M., Gottfried, M.D., Stevens, N., Kapalima, S. & Ngasal, S. 2004: Revised stratigraphy and age of the Red Sandstone Group in the Rukwa Basin, Tanzania. Cretaceous Research **25**, 749–759.

van Straaten, P. 2002: Rocks for crops. Agrominerals of sub-Saharan Africa, 338 pp. Nairobi, Kenya: International Centre for Research in Agroforestry.

van Straaten, P. 2006: Farming with rocks and minerals: challenges and opportunities. Anais da Academia Brasileira de Ciências **78**, 731–747.

Vanaluwe, B. & Giller, K.E. 2006: Popular myths around soil fertility management in sub-Saharan Africa. Agriculture, Ecosystems and Environment **116**, 34–46.

Authors' addresses

P.K., *Geological Survey of Denmark and Greenland, Øster Voldgade 10, DK-1350 Copenhagen K, Denmark*. E-mail: *pka@geus.dk*

N.F., *Department of Geography and Geology, University of Copenhagen, Øster Voldgade 10, DK-1350 Copenhagen K, Denmark.*

J.B.J., *School of Geographical & Earth Sciences, University of Glasgow, Glasgow G12 8QQ, Scotland, UK.*

E.E.M., *Department of Geology, University of Dar es Salaam, P.O. Box 35052, Dar es Salaam, Tanzania.*